The Aerosol-Chase Project

A continental Lagrangian experiment

DIPLOMA WORK FOR MASTER OF SCIENCE IN PHYSICS, FYSM30
LUND UNIVERSITY
20TH OF JUNE 2021

ADRIAN REYES MARTIN
ad6620re-s@student.lu.se

SUPERVISOR
ADAM KRISTENSSON

CO-SUPERVISOR
MATTHEW STANLEY JOHNSON

LUND
UNIVERSITY

Abstract

Determining how aerosol particle number size distributions evolve during long range transport and how aerosol sources contribute to the aerosol population is one of the greatest conundrums in aerosol science. Current monitoring of particle size distribution is done in fixed stations that provide limited information about the reasons why size distribution changes with time. In this project, the Lagrangian approach was applied to measure particle size distribution in an air mass while it was being transported. This was achieved by installing a Scanning Mobility Particle Sizer (SMPS) and a collection of sensors for temperature, humidity, ozone, CO_2, NO_2, PM_{10} and $PM_{2.5}$ inside a car, measuring the conditions of the air mass for 6-7 hours during its transport in the atmosphere. The results of this pilot project, divided into three case studies, have proven the method to be effective for the application of the Lagrangian approach in continental measurements. This study aims at becoming the beginning of a new line of research.

Contents

1 Introduction

Anthropogenic aerosol particles in the atmosphere have severe effects on climate and human health [1, 2]. The World Health Organization estimates that exposure to fine particles in polluted air causes around 7 million deaths per year by diseases such as stroke, heart disease, lung cancer or respiratory infections [3]. In addition, aerosol particles have a direct impact on climate by absorption of solar radiation and scattering. The effect can also be indirect, since aerosol particles act as condensation nuclei for cloud formation, creating cloud droplets and ice crystals that effectively scatter light. With an increasing population of aerosol particles due to human activities, the net effect of this direct and indirect anthropogenic forcing is a cooling. It comprises the largest uncertainty in the radiative forcing, defined as the increase of trapped radiation in the earth and atmospheric system compared to pre-industrial times [4] (Figure 1).

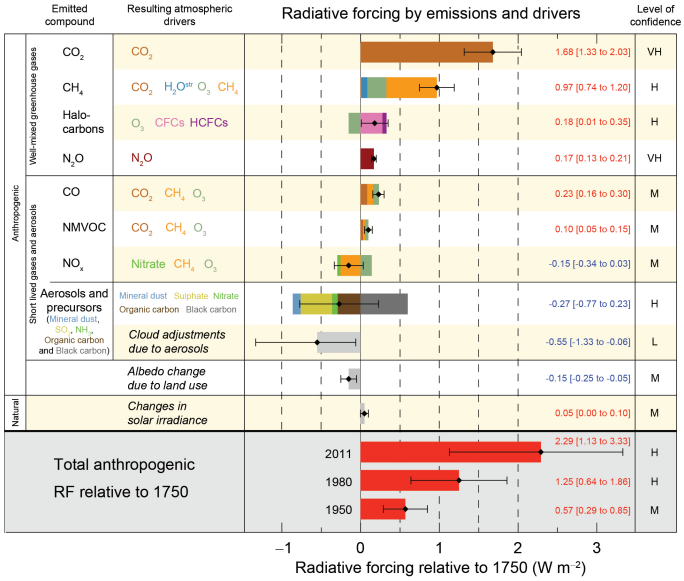

Figure 1: Radiative forcing estimates in 2011 relative to 1750 and aggregated uncertainties for the main drivers of climate change. From European Environment Agency.

Environmental and health effects are dependent on particle size and chemistry. For this reason, particle number size distributions and atmospheric chemistry are essential elements in environmental monitoring, currently measured at fixed stations. There is a movement towards increasing the number of rural background and remote flagship stations for climate effect studies [5] and urban monitoring

networks for air quality purposes. At fixed stations, it is occasionally possible to quantify the contribution from various sources using statistical source/receptor modelling [6] applied on the monitored data. This source apportionment can be performed for the particle number size distribution in urban areas [7, 8]. However, it is very difficult to perform source/receptor modelling in rural areas where long-range transport has a great influence on the aerosol population, because particle transformations change the properties of the particles, making them indistinguishable between different sources at fixed stations. Namely, source/receptor models require that the measured gaseous compounds or the aerosol particle properties are invariant from the source emissions until they reach the field site. Estimating the contribution of particle sources to the aerosol population and understanding the evolution of particle size distribution during long-range transport is one of the greatest conundrums in aerosol science.

One way to solve this problem is the so-called Lagrangian approach, which is based on following the movement of an air mass with the wind and measure the aerosol particles and the precursor gases as they develop [9]. In this way, transformation and emissions from new sources along the air mass path are monitored closely, being possible to quantify. Previous studies have approximated the Lagrangian approach relatively well by integrating measurements from field stations that are close to each other [10]. However, these experiments can only be performed for connected wind flow between the stations, and not for other wind directions. Real Lagrangian experiments have used balloons for air mass tracking over the ocean [11] and Antarctica [12]. However, there are no previous reported Lagrangian experiments over populated continental areas. This kind of experiments can, in principle, be performed with balloons, aircraft, unmanned aerial vehicles (UAV), airships, or mobile road vehicles. Among these options, mobile road vehicle experiments are the most cost-effective and require less extensive infrastructure and planning.

The aim of this pilot project is to test a novel method to perform Lagrangian measurements over continental areas employing mobile vehicle measurements at ground level. If successful, it would provide a reliable and cost-effective method to quantify particle emissions and transformations from various aerosol processes. In addition, this method allows the validation and improvement of the 2D-Lagrangian model for Aerosol Dynamics, gas-phase CHEMistry and radiative transfer (ADCHEM) [13]. The methods used in this first continental Lagrangian experiment can be replicated to other studies at other seasons and other geographical regions.

The newly developed equipment consists of a monitoring system composed of a particle number size distribution instrument and low-cost sensors to measure

size-dependent aerosol number concentrations and atmospheric chemistry. The portable monitoring system was installed inside of a car with a power station that allowed following a single air mass for up to, at least, 10 hours. The results were validated with measurements from the fixed Hallahus and Hyltemossa research field stations.

This report begins by introducing theory about aerosols and their sources, and describing the aerosol processes that transform the particle size distribution during long-range transport in an air mass. Secondly, the methods and setup used in the project are described, expecting to provide a manual for future Lagrangian experiments. After explaining the methods, the measuring campaigns for each of the three case studies are described, showing the obtained results and discussing potential explanations of the observations. Following this, some conclusions are drawn by comparing the results from the different campaigns. Lastly, potential future research projects that could follow this diploma work using the Lagrangian approach for continental measurements are described and proposed.

2 Theoretical background

An aerosol is a mixture of gases and particles. The lowest layer of the terrestrial atmosphere, which this study focuses on, is an example of an aerosol. The particles present in an aerosol are also referred to as aerosols or aerosol particles, and can be both solid and liquid. They are characterised by an average lifetime of about one week in the boundary layer of the atmosphere. However, the lifetime depends strongly on size, where micrometre sized aerosol particles and particles of a few nanometres are removed most quickly [14].

2.1 Aerosol sources

Aerosol particles are classified as primary and secondary particles [15]. Primary particles are formed directly at the source, while secondary particles are formed through gas-to-particle conversion a while after the first gaseous emissions. However, this distinction is not always clear and, for example, particles that are formed through gas-to-particle conversion from human activity are secondary in nature but considered as primary when they are formed within a few seconds after their source emission. The two types of particles can have both natural and anthropogenic origins, and they can be divided into sub-categories based on how they are generated.

Primary particles can be biological, mechanically generated or emitted during combustion. Biological particles include bacteria, fungal spores, pollen, viruses, algae and biological crusts [16]. Mechanically generated particles have different origins such as wave breaking, wind-borne dust or road abrasion by vehicles. Similarly, combustion particles can be generated by natural sources, such as forest fires or volcanoes, or anthropogenic sources, such as vehicle engines, power plants or domestic biomass combustion.

Secondary particles are formed by secondary formation and new particle formation. Secondary formation occurs by condensation of gases on existing particles, increasing the mass concentration of particles without affecting the number concentration, since no new particles are formed. Conversely, new particle formation mechanism produces new nanoparticles around 1 nm diameter from precursors gases, increasing the number concentration while negligibly affecting the mass concentration at the time of formation.

Many of the emitted precursor gases from natural and anthropogenic activities have relatively low volatility, which is required for condensation or new particle formation to occur. Conversely, many other precursor gases which have recently been emitted can be of much higher volatility, and they need to pass through several oxidation steps before acquiring low enough volatility for condensation or new particle formation to occur. This is realized mainly by oxidation with ozone, OH-radicals, or nitrates. Additional compounds oxidize the aerosol when it is in the cloud droplet phase [15, 17].

There is a permanent competition between condensation and new particle formation in the atmosphere. When there is a large available surface area of existing particles, the low-volatility compounds preferably condense on the existing particles, suppressing new particle formation. This happens mainly in the presence of a high surface area concentration of particles in the accumulation mode (larger than 100 nm diameter). Conversely, when the surface area of pre-existing particles is low, secondary formation is preferred via the new particle formation route [18].

2.2 New particle formation

New particle formation (NPF) occurs when gas molecules undergo a phase transition to liquid or solid particles with sizes around 1-2 nanometres [19]. This often happens early in the morning and until midday, after oxidation taking place by ozone or OH-radicals, which have higher concentrations after sunrise. After formation, the particles also need to go through a growth activation phase before they are detected by most instruments measuring aerosols above 10 nm diame-

ter, likely involving other compounds than those during the initial formation [19]. This growth takes place by condensation on these already preexisting atmospheric particles.

Evidence of new particle formation in the atmosphere was first reported by Aitken in 1897 [20], but it could not be detected until further development of instruments allowed observing particles in the nanometre scale [21, 22]. Currently, new particle formation has been observed at field sites around Europe about one third of the days, with the recently formed particles being observed to grow to sizes of several tens of nanometres during the course of the day. These particles provide an important fraction of the existing aerosol population by number [23]. Currently, the Scanning Mobility Particle Sizer (SMPS), used for this Lagrangian experiment, is one of the most widely used instruments to measure newly formed particles and observe the evolution of the particle number size distribution [19]. A case of NPF followed by particle growth due to condensation observed during this Lagrangian experiment is discussed in *Results and Discussion*. Figure 2 illustrates this process.

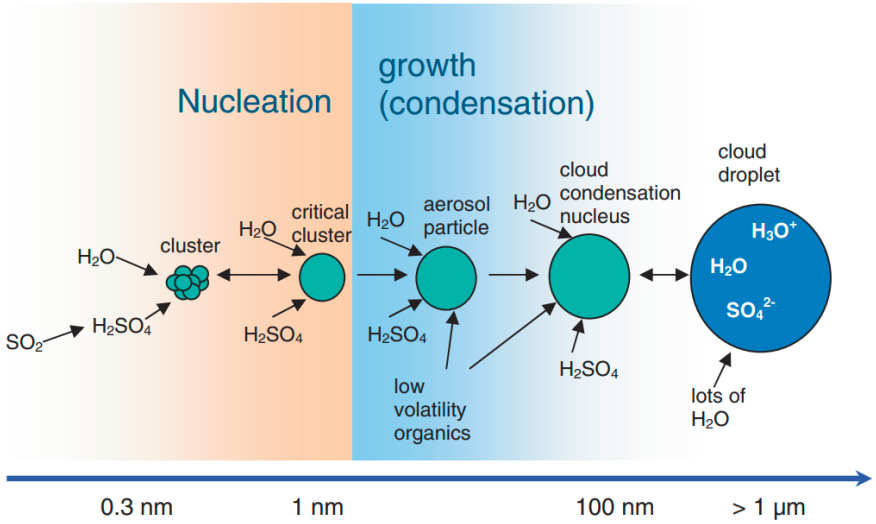

Figure 2: Schematic representation of nucleation and subsequent particle growth by condensation. From [24].

The sources that contribute to particle formation can be both natural and anthropogenic. Vegetation sources usually release high amounts of monoterpenes, like alpha-pinene or isoprenes of high volatility through stomata in leaves and needles that cannot produce NPF by themselves [25]. However, particle formation

has been observed in boreal forests by oxidation of these substances [23]. On the other hand, anthropogenic sources have different volatilities, and some of them lead to NPF without oxidation. In the case of vehicle exhaust emissions, which are important in this study, some of the particles condense immediately after the emissions (which are considered primary particles), while others are transported a long distance before they are oxidized to receive lower volatility and contribute to NPF or condensation.

The production of oxidants is often taking place via photochemical processes in the atmosphere, and therefore, sun radiation drastically affects NPF, which is a factor to consider in addition to the existing aerosol population. During winter, limited sun hours and less availability of precursor gases from tree emissions make NPF less likely at this period. Although tree emissions are more intense in summer, the relatively higher abundance of accumulation particles in the summer months in Europe makes condensation more favourable than NPF during this time [18], hence NPF events peak in spring and autumn. There is also an additional reason for diurnal variation in NPF; while the atmosphere presents stable stratification that traps the pollutants during the night, morning sun radiation initiates warming of the ground surface and creates turbulence. This process turns the stable night layer into a turbulent boundary layer, which becomes more vertically extensive during the course of the day, decreasing the concentration of particles in the accumulation mode as the air from above layers with fewer accumulation particles is mixed downwards to the boundary layer, where the NPF eventually takes place.

2.3 Atmospheric particle processes

Aerosol particles can be affected by several atmospheric processes that can change their size and composition and affect their lifetime. Some of the particle transformations that are more relevant for this study are briefly explained below.

- **Condensation**

  As described in the previous subchapter, condensation occurs when gases adhere to an existing aerosol particle. This process makes the particles grow in size, contributing to an increase in the particle mass concentration without changing the number of particles. Depending on the characteristics of the molecules, the condensing gases can either adhere to the particle surface or dissolve and alter its chemical composition (Figure 3). Condensation of sulfuric and nitric acids, ammonia, and secondary organics onto existing

particles is the dominant process that contributes to the increase of particle mass distribution [25]. Evaporation is the opposite process to condensation, where an aerosol particle decreases in size because of the transition to the gas phase of compounds forming the particle.

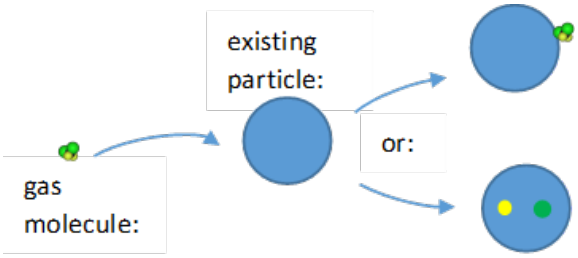

Figure 3: Simplified diagram of condensation of gases on pre-existing particles. Image: Adam Kristensson.

- **Coagulation**

  Coagulation is a process in which two particles collide, adhering to each other and forming a larger particle than its precursors. The process of coagulation increases the size of the particles but reduces the number concentration. Depending on the phase of the colliding aerosols, they can dissolve into each other, agglomerate, or form a solid core in a liquid particle (Figure 4). Coagulation is especially efficient when the size difference of the two colliding particles is large, for example, nucleation particles colliding on particles in the accumulation mode.

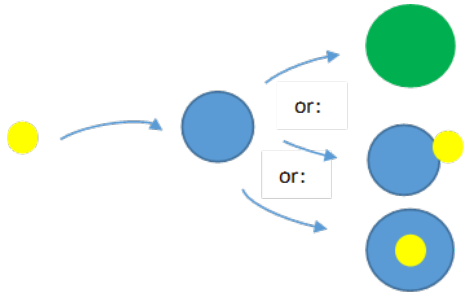

Figure 4: Simplified diagram of coagulation process between two particles. Image: Adam Kristensson.

- **Cloud activation**

  Aerosol particles can also change in size and composition by becoming cloud condensation nuclei (CCN). Clouds are usually formed by condensation of water molecules on existing particles, since this process is more energetically efficient than forming new pure droplets. For moderate values of water supersaturation, aerosol particles can become activated as CCN and start growing by condensation of water. While the cloud droplets continue growing, they can incorporate other particles and gases, changing their chemical composition [26, 27].

  When the cloud droplet evaporates, the aerosol particles are released to the atmosphere, usually with larger sizes due to the assimilation of salts and other elements during growth. The process of an aerosol population changing in size by cloud activation can be seen in Figure 5.

- **Wet and dry deposition**

  Wet deposition is responsible for the removal of 80-85 % of the aerosol particles in the atmosphere. In areas with intense precipitation, most of the CCN that were activated into cloud droplets are removed by precipitation directly (in-cloud scavenging). Wet deposition can also happen through below-cloud scavenging, where aerosol particles are captured by falling rain droplets below the cloud.

  Dry deposition only surpasses wet deposition rates in very arid regions. While wet deposition can take place anywhere in the troposphere, dry deposition only occurs when the aerosol particles are close enough to the ground or surface objects. Different factors affect dry deposition such as roughness of the surface, wind velocity, stability of the atmosphere and particle diameter [28, 29].

2.4 Particle size distribution

It has been shown that several of the processes described in the previous chapter are continuously changing the size of particles, which leads to aerosol populations with very diverse sizes. The gravitational and sedimentation velocity establishes a maximum limit in particle diameter at 100 µm. The structure of the aerosol particles as an assembly of gases, molecules or atoms, establishes a lower limit in particle diameter of 1 nm [14]. Therefore, the aerosol particles are present in a

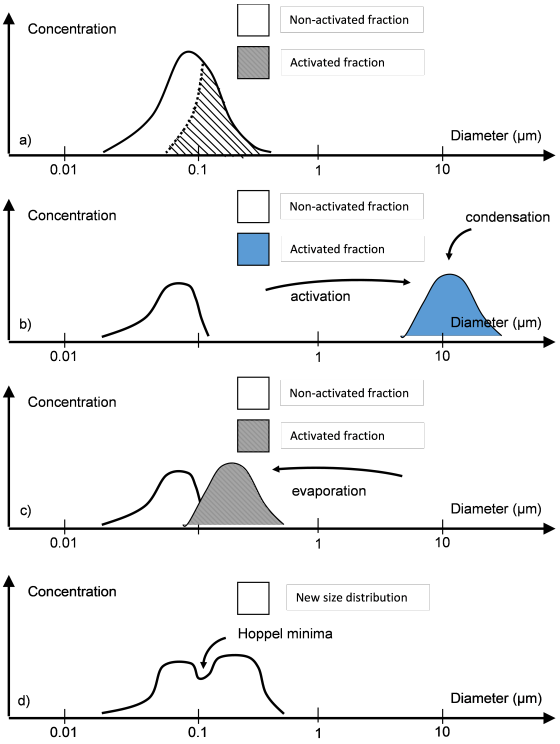

Figure 5: Cloud activation process of CCN a). a) Activation of part of the aerosol population into cloud droplets of larger sizes. b) Increase in size and chemical components of cloud droplets due to effective condensation of gases. c) Cloud droplet evaporation leaving activated aerosol particles at a larger size than a). d) New cloud-free atmospheric particle number size distribution with a Hoppel minimum between previously activated and unactivated aerosol particles. Image: Adam Kristensson.

range of sizes that covers five orders of magnitude for particle diameter which, scaled to volume, corresponds to 15 orders of magnitude.

The wide variability in sizes of the aerosol population is handled by classifying the particles in a size distribution. An example of particle size distribution for a rural environment, obtained during the first case study of this Lagrangian experiment, can be seen in Figure 6. The distribution in Figure 6 presents two pieces of modes of different sizes, and it is shown on a logarithmic size scale, weighted with the logarithmic difference of the size interval limits, $dNi/d\log_{10}(Dp)$. This lognormal distribution is the most conventional layout in aerosol physics due to its tendency to show symmetry and the reduction of input values to three parameters for each size mode: total number concentration N, geometric standard

deviation σ_g and geometric mean diameter d_g. These values form the lognormal distribution as in Equation 1.

$$dN/dlog_{10}(d) = \frac{N}{\sqrt{2\pi}log_{10}(\sigma_g)} e^{-\frac{(log_{10}(d)-log_{10}(d_g))^2}{2(log_{10}(\sigma_g))^2}} \quad (1)$$

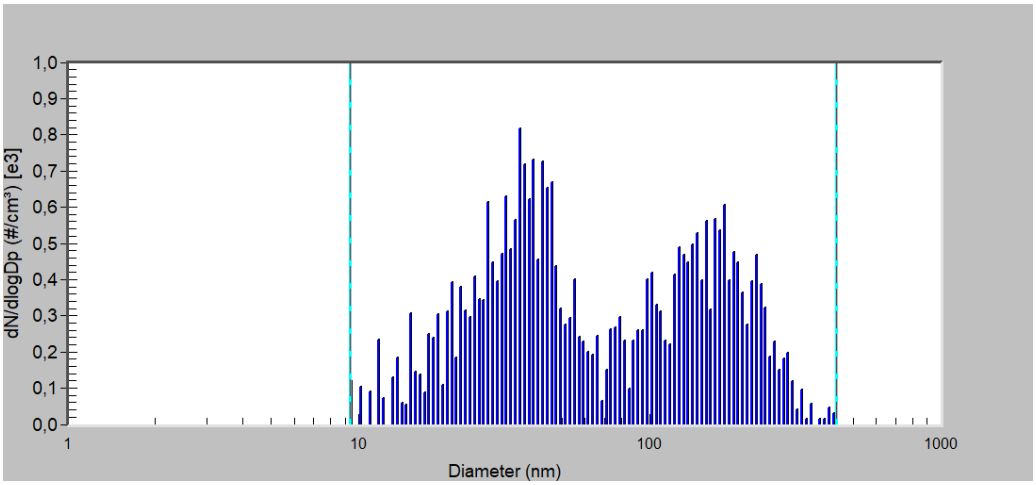

Figure 6: Particle size distribution measured during the first case study of the continental Lagrangian experiment, 23rd of March, 2021.

2.5 Particle modes

Equation 1 allows to classify the particles in several size modes, as illustrated in Figure 7. These lognormal modes are related to different source emissions and transformation processes such as condensation, coagulation, evaporation or cloud activation, explained in the section *Atmospheric particle processes*. These modes overlap in the size spectrum because of the continuous changes in particle sizes due to the atmospheric particle processes [30]. Figure 7 depicts some of the transformation processes that contribute to transitions between modes, as well as examples of atmospheric particles in the different modes.

The particles in the nucleation mode, smaller than 30 nm, are originated from new particle formation events (*nucleation*) or primary emissions of fossil fuel or biomass combustion. Nucleation particles grow by condensation of gases, transitioning to the Aitken mode when they reach diameters larger than 30 nm, a

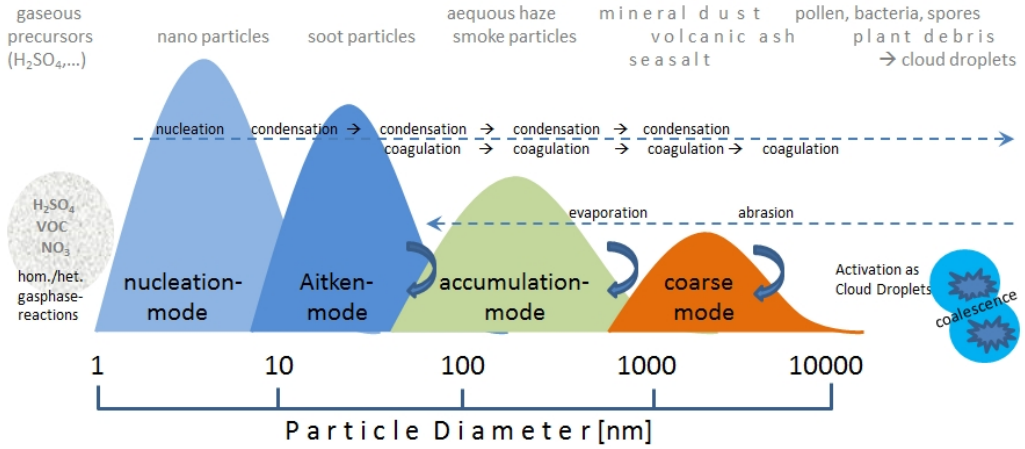

Figure 7: Schematic multi-modal particle size distribution with typical transformations and example particle types within each mode. From [30].

process that occurs after being transported for several hours or days in the atmosphere. When the concentrations in Aitken and larger size modes are sufficiently high, nucleation particles also coagulate with them, decreasing the concentration in the nucleation mode.

The Aitken mode includes particles with different ageing times. A fraction of them were nucleation mode particles that experienced growth from condensation. A second group present in this mode are aerosols originated by combustion processes, such as vehicle exhaust emissions. Particle size distributions cannot clearly distinguish evolved particles from newly emitted particles, which makes it very hard to estimate the contribution of the two groups to the Aitken mode when long-range transport effects are significant. A Lagrangian experiment like the one performed in this pilot project allows observing the transformation of particles from the nucleation to the Aitken mode during transport. Therefore, it enables to estimate the effect of atmospheric processes while detecting new sources of pollutants.

Particles in the accumulation mode, with sizes above 100 nm, have longer ageing times, and they usually reach larger sizes by condensation and cloud activation of Aitken mode particles. Due to their intermediate size, where neither coagulation, dry deposition or sedimentation are significant, these are predominantly removed by wet deposition. Since only one loss process is acting on these particles, they have the longest lifetime of all aerosol particles, with at least one week.

The coarse mode, above 1 µm in diameter, is generally not formed from the evolution of particles in smaller size modes, but by primary particles that are mechanically generated directly into this size mode. This leads to a high mass concentration of particles for diameters larger than 1 µm. The number concentration of particles in the coarse mode is, however, often several orders of magnitude smaller than for the other modes.

Mass concentration measurements of particles are usually separated by two main size fractions called $PM_{2.5}$ and PM_{10}, which are all particles in the population smaller than 2.5 and 10 µm in diameter, respectively. Traditionally, 2.5 µm was supposed to be the separation between coarse mode particles above 2.5 µm and fine particles below 2.5 µm, although it has been recognised later that 1.0 µm diameter is a more appropriate separation between fine and coarse mode particles. However, since many measurements of the $PM_{2.5}$ fraction remain worldwide, this separation remains in the nomenclature of air quality and aerosol research.

3 Methods

This chapter aims at describing how the experimental preparations were made, how the instrumental setup was used and how the Lagrangian experiments were conducted, and should become a manual for future experiments where the Lagrangian approach can be applied for similar purposes. Some of these potential projects are described in the chapter *Future research*. The different components of the methods or instrumental apparatus, which are described in detail in the following subchapters, can be extended or modified for future projects depending on the characteristics and the focus of the experiments.

3.1 Measurements area and field sites

3.1.1 Study region

The Lagrangian measurements were performed in the regions of Skåne and Blekinge. The terrain of these regions is relatively flat in most parts, which should allow neglecting effects from changes in altitude. The majority of the municipalities in the area are small in population and there is no intense industrial activity, with the only exception of Malmö, in western Skåne. However, several highways and smaller roads connect different urban areas, which are significant sources of pollutants. The southern part of Skåne and Blekinge consists mainly of agricultural

or pasture areas, whereas the Northern part consists mainly of managed forest areas, with a portion of natural broadleaved forests.

The geographical route for the Lagrangian experiments with the mobile system was always selected to pass very near the Hyltemossa and Hallahus field stations in Skåne (Figure 8). This allowed validating the concentrations measured with the mobile system and to extend the analysis to contain additional valuable measurement parameters. The details about Hyltemossa and Hallahus stations are described in the following sections.

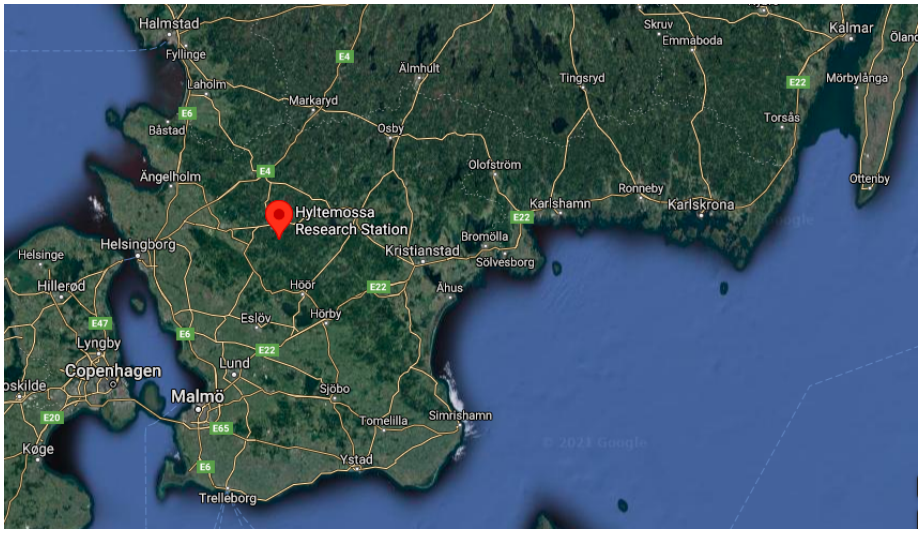

Figure 8: Map of the Skåne and Blekinge region and location of Hyltemossa Research Station. From Google Maps.

3.1.2 Hyltemossa field station

The Aerosol, Clouds and Trace Gases Research Infrastructure (ACTRIS) station Hyltemossa is located a few kilometres south of Perstorp (56.10 N, 13.42 E), in northwestern Skåne (Figure 8), at an elevation of 115 m [31]. The research station is inside a 37 year old Norwegian Spruce forest, with the forest canopy around 15-19 m height. It is far away from strong local sources of pollutants (Figure 9), which makes it a background reference station for urban measurements in southern Sweden and for studying the effect on pollution from long range transport. An inlet is placed at 30 m height above ground in a scientific tower. Air is drawn through the inlet to the laboratory house at the ground, where it is split in several

flow tubes to different continuously operated instruments in the house. The Hyltemossa station provides continuous measurements of the particle number size distribution (with differential mobility particle sizer [32]), absorption and scattering (with aethalometry and nephelometry respectively [33, 34]), cloud activation (with cloud condensation nuclei counter [35]) and aerosol chemical composition of sub-micron particles (with aerosol and chemical speciation monitor [36]).

Gases are measured from a 150 m mast, 50 m from the 30 m tower (Figure 9). Nitrogen oxides (with Thermo Electron Corporation Model 42 C chemiluminescence gas analyser), ozone (with Teledyne T400 photometric ozone analyser), and CO_2 (with Picaro G2401) are monitored at different heights in the forest canopy and above.

Figure 9: 150 meter tower in Hyltemossa used for gaseous measurements. From Hyltemossa Research Station, LU, Twitter, @SE_Htm, 21 Mar. 2019.

3.1.3 Hallahus field station

$PM_{2.5}$ and PM_{10} sensor node data were compared to measurements with a PALAS-FIDAS 200S optical particle counter instrument at Hallahus field station (56.04 N, 13.15 E), located about 19 km to the WSW of Hyltemossa station. The surroundings at Hallahus are a mix of coniferous and deciduous forests with pastures and agricultural fields nearby and a grass field just at the station (Figure 10). Hallahus is far away from local pollution sources, except for a small house 100 m to the SW

of the station, where domestic wood combustion is sometimes used, and a countryside road, about 300 m south of the station. The traffic count on this road has not been estimated, but a qualified guess is that roughly 500 vehicles pass on this road every day on average.

Figure 10: Hallahus field site with surroundings. Photo: Marcin Jackowicz Korczyński.

3.2 Instrumental equipment

3.2.1 Mobile measurement setup

The mobile measurement equipment system that was used in the Lagrangian experiments was built and tested in the Aerosol Laboratory at Ingvar Kamprad Design Center (IKDC) in Lund. The potential hazards of the project were evaluated in the risk analysis document that can be found in Appendix 1.

The system (Figures 11 and 12) was installed in a car with a large luggage compartment and relatively large space for passengers in the backseats, and secured with rope ties in case of an accident. The entire system was supported with electricity from a power station in the luggage compartment.

Air was drawn into the car via the inlet system with rain protection outside the backseat window with a flow rate of 4.0 l/min. The particles above 1 µm diameter could have been subject to size-dependent particle losses through the

inlet system, although these losses will be characterized only after the end of this diploma work. The air was transported further through a mixing volume chamber of about 1 L volume, where potential fluctuations of aerosol concentrations were smoothened, and then to the box containing the Scanning Mobility Particle Sizer (SMPS) and sensor node system in the backseat.

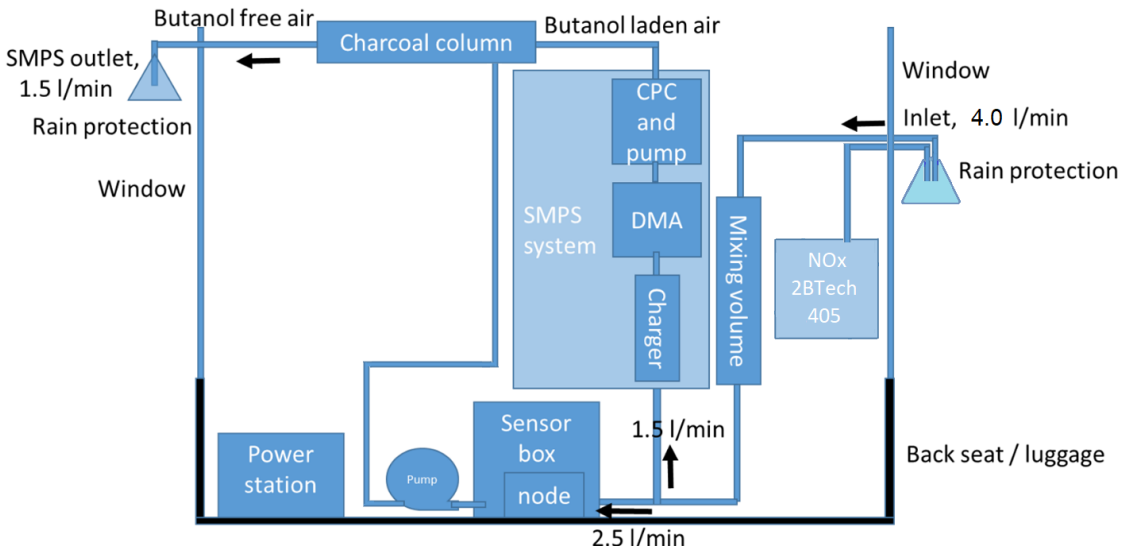

Figure 11: Principal drawing of the equipment used in the Lagrangian mobile experiments and flow rates in tubing lines.

After the mixing chamber, the flow was split into two parts. One part of the flow, with 1.5 L/min, went to the SMPS for the measurements of the particle number size distribution. The other part, with 2.5 l/min, was drawn through the sensor box containing an AirNode sensor, capable of measuring CO_2, NO_2, O_3, temperature, relative humidity, and $PM_{2.5}$ and PM_{10} mass concentrations with an optical counter.

The condensation particle counter (CPC) of the SMPS contained the pump that suctioned the air through the SMPS system. The exhaust air from the CPC contained butanol, hence it had to be cleaned with a column containing baked charcoal. The exhaust air from the charcoal column was transported outside through the opposite placed backseat window of the car. Conversely, air was drawn through the sensor box with a commercial mini pump with a flow rate of 2.5 l/min regulated with a needle valve. Although the air passing through the sensor box was not health hazardous, the outlet of the mini pump was connected to the charcoal column to eliminate part of the noise inside the car.

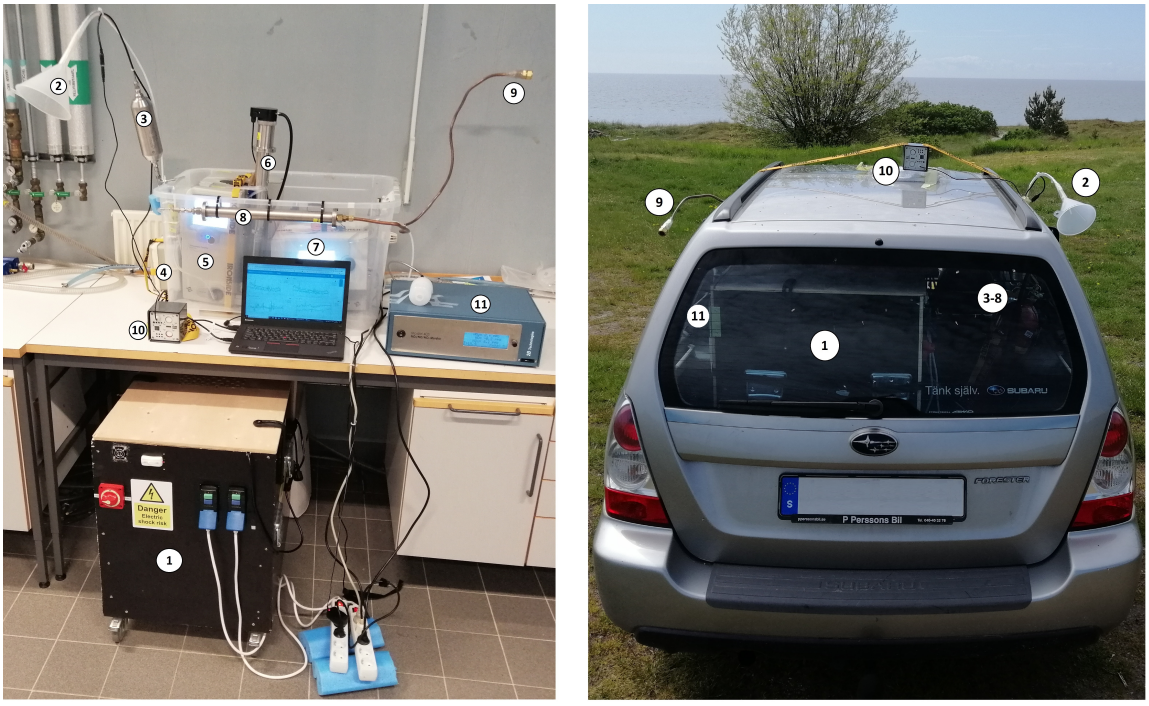

Figure 12: Mobile measurement system used in the Lagrangian experiments. Photos: Adrian Reyes.

Apart from the sensor node in the box, an additional AirNode sensor node was placed directly on the roof of the car used in the mobile Lagrangian experiments. Since the sensor node operates with a built-in fan drawing air through the system, no pump or inlet system was needed for the node on the roof. By using this second node, it was possible to compare their performance and estimate the losses in the inlet tubing affecting the indoor sensor.

3.2.2 Power station

The instruments were powered by a portable power station that allowed uninterrupted operation for at least 10 hours. Having an independent power supply for the instruments with electrical batteries in the car allowed measuring with the engine off, avoiding self-contamination. Since the available options in the Swedish market were limited, a battery box was designed and home-built out of several components (Figure 13).

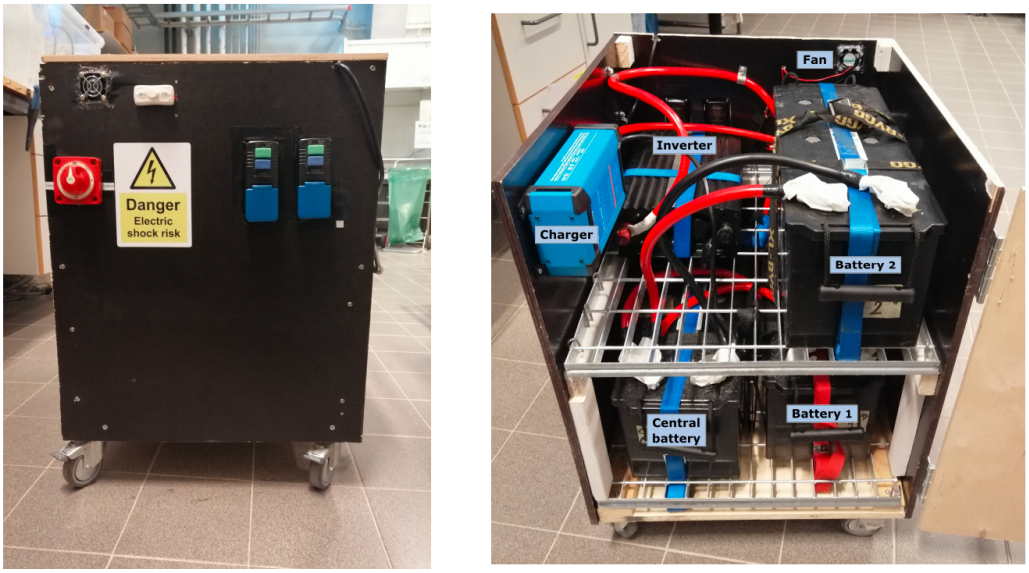

Figure 13: Exterior and interior of power station. Photos: Adrian Reyes.

The power supply consisted of three gel 12 V batteries of 120 Ah capacity each, connected in parallel, and a 1500 W inverter that transformed the 12 V direct current to 230 V pure sine wave alternating current. The three batteries were charged at the same time with a charger that was permanently installed inside the box. A switch change over allowed alternating between the use of the charger and inverter. The connections between the different elements are presented in Figure 14.

Since working with powerful batteries implies a high risk of electrical shock and fire hazard, extra precautions were implemented to build the battery box safely. The electrical circuit was discussed with several electrical experts and laboratory safety responsible persons, and the building of the station did not start without a seal of approval. After the system was built, an electricity expert ex-

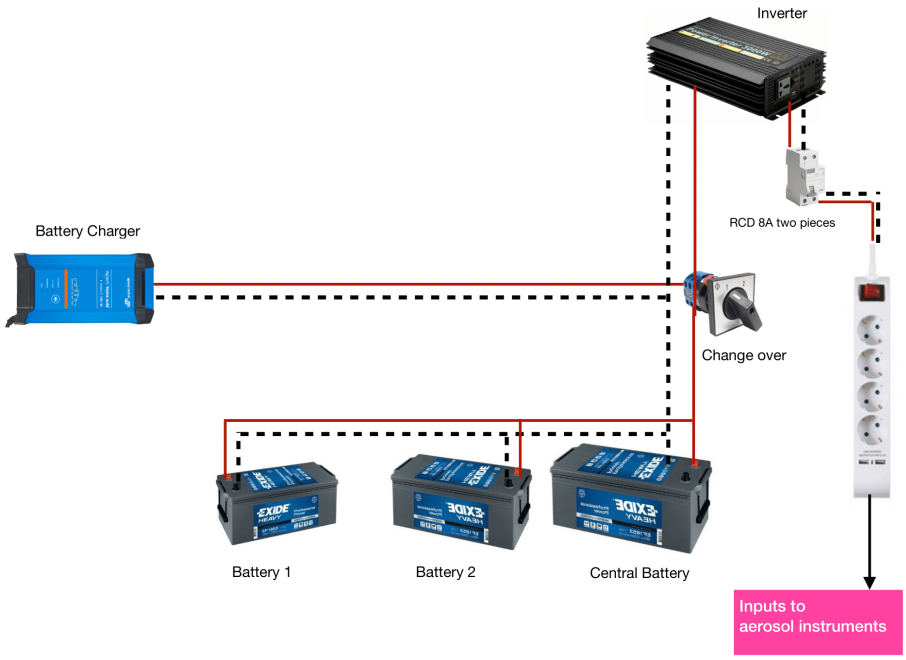

Figure 14: Circuit diagram of the power station.

amined the system one more time to confirm its safety before the first test in the field.

All the elements were arranged to allow for operation without opening the box, to avoid an accidental electric shock. Three danger signs were placed on the outside of the box to discourage untrained personnel from handling the system. The enclosure was non-conductive and the battery poles were covered with isolation tape. Residual current devices (RCD) were connected to the inverter outlets to stop the current in case of electrical shock or faulty instruments.

In order to avoid overheating, holes were drilled on the door and top surface, and a fan provided air circulation in the box. The batteries rested on two metal grids that allowed air to flow below and above them. The fan was always on when the batteries were powering the instruments.

However, when charging batteries, even more cooling was necessary to minimize risk of overheating and fire. For this, the box lid and door were opened. An extra warning sign was placed beside the power station to discourage people from handling the batteries while the top lid was open.

3.2.3 Scanning Mobility Particle Sizer (SMPS)

The main instrument of the system was the Scanning Mobility Particle Sizer (SMPS, TSI 3080 system). The SMPS measured the particle number size distribution concentration in the range of 9.3 - 437 nm electrical mobility diameter. The main components of the instrument are the bipolar charger, the differential mobility analyzer (DMA) and the condensation particle counter (CPC).

The particles pass at first through a radioactive source charger that applies a known charge distribution as a function of size. Then, the particles pass further through the DMA, where they are deflected towards the oppositely charged inner rod (Figure 15). Particles with an appropriate size and charge manage to pass by a narrow slit at the end of the flow tube in the DMA. By adjusting the voltage of the inner rod, it is possible to choose which electrical mobility diameter is allowed to pass through the narrow slit. These particles are later passing through the CPC, which counts the number of particles as a function of the selected size. Hence, by varying voltage, it is possible to measure a particle number size distribution.

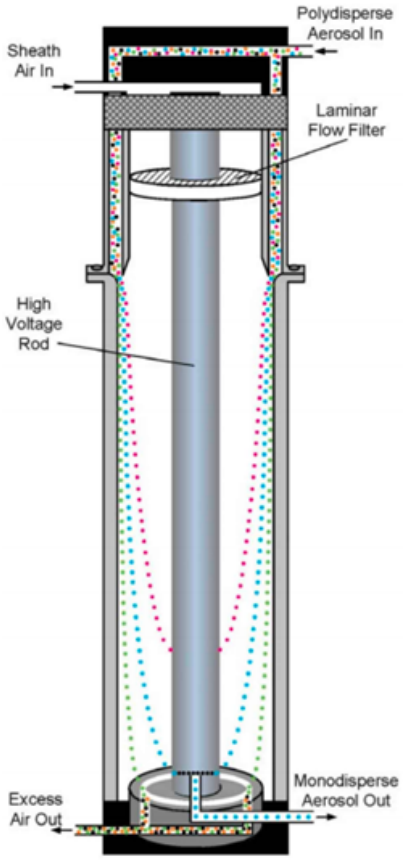

Figure 15: Principal drawing of a Differential Mobility Analyzer (DMA). From TSI ©.

The bipolar charger could contain different types of radioactive sources emitting beta radiation. In the current experiment, a homemade cylinder with a ^{85}Kr source was used. The particles exiting the charger are charged with a known bipolar charge distribution according to Table 1.

The charged particles of different sizes (polydisperse) contained in the aerosol flow enter the DMA model 3081. The DMA has a laminar and particle-free sheath flow pushing the collected polydisperse aerosol particles through the DMA column faster than the aerosol flow would allow by itself. This gives better flow conditions and size resolution of the DMA. The DMA has a positive voltage on the inner rod that makes the negatively charged particles with the

Table 1: Bipolar charge distribution of particles as a function of size and charge around atmospheric pressure and room temperature. From [37].

	$f(N)$ (%)					$\frac{f_s(N)}{f(N)} - 1$ (%)				
D_p(nm)	−2	−1	0	1	2	−2	−1	0	1	2
1	0	0.47	99.09	0.44	0	—	1.9	0.8	1.9	—
1.3	0	0.58	98.88	0.54	0	—	−1.1	−0.8	−1.3	—
2	0	0.85	98.38	0.77	0	—	−2.5	−1.0	−2.4	—
3	0	1.27	97.62	1.11	0	—	−1.3	0	−0.8	—
5	0	2.21	95.92	1.86	0	—	1.8	1.1	1.7	—
7	0	3.28	94.03	2.69	0	—	2.6	1.0	2.3	—
10	0	5.03	90.96	4.02	0	—	2.2	0.3	1.9	—
13	0	6.87	87.73	5.40	0	—	1.1	−0.4	0.8	—
20	0.02	11.14	80.29	8.54	0.01	0.3	−1.7	−1.2	−1.6	1.0
30	0.17	16.35	71.03	12.35	0.10	−1.0	−3.5	−1.0	−3.2	−3.3
50	1.13	22.94	58.10	17.20	0.63	1.3	−3.0	0.1	−2.6	4.1
70	2.80	26.02	49.99	19.53	1.57	0.2	−1.1	0.7	0.7	0.8
100	5.67	27.42	42.36	20.75	3.24	−0.7	1.6	0.6	1.6	−1.9
130	8.21	27.30	37.32	20.85	4.77	−0.5	3.1	0.3	2.5	−1.9
200	12.18	25.54	29.96	19.65	7.21	0.1	3.0	−0.1	2.5	0.1
300	14.56	22.71	24.16	17.51	8.65	0.5	0.7	−0.3	0.6	2.1
500	15.09	18.60	18.28	14.33	8.95	0.1	−3.0	−0.3	−2.6	0.5
700	14.29	15.94	15.15	12.27	8.46	−0.5	−3.1	−0.1	−2.8	−1.9
1000	12.86	13.33	12.36	10.24	7.59	0.2	2.8	0.3	2.5	0.7

right size escape through the slit in the monodisperse aerosol out flow depicted in Figure 15. The particles that do not have the appropriate size and charge might escape with the excess sheath airflow or impact on the inner rod or outer wall.

By adjusting the voltage, aerosol flow and sheath flow, different sizes can be selected to pass through the narrow slit. The electrical mobility of the particles (Zp) in the DMA for each voltage setting depends on the number of charges on the particles and the air drag force acting on them, which in turn depend on the particle diameter and the air viscosity as:

$$Z_p = \frac{n \cdot e \cdot C_c}{3\pi \cdot \eta \cdot D_p} \tag{2}$$

where n is the number of charges, e is the elementary charge, C_c is the Cunningham slip correction factor, η is the air viscosity and D_p is the particle diameter [38]. The exact electrical mobility of the particles in the DMA exiting the slit is a function of the properties of the DMA, and can be related to Equation 2 as:

$$Z_p = \frac{Q_{sh} \cdot ln(\frac{r_1}{r_2})}{2\pi \cdot V \cdot L} \tag{3}$$

where Q_{sh} is the sheath flow, V is the voltage applied to the central electrode, L

is the length and r_1 and r_2 are the inner and outer radius of the DMA respectively. This equation is valid when the sheath and excess flows are equal.

Since the slit is not infinitesimally narrow and the air trajectory path of the particles is not exactly defined, the selected particle mobility has a certain width given by:

$$\Delta Z_p = 2 \cdot \frac{Q_a}{Q_{sh}} \cdot Z_p \tag{4}$$

where Q_a is the aerosol flow entering the DMA [38]. Equation 4 shows that a decrease of the aerosol to sheath flow ratio gives a better size resolution. For the last case study of this project, the selected flows were 1.5 L/min for the aerosol flow and 7.5 L/min for the sheath flow, providing a 1/5 ratio. Equation 3 also shows that a short DMA with low voltages applied is more suitable for smaller particles.

After the DMA, the almost monodisperse particles are counted by the CPC, in this case, the TSI model 3775. When passing through the CPC, the aerosol is exposed to air saturated with butanol vapour. In the next step, the air is cooled down in a condenser, where butanol condenses on the particles making them grow into droplets and can be measured with a laser and photodetector. The photodetector sends an impulse signal to a computer for each detected particle, and the number concentration can thereby be estimated. The CPC has a lower size detection limit due to the difficulty of growing the smallest particles fast enough to larger sizes detectable by the photodetector. For safety reasons, no butanol was supplied to the CPC during the measuring campaigns in this project, which did not seem to be a problem for a car ride of, at least, 10 hours.

Ideally, each mobility diameter, D_p would correspond exactly to a certain voltage and sheath flow rate. However, the final size distribution has to take into account the width of the transfer function (Equation 4) and the charging probability of singly charged particles. Another problem arises from doubly charged particles of larger sizes passing through the narrow slit, being counted as smaller particles. In addition, with decreasing size, Brownian diffusional losses of particles increase, and there is a certain collection efficiency of the CPC as a function of particle diameter. The final size distribution has to be corrected to take these artefacts into account [38].

The operation of the SMPS is based on continuously ramping the voltage of the DMA, which entails other issues in the calculation of the size distribution, since the voltage between DMA and CPC is changing while the aerosol particles are passing through the instruments. The time that the particles take since they leave

the DMA until they reach the CPC is called plumbing time, and it can affect the measurement of the particle size. Additionally, the average residence time of the particles in the CPC, defined as smearing time, can make the particles that enter the CPC at the same time be smeared out over several size bins. The plumbing and smearing effects are more significant for faster changes in voltages, and they have to be taken into account in the calculation of the final size distribution [39]. For the measurements in this Lagrangian experiment, a time resolution of three minutes was used for each size distribution voltage scan.

3.2.4 AirNode sensors

The monitoring system was equipped with two AirNode sensors that measured PM values, gases and meteorological parameters. The sensors are compact, low-powered and low-cost, and they provide real-time data for PM_{10}, $PM_{2.5}$, nitrogen dioxide (NO_2), ozone (O_3), carbon dioxide (CO_2), temperature (T) and relative humidity (RH) with 1-minute resolution. The monitored gases are involved in some of the chemical processes that contribute to particle formation and evolution such as oxidation, condensation and evaporation, and changing cloud droplet chemistry after cloud formation. Therefore, the sensors data were expected to help explain the changes in particle size distribution measured by the SMPS, by providing information about the atmospheric processes that might have happened in the air masses that were followed in the Lagrangian measurements.

The AirNode sensors were provided by the company AirLabs, based in Copenhagen [40] (Figure 16). Calibration of the sensors in AirLabs laboratories was planned before the beginning of the measurements but, due to the regulations in Denmark, Sweden and Lund University during the COVID-19 pandemic, it was not possible to travel to Copenhagen for these matters. Only a preliminary testing phase was performed during this diploma work, which should be enough for the experiment since, according to the manufacturer, the sensor node is delivered calibrated [41]. A more accurate calibration in AirLabs laboratories is still planned after the culmination of this diploma work, with the idea of using the sensors, together with the rest of the equipment, for further projects that have been introduced in the section *Future research*.

Two AirNode sensors were used during the measurements to compare their performance and obtain more accurate results. The first sensor was placed in a sealed box with air pumped from the outside. The second sensor was installed on the roof of the car, protected by an enclosure that made it rain and solar shielded. The sensors needed to be plugged in the power outlets of the battery box by a USB

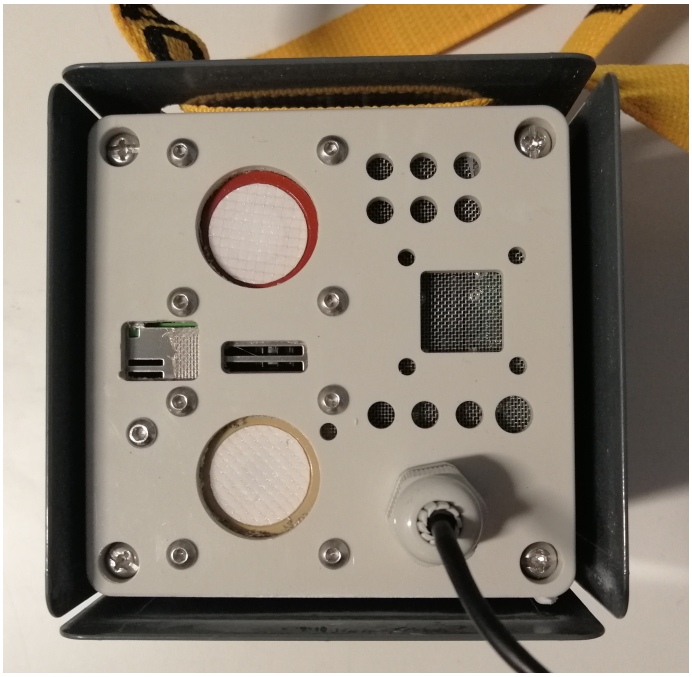

Figure 16: Exterior of AirNode sensor. Photo: Adrian Reyes.

cable, and they were connected to the Internet by a WiFi mobile hotspot provided by a mobile phone. The data could be seen in real time from a computer, and they were saved online (Figure 17).

The AirNode contains multiple sensors in a compact format that facilitates local monitoring with relatively short response time and low power requirements [42]. The PM sensors detect particles by light scattering, determining particle density distribution by analyzing the intensity distribution patterns produced when particles scatter a laser beam [43]. Continuous flow is kept through the sensor by a built-in fan. The NO_2 and ozone measurements are made by an amperometric electrochemical gas sensor that contains four electrodes working under the principle of electrochemistry [44]. CO_2 is measured by non-dispersive infrared spectroscopy [45], integrating the temperature and relative humidity sensors in the same module [46].

3.2.5 NOx 2BTech 405 monitor

The Model 405 nm NOx Monitor is designed for the direct measurement of atmospheric nitrogen dioxide (NO_2), nitric oxide (NO) and total reactive oxides of

Figure 17: Dashboard of the AirNode sensors, data from the second case study of the aerosol-chase project.

nitrogen (NOx = NO + NO_2) in the concentration range 0-10 ppm for NO_2 and 0-2 ppm for NO with high precision and accuracy. In this instrument, NO_2 is measured directly by absorbance at 405 nm while NO is measured by selective conversion using the highly selective reaction of NO with ozone. Total NOx is obtained by the addition of NO and NO_2 (From Ubitech ©).

3.3 Route planning and execution of experiments

The measurements for this pilot Lagrangian project consisted of three case studies where an air mass was followed for 5 or 6 hours measuring particle size distribution and atmospheric chemistry at several measurement spots with one hour difference. To achieve this, it was necessary to perform a prediction of the wind trajectory and design a route that allowed following the air mass path, choosing spots far away from strong local sources to measure a representative sample of the

air mass. The details of this process and description of the measuring campaigns are described in this section.

3.3.1 Construction of trajectories

To ensure that the same air mass is followed through the entire experiment in each Lagrangian case study, an attempt was made to predict the movement of the mixing boundary layer (MBL) of the atmosphere. It is within the MBL, at ground level that new emissions along the air mass path are taking place. After several minutes downwind of the emissions, the emitted compounds in the MBL should distribute almost evenly in the entire MBL due to turbulent vertical mixing. Hence, by measuring further away from local emission hot spots during the Lagrangian case studies, the measured concentrations represented the well-mixed concentration of the mixing layer. It was assumed that half the MBL height represented the average movement of the entire MBL. Half the MBL height could be calculated with forecast trajectory data, in this project, with the National Oceanic and Atmospheric Administration (NOAA) Air Resources Laboratory's (ARL) Hybrid Single-Particle Lagrangian Integrated Trajectory model (HYSPLIT) [47].

HYSPLIT is one of the most broadly used atmospheric transport and dispersion models, allowing the computation of air parcel trajectories while studying complex transport, dispersion, chemical transformation, and deposition simulations [47]. For the measuring campaigns of this Lagrangian project, forward trajectories were calculated with HYSPLIT to predict the path that an air mass would follow during its journey over the continental area where the measurements were performed. The forward forecast trajectories were run with the starting position of half of the MBL height. Since the forward trajectory might have deviated from this height after some time, a new forward trajectory was made for each hour to adjust to half the MBL height. To increase the accuracy of the prediction, the trajectories were calculated a few hours before the beginning of the measurements with the latest HYSPLIT forecast available. Introducing these data in MATLAB allowed plotting the wind trajectory and visualize other important meteorological parameters along the Lagrangian path for the campaigns (Figure 18).

Since wind speed and direction is significantly different at different heights within the MBL, following the winds at half the MBL height, does not represent exactly the movement of the entire MBL. In other words, there is intrusion of air from other horizontal wind directions and differences in wind speed at different heights along the followed air mass path. In addition, there is also intrusion of air from above the MBL.

(a) An example of a horizontal Lagrangian air mass trajectory path.

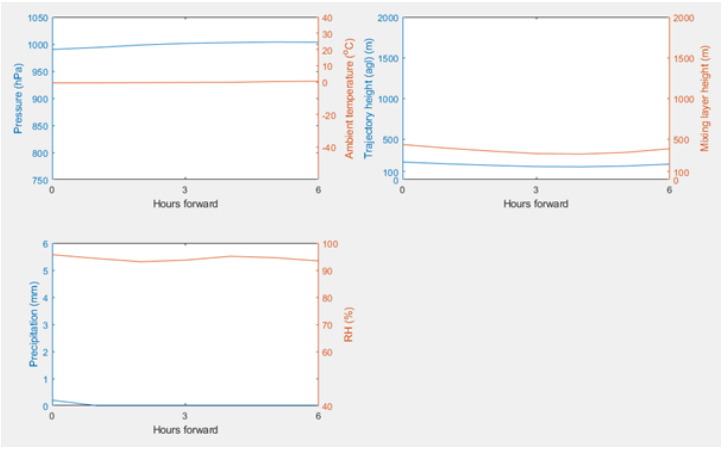

(b) Values of temperature and pressure, mixing layer and trajectory height and precipitation per hour along the Lagrangian air mass path.

Figure 18: MATLAB plots obtained with HYSPLIT data.

Hence, in reality, observing new emissions along the air mass path and the particle processes acting on the particles would require measuring winds and aerosols at additional heights and horizontal locations, different from the chosen ones. Following the average MBL movement is an approximation and compromise. A campaign with observations made at different locations and different heights would not be feasible. Nevertheless, the wind distributions can be modelled using 3D trajectories from the FLEXPART model [48], and intrusion with air from above can be simulated by knowing the height dependent pressure, temperature and wind structure as a function of height. In addition, when performing Lagrangian modelling, several different heights and horizontal locations can be simulated.

Since the horizontal and vertical resolution of winds in the HYSPLIT model is on the order of tens of kilometres, and the meteorological HYSPLIT forecast is uncertain, the forecast trajectory also needs to be compared to the trajectory created from meteorological observations in retrospect. However, this was out of the scope of the current study, which was more focused on the possibility to make a trajectory path forecast and to see if it was possible to follow the predicted path

with a car and to measure at the same time.

3.3.2 Route planning

Several measurement spots were selected for the measurements along the HYSPLIT wind trajectories, like the one pictured in Figure 18a. The purpose of choosing measurement spots instead of having continuous measurements was to avoid pollution from road vehicles on the same road and to measure with the car engine off to avoid self-contamination. In addition, measuring for several minutes on each spot allowed averaging noisy data. Since the sampled air mass should have been representative of a well-mixed MBL without peak concentrations due to local emission sources, the spots were located far away from strong local sources such as towns or highways. When there was a road close to the selected area, the measurement spot was chosen to be upwind of the road.

The separation between each spot along the Lagrangian path was one hour. This also made the planning easier, since HYSPLIT data is presented for each hour. Although the wind follows an almost straight trajectory, the roads between different spots have different lengths and speed limits, which should be considered when planning the route. In reality, it was necessary to arrive at each spot a few minutes earlier than the trajectory arrival, and to leave the spot a few minutes later. Otherwise, it would not have been possible to stay for a certain time at each spot. The duration of measurements at each spot is governed by the wind speed. At a wind speed higher than roughly 13 m/s it is not possible to find the time to stay at each measurement spot, since this wind speed is close to the average speed of the car.

The total duration of the measuring campaigns was limited by geographical and human constraints. Road vehicles can only follow the air mass while it travels over land, hence the measurements had to be restrained to the area between shorelines. However, human limitations were more important for this experiment, since having only one person driving for too many hours could result in tiredness and distractions that could jeopardise safety. The battery life of the power station could also be a limitation for longer campaigns, although this was not a problem for this pilot experiment where the batteries were supporting the instruments for, at least, ten hours without interruptions.

Taking this limitation into consideration, a route of five to seven hours with six to eight measurement spots was designed, counting on the extra driving time that was required to reach the first measurement spot and come back to the laboratory from the last spot. For the campaigns where geographical limitations were not af-

fecting the duration of the measurements, the final number of measurement spots was decided on the run, and was dependent on the tiredness of the driver. The route for the three case studies was chosen to pass near Hyltemossa and Hallahus field stations for a comparison of the results.

3.3.3 Measuring campaigns

The instrumental equipment was arranged for efficient use of the available space in the car and to secure all the elements to avoid accidents and malfunction of the instruments. The distribution of the different components was modified through the different campaigns, with the aim of loading the car in the fastest way while shortening the tubes of the inlet system to minimize particle losses. The distribution and procedures described in this section correspond to the latest case study, which integrates the knowledge obtained from the two first case studies.

The power station was placed in the boot of the car with the help of a forklift, since the box had a weight of 140 kilograms. The SMPS and CPC were attached to the bottom of a plastic box that would allow securing the instruments to the backseats while protecting tubes and cables from being broken or compressed. The mixing chamber, sensor box, sensor pump and charcoal column were attached to the SMPS box, as can be seen in Figure 12, minimising the length of the inlet system while allowing a fast load of the car. This box was placed on the backseats next to one of the windows with the inlet tube and rain protection facing the outside. The outlet tube connected to the charcoal column was taken out of the opposite window. The NOx 2BTech 405 monitor, only introduced in the second case study, was placed on the backseat next to the SMPS box. The outside sensor was placed on the roof of the car, secured with long straps. Swedish safety regulations required that a fire extinguisher was carried in the boot of the car, and a document showing there was a radioactive source in the car in the form of the charger was carried in the glove compartment.

In the original plan of this pilot project, two people should have been in the car at all times during the execution of the measurements, with the intention of having one person who would only focus on driving while the other one could oversee the performance of the instruments and analyse the preliminary data, having the possibility to switch roles after some hours of driving. However, the regulations in Lund University during the COVID-19 pandemic did not allow to follow this plan, and the measurements were performed by one person that was keeping permanent contact with the other one by text and phone calls during the measuring stops. This change of plans did not only shorten the duration of the measure-

ments, as explained before, but it also made it harder to solve the issues that arose during the campaigns, leading to limitations in the data and significant delays in project execution.

Although only one person was allowed to be in the car during the measurements, two people were needed to install the equipment in the car before the start of the campaigns, mainly because of the weight of some of the components. While the driver was travelling to the first measurement spot, a new wind trajectory was calculated by the other person, slightly modifying the original route to have a more accurate approximation of the air mass path. The driver arrived at the first measurement spot a few minutes before the established beginning of the measurements, and both would discuss the duration of the measurement times at each spot based on the conditions of the new wind forecast.

The subsequent measurement spots were reached by following their coordinates with a GPS, although several of them had to be slightly modified because of being located in private properties that could not be seen when planning the route. Nevertheless, all spots that were selected were far away from local pollution sources or upwind of roads. For each spot, the characteristics of the area were noted for future analysis, noting the character of the location and taking a photograph of the car (Figure 19). The performance of the instruments was checked in a computer placed in the passenger seat next to the driver, and the SMPS and sensors data would occasionally be sent to the researcher at home, who would perform a comparison with Hyltemossa and Hallahus field stations for preliminary validation.

Before the three case studies were conducted, a test campaign was performed to assess the performance of the instruments and the potential difficulties of the measurements. The results of this campaign, shown in the following chapter, helped to improve the system and discover flaws in the original plan. However, for every new measurement, new issues arose and new knowledge was gained, refining the system after every campaign and improving the experiments. The lessons learned from this campaign should be of value for other future Lagrangian experiments.

Figure 19: The car with the mobile monitoring system at the different measurement spots during the test campaign (4th of March, 2021), first case study (23rd of March, 2021), second case study (21st of April 2021) and third case study (24th of May 2021). Photos: Adrian Reyes.

4 Results and Discussion

The following sections show the results from the test campaign and the three case studies of this pilot Lagrangian project. Each section corresponds to a measuring campaign with a specified Lagrangian route plan. The mobile monitoring system provided information about particle size distribution and atmospheric chemistry, and the data were compared with measurements at the permanent field stations Hyltemossa and Hallahus.

The SMPS instrument provided data for particle size distribution and total concentrations for particle number and mass. The particle size distributions covered a range of particle diameters from 9.30 nm to 437 nm. These data were com-

pared to the particle size distributions measured in Hyltemossa.

The AirNode sensors measured PM_{10}, $PM_{2.5}$, NO_2, O_3, CO_2 and temperature and humidity. All values from each case study have been presented for the entire duration of the case study. Then, average data from each spot, when the vehicle was stationary, was also plotted, after removing data influenced by local pollution sources. The data was compared to PM values and atmospheric gases measured at Hyltemossa and Hallahus stations. For the third case study, NOX concentrations were also measured with the instrument NOx 2BTech 405.

To the author's knowledge, the three case studies presented in this pilot project are the first reported continental Lagrangian experiments. The inexperience created several problems when performing the experiments, and the lessons learned from these should be useful for other researchers taking on Lagrangian experiments in the future. As shown in *Future research*, this diploma work aims at becoming the beginning of a line of research that will improve with time and gain in complexity.

4.1 Test campaign

The test campaign of this pilot Lagrangian experiment was performed on the 4th of March 2021, with the aim of testing the equipment in the mobile vehicle and find possible limitations in the application of the Lagrangian approach for continental measurements. The SMPS system was placed inside a plastic box attached to the backseat, and only one AirNode sensor was used for the measurements, placed in a sealed box with air pumped in through the inlet system. Several issues arose during the day, which delayed the data collection and required the execution of a new wind trajectory and route. The main issues were the interruption in the aerosol flow in the SMPS and the loss of internet connection at the beginning of the measurements.

The SMPS reported faulty data at the first preliminary measurement spot. This was caused by the instability of the instruments in the box, where the inlet tubing was squeezed because of the vehicle movement. Despite replacing the tube and rearranging the position of the instruments, the issue was only fixed intermittently during the remaining duration of the field test.

The internet connection provided by the mobile hotspot, necessary for the AirNode sensors and the GPS, stopped working shortly after the preliminary fix of the SMPS system. This showed the necessity to secure a stable internet connection and access to unlimited mobile data. During the duration of this issue, the wind direction changed substantially, which required a change of plans for the car

route.

The revised plan meant measuring upwind and downwind of Landskrona, expecting to observe differences in particle size distribution, PM values and atmospheric gases due to Landskrona emissions. The followed route (Figure 20) included three stationary measurement spots to observe the air mass before it crosses Landskrona, immediately after the town, and about ten kilometres downwind of Landskrona. The air mass travelled for approximately half an hour between each spot, allowing to measure for about 10 minutes each time. Two additional measurement spots were planned further downwind of Landskrona, but the experiment was interrupted after the third spot due to the tiredness and stress experienced by the driver that could compromise safety on the road.

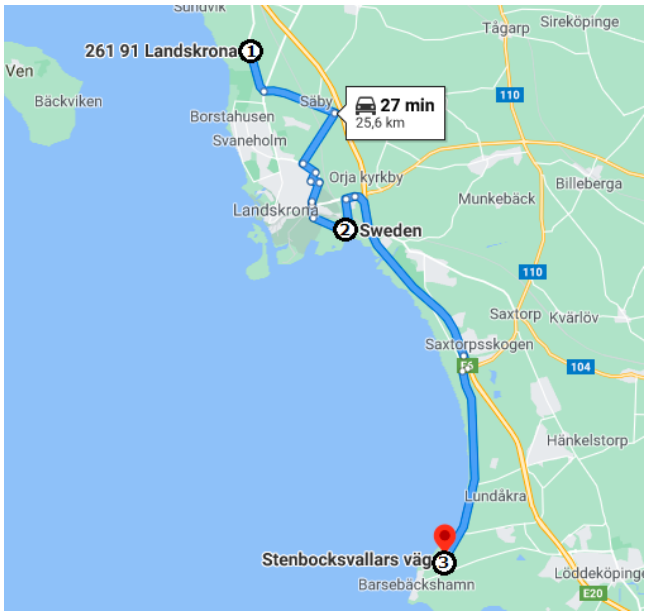

Figure 20: Route for the test campaign of the continental Lagrangian experiment, 4th of March 2021. From Google Maps.

4.1.1 Particle size distribution

Because of the instability of the SMPS instrument inside the box and the problems with the inlet tubing, the particle size distribution data was very limited. Figure 21 shows the data during the period when the SMPS was functioning, during the route from the first to second measurement spot and the time when the car was standing still at Spot 2.

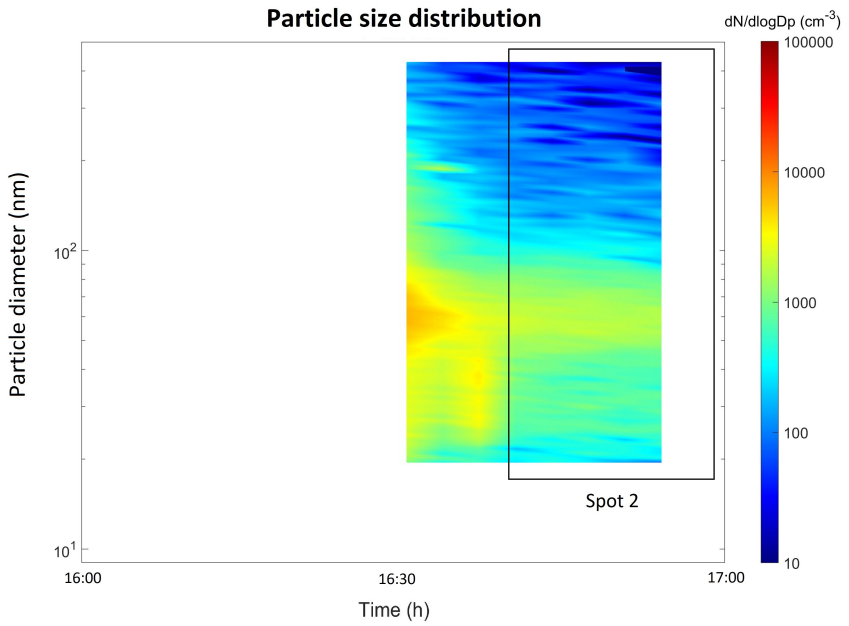

Figure 21: Particle size distribution measured during the test campaign of the continental Lagrangian experiment, 4th of March 2021.

The instrument started measuring when the car was passing close to Landskrona around 16:30, where a high concentration of particles could be seen for all sizes, with the highest peak concentrations between 50 and 80 nm diameter. The high concentration of particles reflected emissions from the town and the highway where the car was travelling. While going away from the town at around 16:40, the particle concentration seemed to decrease, although there was a mode of particles below 50 nm that lingered on for some time. This pattern suggests that the mode of 50-80 nm corresponded to emissions from Landskrona while the smaller particles came from the cars on the road along the route.

When Spot 2 was reached shortly after 16:40, and the car engine was turned off, the particle modes below 50 nm, and between 50 and 80 nm remained, but the concentration decreased further. A comparison of the particle size distribution in Spot 1 with the distribution in Spot 2 could not be made due to missing data from Spot 1, but it would have enabled the estimation of the contribution to pollution from emissions in Landskrona.

Such limited data did not allow to determine the reliability of the results, but the observations of the particle size distribution suggested that it was possible to apply the Lagrangian approach in this kind of continental measurements. Sig-

nificant differences could be observed from the measurements on the road and the data obtained at the measurement spot, which motivates why measurements are not valid with the moving vehicle. The size distribution observed in Spot 2 seemed relatively stable from the beginning until the end of the measuring period.

4.1.2 Sensors analysis

After the issues with the Internet connection were solved, the AirNode sensors were functioning for the rest of the campaign. Figure 22 represents the values of PM_{10} and $PM_{2.5}$ mass concentrations between Spots 1 and 3. The difference between the average values in Spot 1 and Spot 2 revealed a remarkable contribution of the emissions in Landskrona to the PM concentrations. The concentration values at Spot 2 and 3 were similar within the statistical uncertainty of the instrument, indicating that there were no additional significant source emissions downwind of Landskrona. The continuous measurements showed high concentrations during driving, reflecting the emissions from the road. The PM_{10} concentration was systematically higher than $PM_{2.5}$ indicating that there were also coarse mode particles present in this air mass between 2.5 µm and 10 µm diameter.

The reliability of the NO_2 and ozone values showed in Figure 23 was unknown, since the inlet system might have caused losses that could not be assessed with a single sensor. However, the increase in NO_2 between Spot 2 and Spot 3 might have reflected the influence of the E6 highway and was realistic, since NO_2 is a compound commonly produced during vehicle exhaust emissions. The increase in NO_2 concentrations when driving between Spots 2 and 3 would support this hypothesis.

Ozone is consumed by the reaction with NO within tens of meters downwind of car exhaust emissions of NO. However, the ozone concentration increased when driving on the highway between Spots 2 and 3 instead of decreasing. The reason for this is unknown, but it might be that measurements were not reliable during driving. The NO_2 measurements were potentially not trustworthy either during driving.

The continuous measurements of CO_2 in Figure 24 showed a decrease of the values towards background levels during the measurement spots in contrast to the values measured while driving. This is an indicator of the absence of strong local sources when measuring at the spots, which is preferred since the data should not be affected by the influence of local combustion pollution. Although CO_2 values were not relevant for chemical reactions, the observations from this test cam-

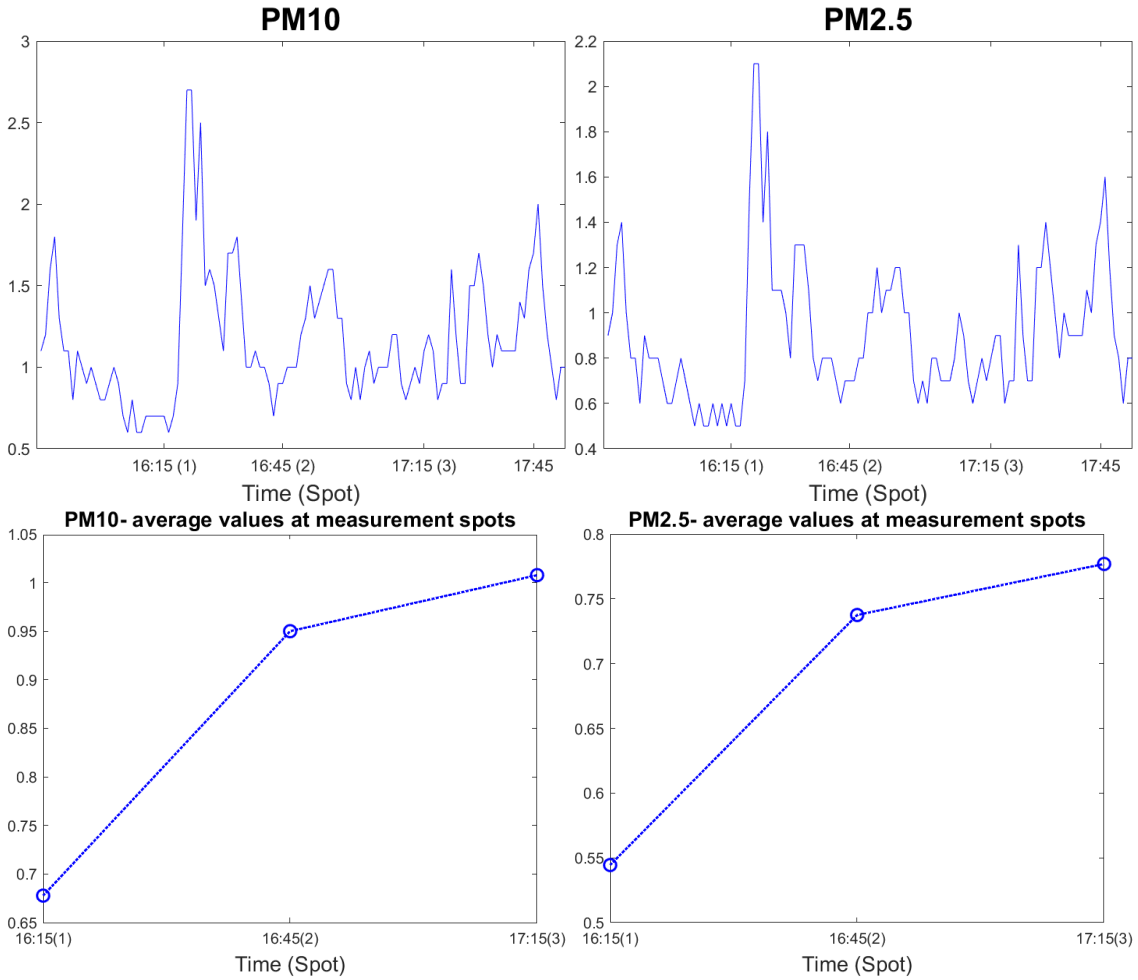

Figure 22: PM_{10} and $PM_{2.5}$ mass concentrations during the test campaign, 4th of March 2021. Continuous measurements in upper panel and average measured concentrations at the spots with stationary vehicle in the bottom panel.

paign showed that the CO_2 measurements could be used to investigate potential influence from local pollution at the spots.

The temperature and relative humidity values in Figure 24 did not show reliable results and therefore were not used further in the study. Although it was expected that the inlet system would warm and dry the air before reaching the sensor box, this effect could not explain the 15 to 20 C difference with respect to the real temperature. Likely, the temperature reported by the AirNode reflected

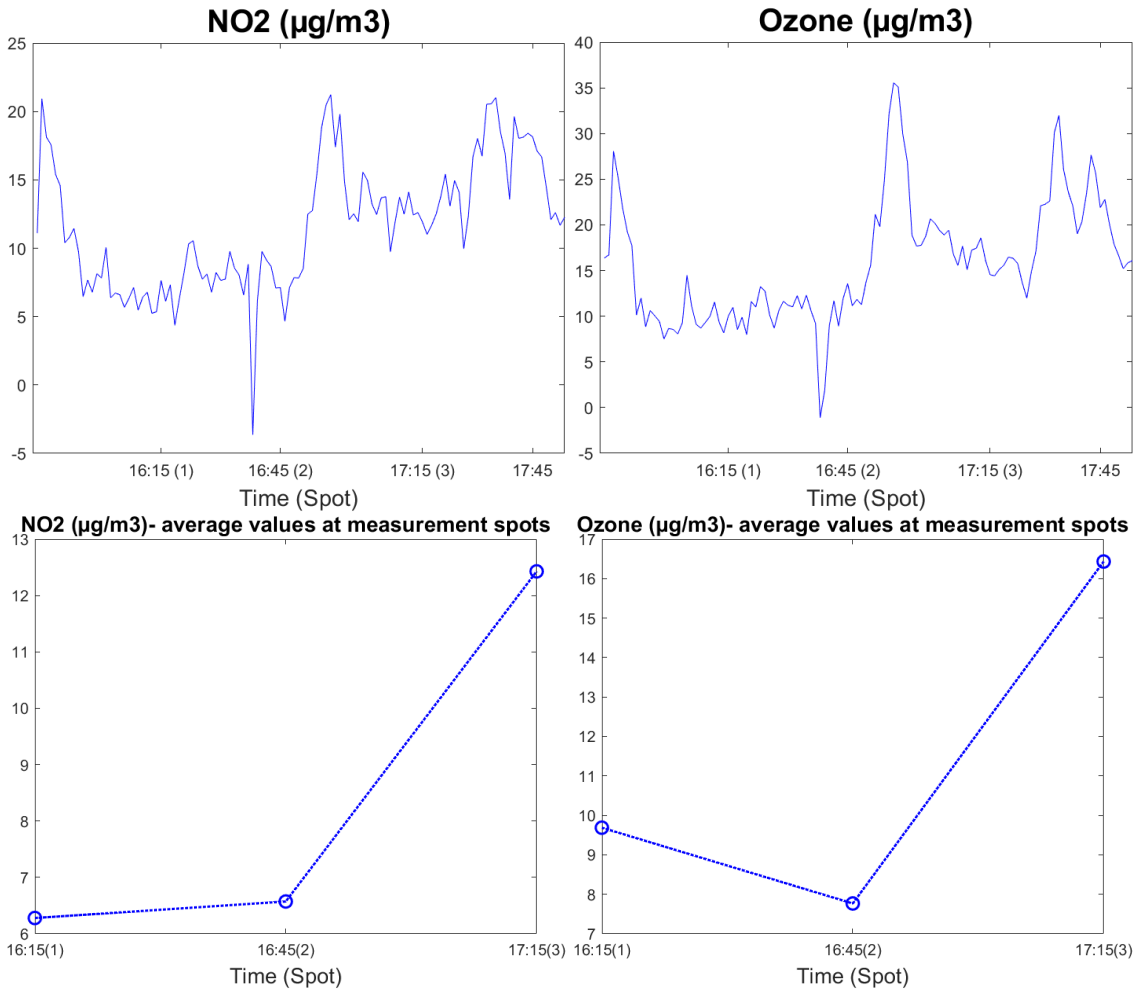

Figure 23: Nitrogen dioxide and ozone concentrations during the test campaign, 4th of March 2021. Continuous measurements in upper panel and average measured concentrations at the spots with stationary vehicle in the bottom panel.

more the internal temperature of the sensors rather than the air temperature in the tubing.

Because of the difficulty to estimate the statistical and systematic errors affecting the AirNode sensors, no error bars were presented for the sensor graphs of the test campaign nor the three case studies. A fine calibration of the sensors and a detailed analysis of the results would be needed to calculate the errors in the data, which was not within the scope of this diploma work.

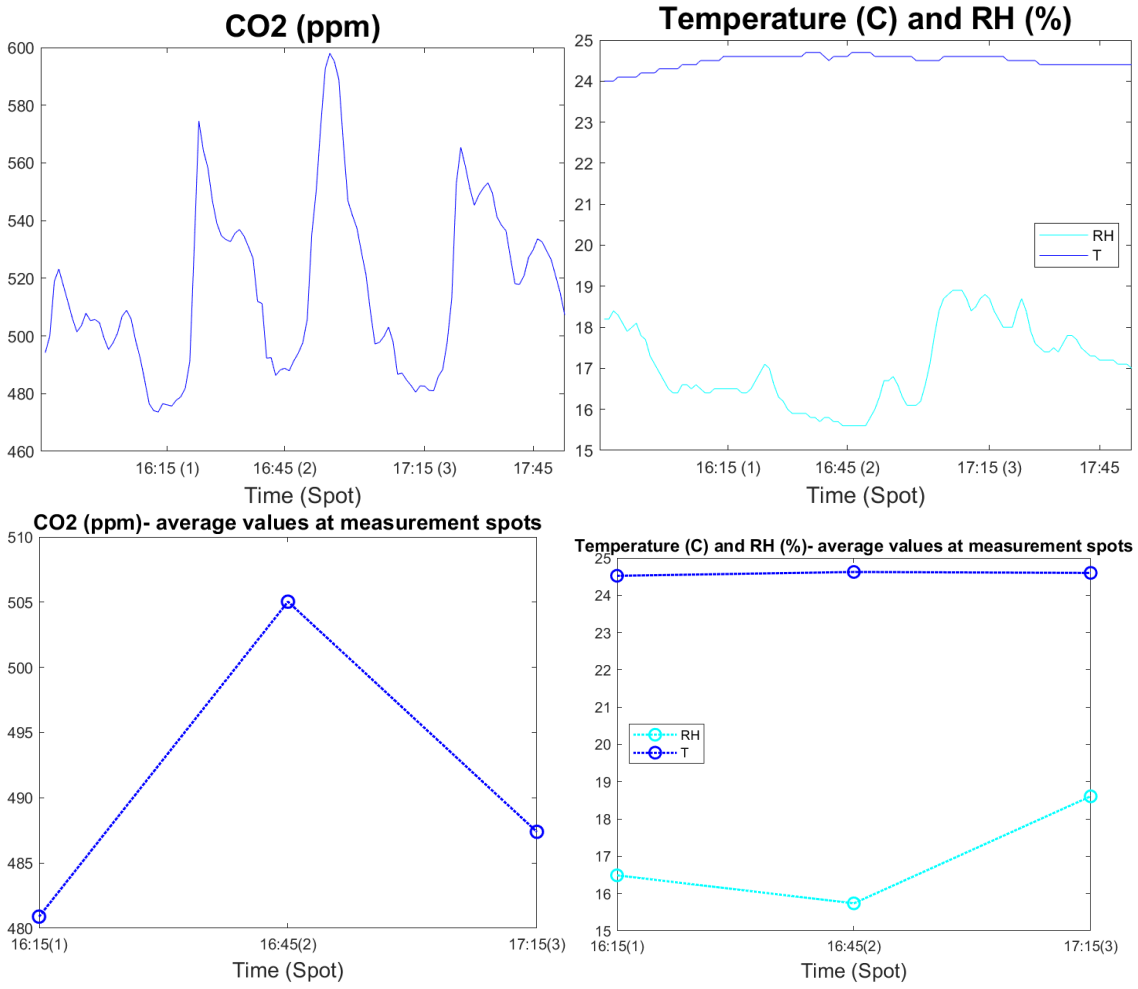

Figure 24: Carbon dioxide concentration and temperature and relative humidity during the test campaign, 4th of March 2021. Continuous measurements in upper panel and average measured concentrations at the spots with stationary vehicle in the bottom panel.

4.1.3 Limitations and improvements

The issues arising during the test campaign provided valuable knowledge about the application of the Lagrangian approach to continental measurements and the performance of the equipment in a mobile vehicle. Before the first real case study, several improvements were applied to the system to overcome the difficulties encountered during the measurements and prevent incidents and setbacks. Other

modifications were applied to the system to facilitate the load of the car before the measurements, and different procedures were established for the following campaigns, for example, purchasing 24 hours of unlimited internet data before the start of the measurements to avoid another connection loss.

The SMPS and CPC were attached to the plastic box by screwing the legs of the instruments to the bottom, which made the equipment immovable despite the movement of the car, and ensured that the inlet tubes would not be squeezed or broken. Additional holes were drilled on the box to attach the charcoal column and sensors pump to the plastic box, providing more stability and a faster load. A plastic wedge was built to flatten the backseats surface under the box to avoid tilting of the instruments.

The sensor box was sealed with silicone and the joints in the inlet system that connected the tubes to the mixing chamber and instruments were replaced and secured to reduce leakages in the system. Several tests were performed in the laboratory to compare the flow after and before the inlet system, obtaining negligible differences before the following measuring campaign. Additionally, the location of the sensor box in the car was moved from the floor to the rack placed behind the backseats to shorten the inlet tubes and minimize losses in particles and gases.

Despite reducing leakages in the system, the sensor in the sealed box could not provide reliable results by itself, due to the losses in the inlet tubes and the lack of proper calibration. For this reason, the company AirLabs supplied a second AirNode sensor node for the following campaigns, which was installed outside the car very close to the inlet with the rain protector. The combination of the two sensor nodes allowed comparing the behaviour with and without the inlet system and increased the trustworthiness of the results.

For the following campaigns, validation with the field stations of Hyltemossa and Hallahus was planned. This could not be done for the test campaign due to the change in the itinerary and the lack of sufficient data for particle size distribution. However, since the purpose of these measurements was testing the equipment in the experimental setup and checking the feasibility of the plan, the comparison of the results with the fixed stations was not required to achieve the goal of the campaign.

4.2 First case study

The first case study of the car-chase Lagrangian experiment took place on the 23rd of March 2021. An air mass path was followed for six hours from the north of Helsingborg to the northwest of Kristianstad (Figure 25). The wind speed was

around 4-5 m/s at half of the mixing layer height from west to east. The route included seven measurement spots separated by one hour and 15 km distance. Due to the low wind speed, relatively longer stops were possible of about 20-30 minutes, which provided more stable averaged measurement values at each stop.

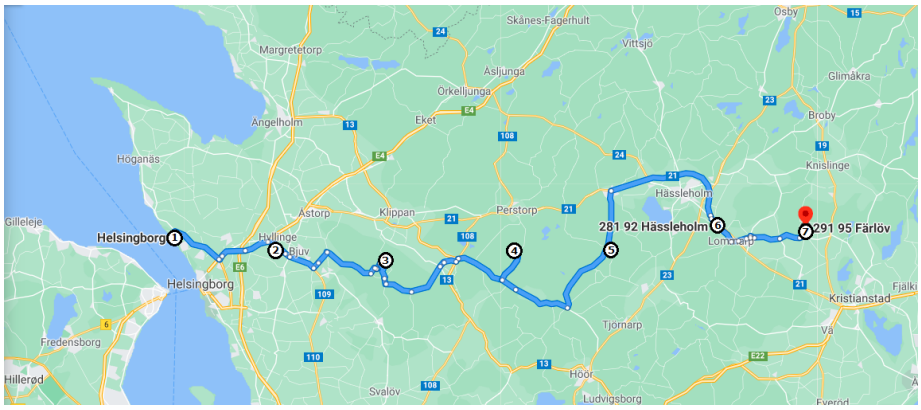

Figure 25: Route for the first case study of the continental Lagrangian experiment, 23rd of March 2021. From Google Maps.

4.2.1 Particle size distribution

The particle size distribution measured during the first case study of the continental Lagrangian experiment is shown in Figure 26. The bottom panel shows the total number concentration of particles and the total $PM_{0.45}$ mass concentration, calculated by integrating the number concentration of all particles smaller than 0.45 µm diameter and transforming to volume and then mass concentration by assuming spherical particles and a density of 1.5 g/cm^3. Due to the different technical issues explained in the section *Limitations and improvements*, only the values for three out of the seven measurement spots could be used for the analysis. The instrument worked and provided coherent results until 13:10, when a power cut switched off the system shortly after departing from the second measurement spot. The instrument resumed working at 15:18, at Spot 4, providing reliable results until 15:36. After that, the SMPS system started reporting problems to detect the DMA and the data could not be used for the study.

Despite the limited data, some conclusions could be drawn. At the first measurement spot, at around 11:30 to 12:00, the particle size distribution contained two particle modes with maximum concentration at around 40 and 180 nm diameter respectively (Figure 27). The 40 nm mode could have had different source

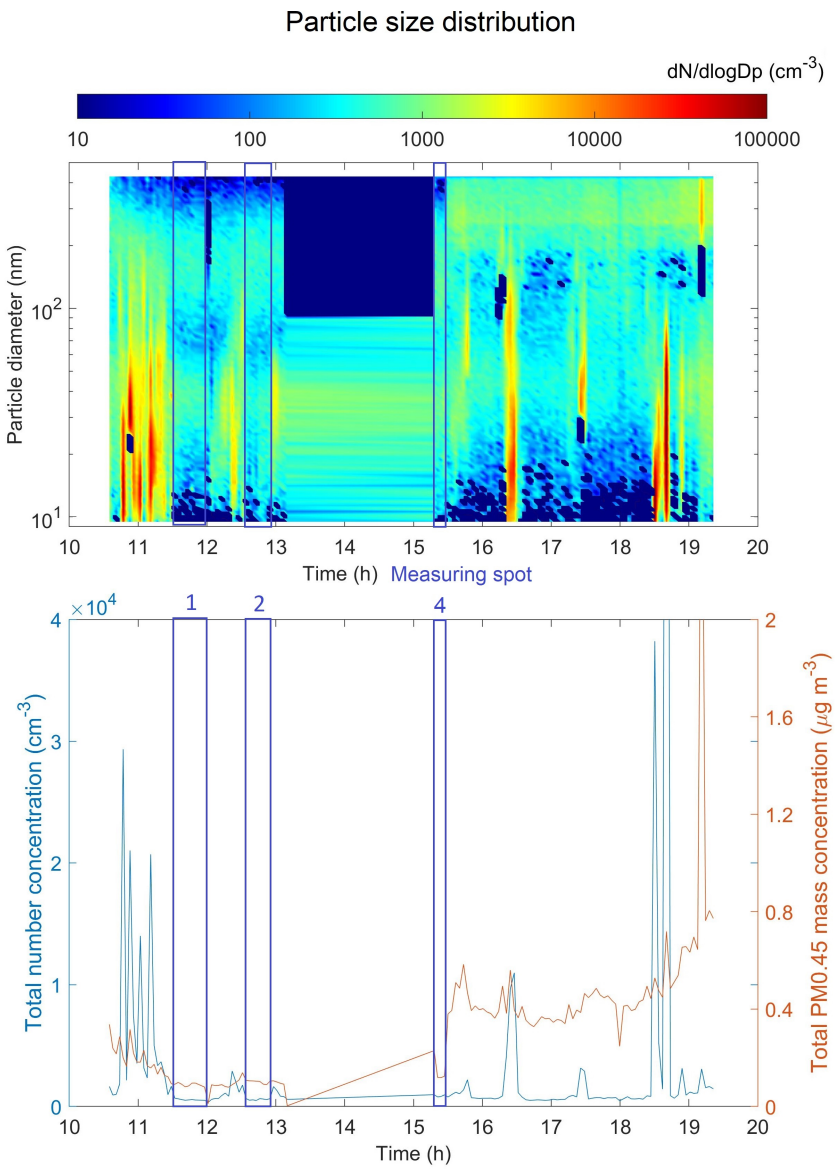

Figure 26: Particle size distribution measured with the SMPS in the car, 1st case study of the continental Lagrangian experiment, 23rd of March 2021.

origins such as Baltic ship emissions or car traffic exhaust at Danish islands from emissions minutes to several hours earlier. The 180 nm mode contained particles generated one to several days before, for example, from Great Britain. A detailed

trajectory analysis that traces the wind direction back in time could confirm the origin of these particles, although such analysis was not within the scope of this diploma work.

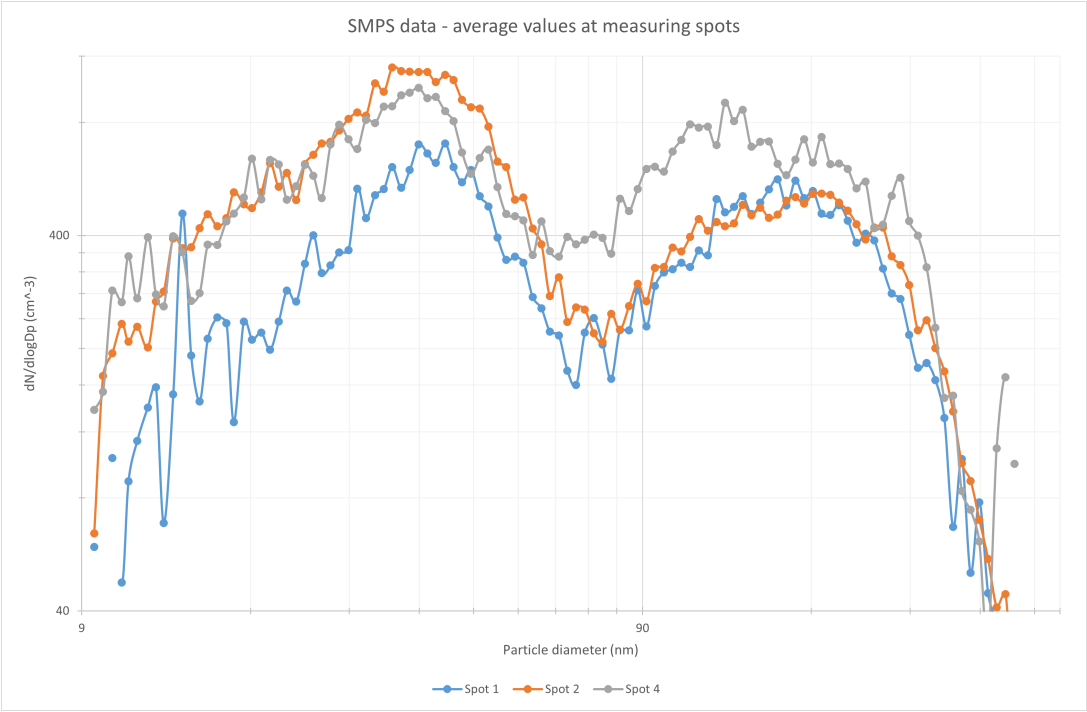

Figure 27: Average values of particle size distribution at the measurement spots, 1st case study of the continental Lagrangian experiment, 23rd of March 2021.

The particle number concentration increased from Spot 1 (12:00) to Spot 2 (13:00), mainly in the 40 nm mode. The increase in the concentration of small particles could be explained by the presence of the highways E-4 and E-6 between Spot 1 and Spot 2, and even by emissions from Helsingborg. While traffic exhaust particles were emitted with diameters around 20 nm at these source areas, the transport time for the emitted particles between Spots 1 and 2 allowed the particles to grow by condensation to diameters around 40 nm before they were measured at Spot 2. Some of the smallest particles in this mode were also likely lost by polydisperse coagulation. Although the particles which were already 40 nm diameter in size were also growing by condensation at the same time, the 40 nm diameter mode did not appear to grow in size any further. This is due to the fact that there have been occasional replenishments of 20 nm diameter particles as

the car passed major highways or towns, which kept the maximum concentration at around 40 nm diameter while it increased the total concentration in this mode.

The increase in concentration in the accumulation mode until Spot 4 showed that intrusion from polluted air masses from other upwind source areas, where these particles were emitted one to a few days before affecting the Lagrangian air mass.

The particle size distribution from Spot 4 was compared to the measurements in Hyltemossa station, located only two kilometres away from this spot. Hyltemossa data showed a total concentration of 500 particles per cubic centimetre, lower than the 800 particles measured by the SMPS in the car. The largest difference could be observed for particles in the range of 30-150 nm diameter. There were no large towns or highways in the vicinity, so local traffic could be discarded as a cause of this deviation. The explanation for this difference could come from the fact that Spot 4 was closer to houses where wood combustion could have been used for heating than Hyltemossa. The SMPS instrument might also have systematically deviated from the Hyltemossa size distribution at this time instance due to instrumental differences between the systems. This instrument intercomparison will be discussed further during the following chapters.

4.2.2 Sensors analysis

While the size distribution data was only valid for three measurement spots, the AirNode sensors inside the sealed box in the car and the non-sealed unit outside were providing data during the entire campaign (Figures 28 - 31). The first thing that could be observed when looking at the graphs is that the values of PM_{10} and $PM_{2.5}$ concentrations correlated with each other for the inside as well as the outside sensor units (Figure 28). The sensors placed in the box detected lower mass concentrations of particles compared to the outside sensors, due to losses in the inlet system.

From the average values measured in the different spots, it could be seen that the values of PM_{10} and $PM_{2.5}$ were almost identical for the sensors in the box and only slightly deviating for the sensors outside. The larger particles in the box were more likely to be removed in the inlet system, hence this was the reason for the almost identical $PM_{2.5}$ and PM_{10} values for the sensor in the sealed box. Since $PM_{2.5}$ and PM_{10} were only slightly deviating from each other in general, it meant that only a small fraction of the particle mass was in the range from 2.5 to 10 µm.

The small increase in PM values measured by the sensors between Spot 1 and the final Spot 7 might have been merely an effect of statistical uncertainty. How-

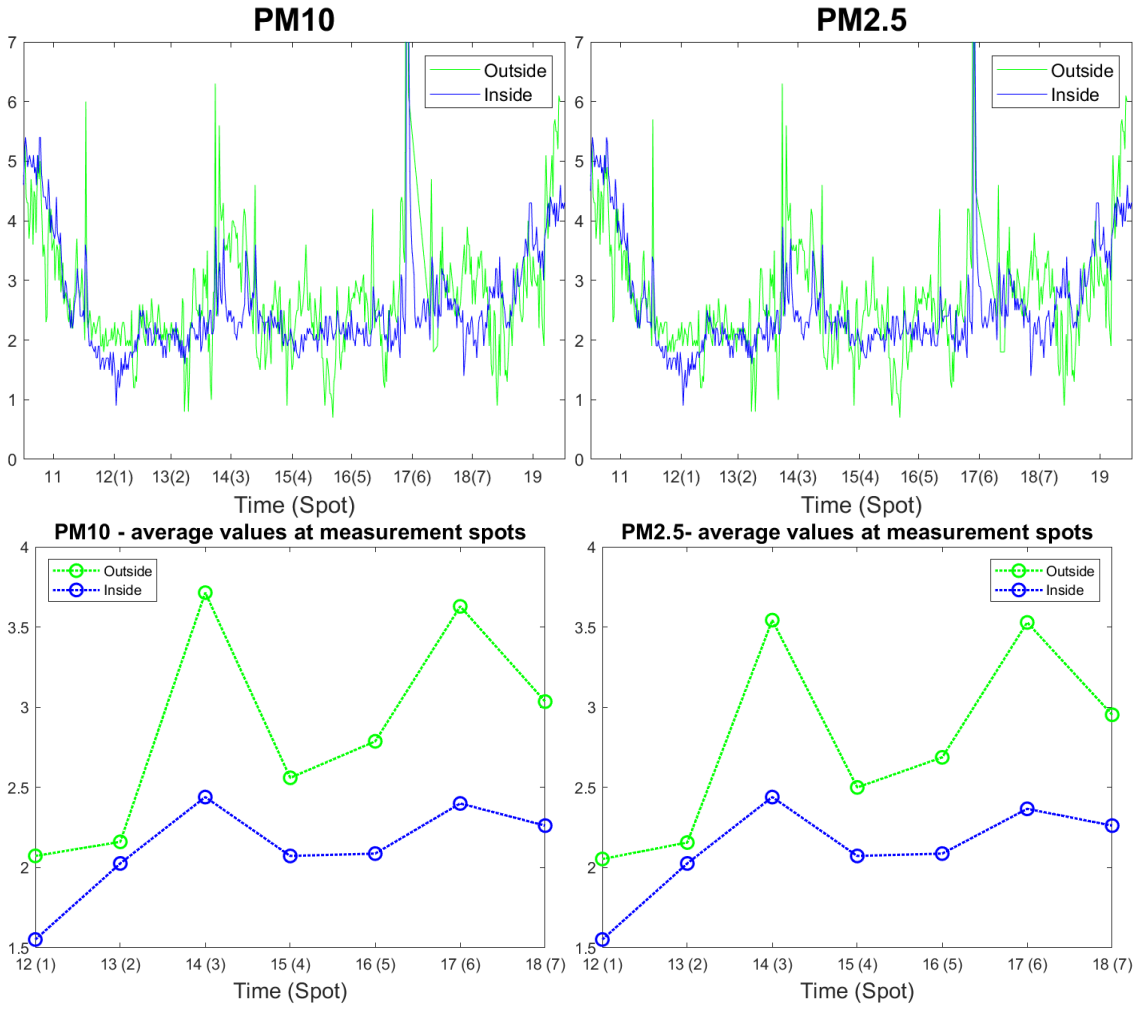

Figure 28: PM_{10} and $PM_{2.5}$ mass concentrations, first case study, 23rd of March 2021.

ever, the increase in accumulation mode particles observed in the SMPS data until Spot 4 makes it likely that the increased PM values were actually true and that it was due to increased accumulation mode concentrations.

During the measurements at Spot 6, a high peak appeared reaching PM_{10} values of 16 $\mu g/m^3$, showing a sudden increase of local generated coarse particles. The peak would have affected the results, as can be seen in Figure 29. Hence, these data with local influence were removed from the calculations before plotting Figure 28. A quarry was observed 800 m away from Spot 6, which could have been

responsible for the local source of coarse particles, generated as wind-borne dust. However, since the quarry was not placed directly upwind of Spot 6 and the wind speed was relatively low, the intermittent source of the large concentrations remained unclear.

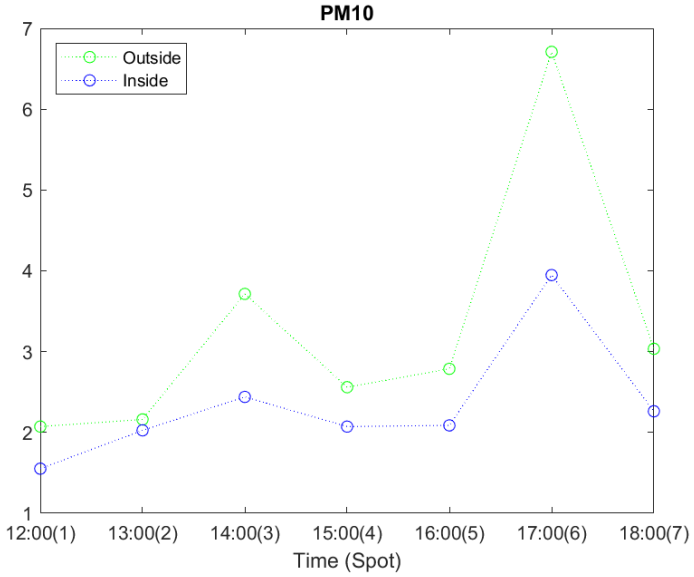

Figure 29: PM_{10} concentration plot before removing peak due to local pollution.

Ozone and nitrogen dioxide data (Figure 30) were difficult to analyse due to the non-quantified losses in the inlet system that affected the sealed sensor node, and the statistical uncertainty affecting the sensors outside. The NO_2 values were very low for the sensor inside, even reaching negative values for the first measurement spot, hence the performance of this sensor in further measurements was evaluated to estimate the reliability of the results. Ozone and nitrogen dioxide seemed to increase from Spot 1 towards the last spot for the outside sensors, which is realistic in the continental boundary layer due to anthropogenic and natural emissions. However, the data were subject to relatively high statistical uncertainty. More analysis of these data is needed with a comparison of data from state-of-the-art instruments in the laboratory to make a dedicated analysis of the performance of the sensors.

The CO_2 values (Figure 31) measured by the sensor in the sealed box were stable for the first six measurement spots, from 464 to 488 ppm, and slightly higher for Spot 7. These values are close to expected background levels, which gave a valuable indication that the measurement spots were not affected by local com-

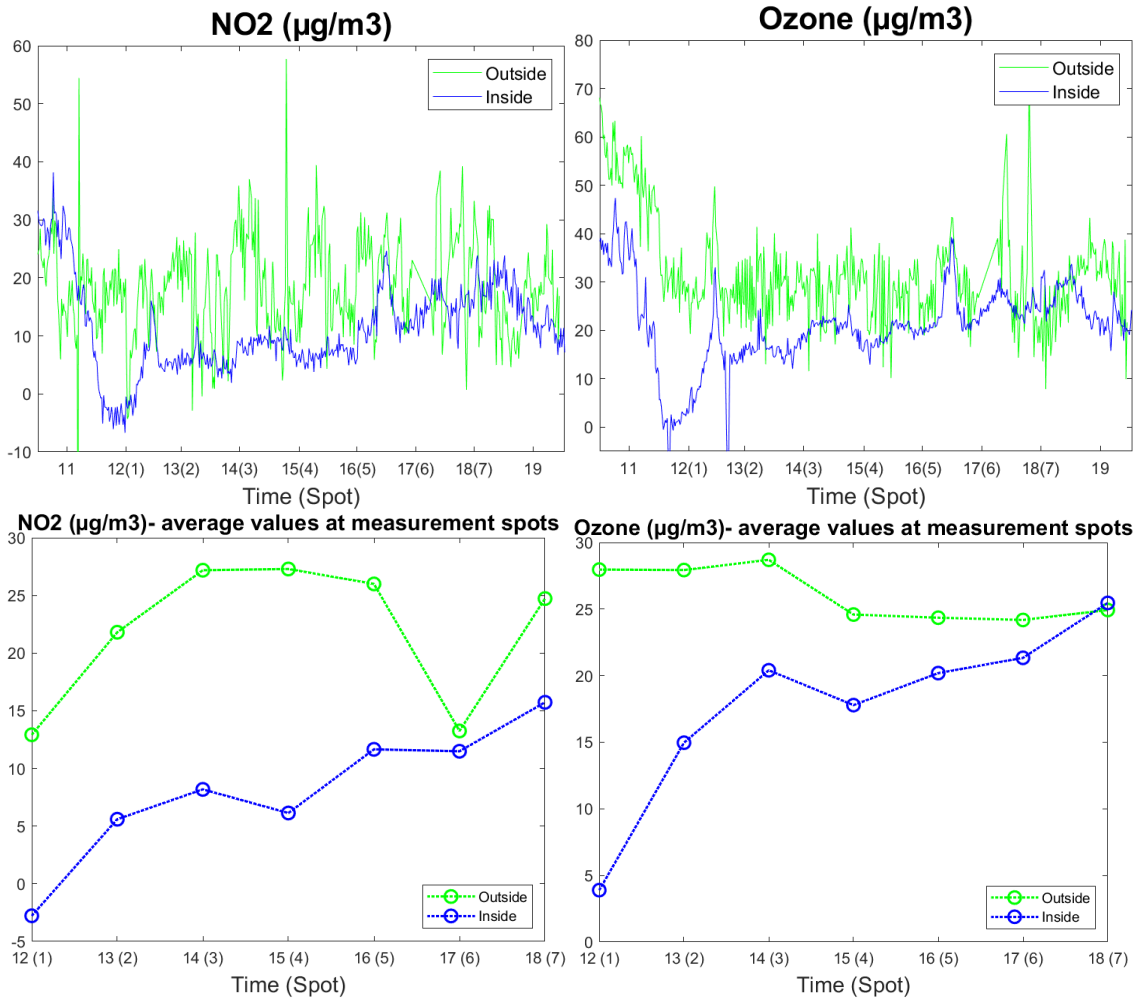

Figure 30: Nitrogen dioxide and ozone concentrations, first case study, 23rd of March 2021.

bustion emissions. However, the CO_2 sensor outside showed too high values that make the measurements unreliable. Since carbon dioxide was not lost in the inlet system, the analysis of the following case studies only used the results from the sensor in the sealed box.

The temperature and relative humidity sensors revealed that the inlet system dried the air that went into the sealed box due to the difference between indoor and outdoor temperatures, giving rather constant values of RH around 21%. For

the sensor outside, the RH varied from 36% to 48%. Regarding the temperature measurements, both sensors showed very high values, reaching 20 C for the sensor outside and 29 C inside, while the real temperatures, according to the car thermometer, were around 6 C.

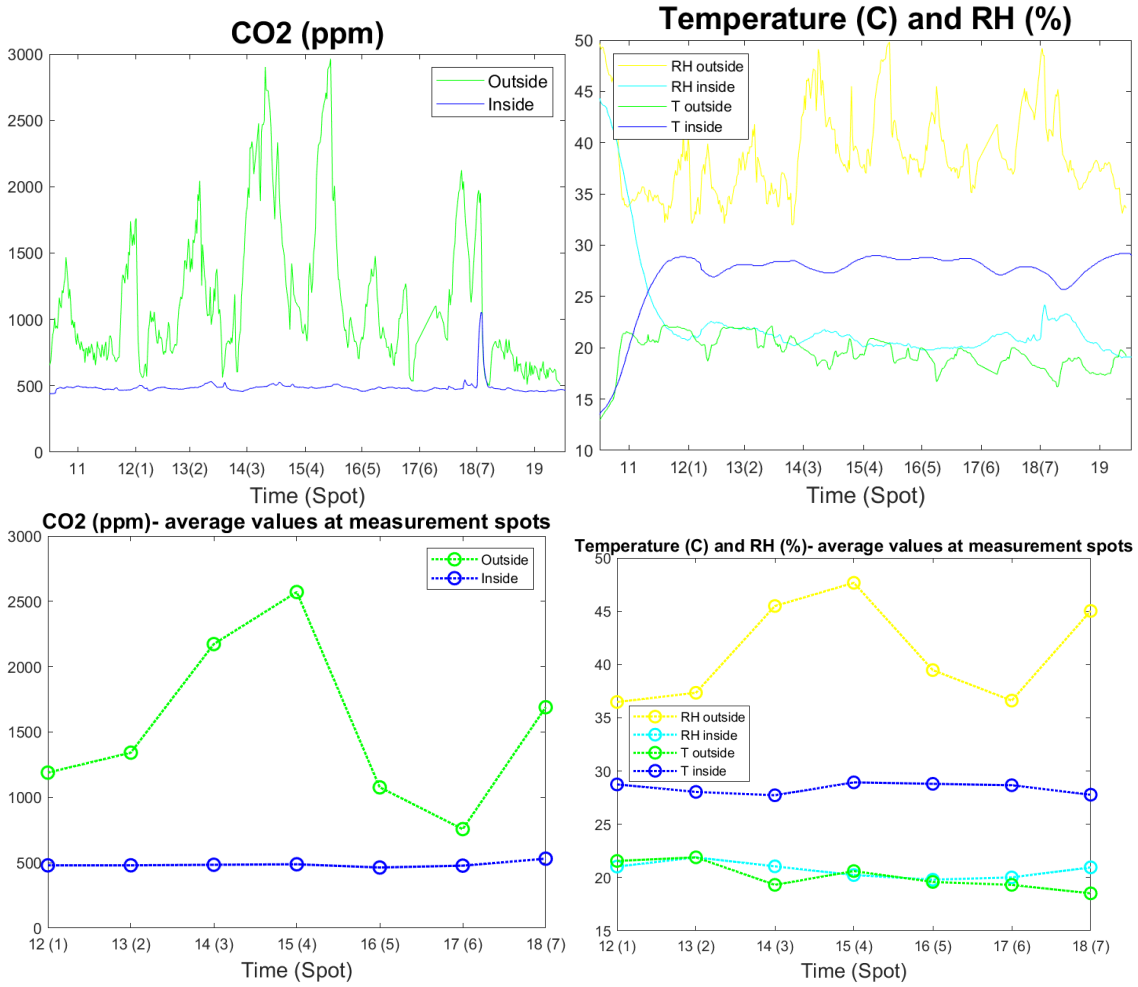

Figure 31: Carbon dioxide concentration and temperature and relative humidity, first case study, 23rd of March 2021.

4.2.3 Limitations and improvements

The problems with the faulty data after Spot 4 was suspected to be caused by the power outages suffered during the performance of the measurements. The power outage in itself would not be a recurrent problem, since it was only due to a loosely connected power cable. Therefore, for future campaigns, the stability of the connections to the power supply was examined after the equipment was installed in the car before the beginning of the measurements.

Nevertheless, the power cuts suffered during the first case study of this continental Lagrangian experiment seemed to initiate additional problems. The particle number size distribution data showed an unusually high concentration of particles larger than 200 nm diameter. The power outage was afterwards simulated in the laboratory, observing that, after restarting the instruments, the SMPS experienced difficulties to detect the DMA, and peaks in large particles were reported for the first one or two scans after the outage. Therefore, the atypical results were attributed to the sudden loss of electricity and they were not expected to be observed in a second Lagrangian case study experiment.

The AirNode sensors showed appropriate agreement with each other for PM values, but the measurements for atmospheric chemistry do not seem to be very reliable. In order to minimize gas and particle losses, the mixing chamber and sensor box were attached to the SMPS box, reducing the length of the inlet tubes while increasing the stability of the system in the car. The outside sensor was moved for future campaigns from the window to the roof of the car to provide better rain protection. To investigate the performance of the NO_2 data, the 2BTech NOx monitor was installed in the car for the second and third case studies.

The forecast of the wind trajectory Lagrangian path created before the measurements could have been substantially different from the real wind speeds and directions, hence, a comparison of the calculated wind path with backwards trajectories from the HYSPLIT trajectory model is planned after this diploma work. Another factor affecting air masses during the case studies was the mixing of air from other horizontal wind directions into the predefined wind path, which might add complexity to the analysis. Additionally, the mixing with air from above the mixing boundary layer is a known factor affecting the mixing layer concentrations, which is not straightforward to consider during the actual experiments. To observe how much other wind directions of air from above the mixing layer were affecting the measurements, a more detailed 3D model, as FLEXPART trajectory model [48], needs to be used with analysed meteorological data in retrospect.

4.3 Second case study

The measurements performed on the 21st of April of 2021 constituted the second Lagrangian experiment of this project and the first one where both the SMPS and AirNode sensors were working without power or internet interruptions. However, the data from the SMPS were still problematic for sizes above 80 nm diameter, as explained in the section *Limitations and improvements*. The 12 m/s wind speed enabled following an air mass for five hours from the Kullen peninsula until the east coast of the Blekinge region (Figure 32). This wind speed was bordering towards a too high wind speed, thus the time to measure on each spot was considerably shorter than during the first case study. An attempt was made to accomplish at least 3 pieces of SMPS size distribution scans, which took 9 minutes in total. Despite the additional stress and tiredness caused by long periods of driving and short active breaks, it was possible to follow the route planning.

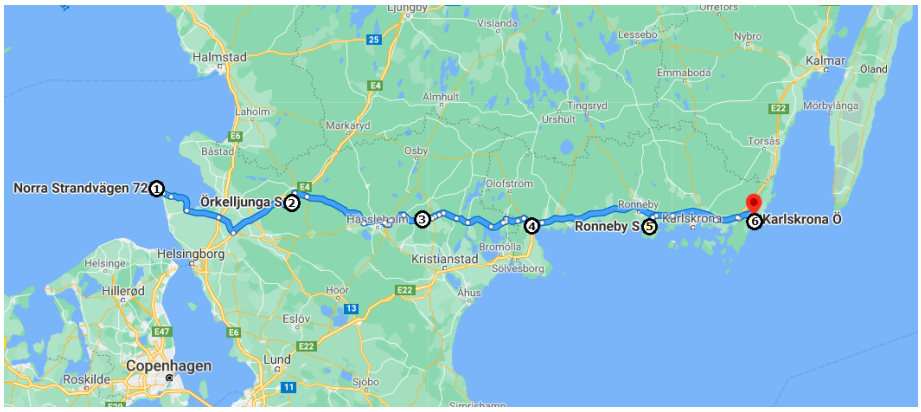

Figure 32: Route for the second case study of the continental Lagrangian experiment, 21st of April 2021. From Google Maps.

4.3.1 Particle size distribution

The particle size distribution and total concentrations measured by the monitoring system for the whole measuring campaign are shown in Figure 33. The SMPS data were compared for validation to the results from the DMPS instrument in Hyltemossa (Figure 34), showing a shift in sizes for particles above 80 nm, as discussed in detail in *Limitations and improvements*. Therefore, the SMPS data for this case study is only shown for particles with diameters smaller than 80 nm. The

$PM_{0.45}$ concentration is not shown either because the calculations were affected by the error in the size distribution above 80 nm diameter.

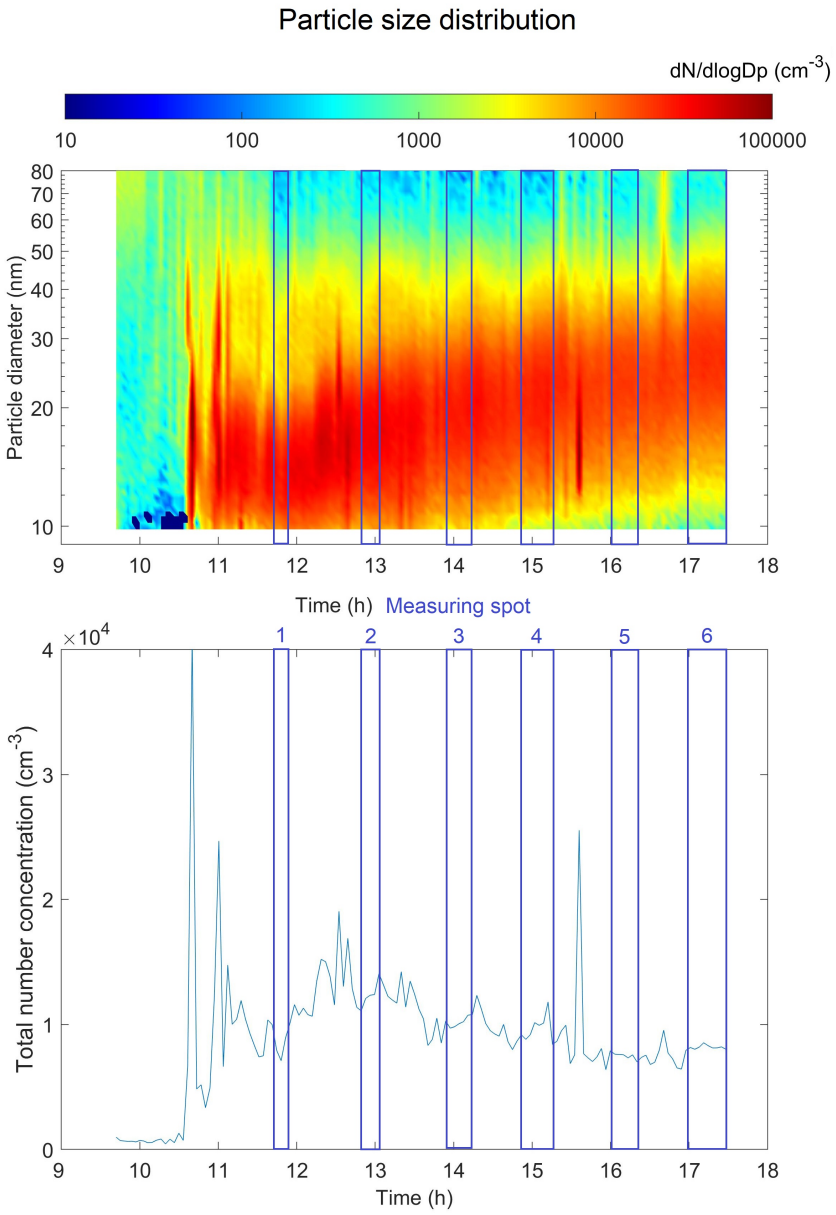

Figure 33: Particle size distribution measured with the SMPS in the car, 2nd case study of the continental Lagrangian experiment, 21st of April 2021.

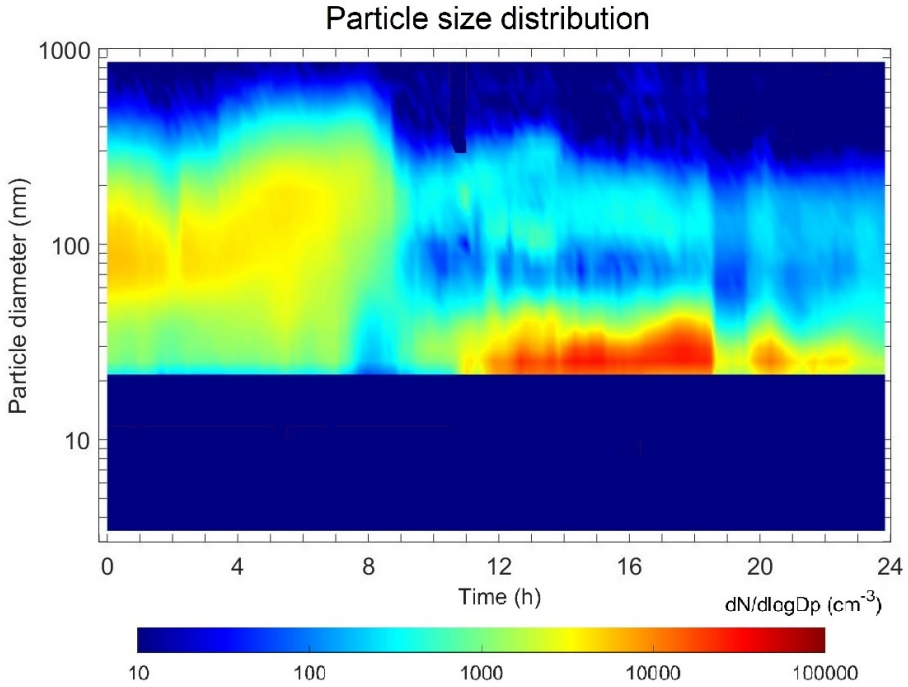

Figure 34: Particle size distribution measured with the DMPS instrument at Hyltemossa, 21st of April 2021. The time is local wintertime, hence one hour shifted compared to the SMPS data.

The earliest SMPS data from the monitoring station in the car was from 9:50, when the car was standing in Lund with the engine off. The Lund data resembled pollution levels close to an urban background station. These data showed close agreement with Hyltemossa for sizes above 200 nm diameter (Figure 35), despite that Hyltemossa and Lund are about 50 km apart. Lund had a higher concentration of particles between 30 and 200 nm. Local car exhaust pollution from Lund likely contributed to these higher concentrations, while the enhanced concentration of Aitken mode particles between 50 to 100 nm diameter approximately was likely caused by pollution from Danish islands and peninsulas. These emitted particles from Denmark likely came from car exhaust, and were grown to Aitken mode sizes due to condensation during the transport between Denmark and Lund. Hyltemossa did not experience the same pollution from populated areas in Denmark, since the air mass over Hyltemossa came from more northerly regions in Denmark. The accumulation mode concentration was similar between Lund and Hyltemossa, presumably because near-regional sources do not influ-

ence the accumulation mode in the Nordic countries to a large extent. These particles were likely originated from transport over longer ranges than Denmark, and were grown by condensation or cloud activation processes to larger sizes during air mass transport for more than one day. However, this relatively high concentration of accumulation mode particles was later not present during the second case-study experiments from Spot 1, at 12:00, until the end of the measurements, as can be seen in Figure 34.

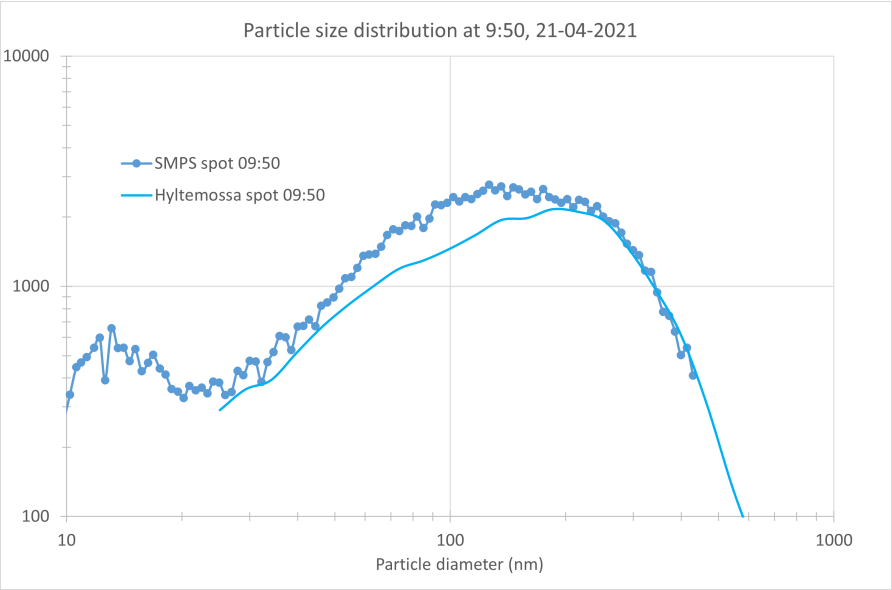

Figure 35: Particle size distribution at 9:50 measured in the car and Hyltemossa. Section of Figure 41.

For the first measurement spot, at 12:00, the particle size distribution measured in the car showed strong new particle formation (Figures 33 and 36). Beneficial conditions for new formation at this time were provided by the decrease of the accumulation mode particles and consequent decline in condensation of gases due to the shift to cleaner air from the North Sea, and the increase in turbulence and mixing with cleaner air from above due to the relatively high solar radiation. New particle formation is normally initiated at around 1 nm particle diameter, but the lowest particle diameter that the SMPS could detect was 9 nm. These particles, which are grown by condensation, are therefore formed a few hours upwind of the measurement spot. The formation was likely initiated over Jutland, Denmark, and possibly over the sea areas surrounding Denmark, such as the North Sea and Kattegat.

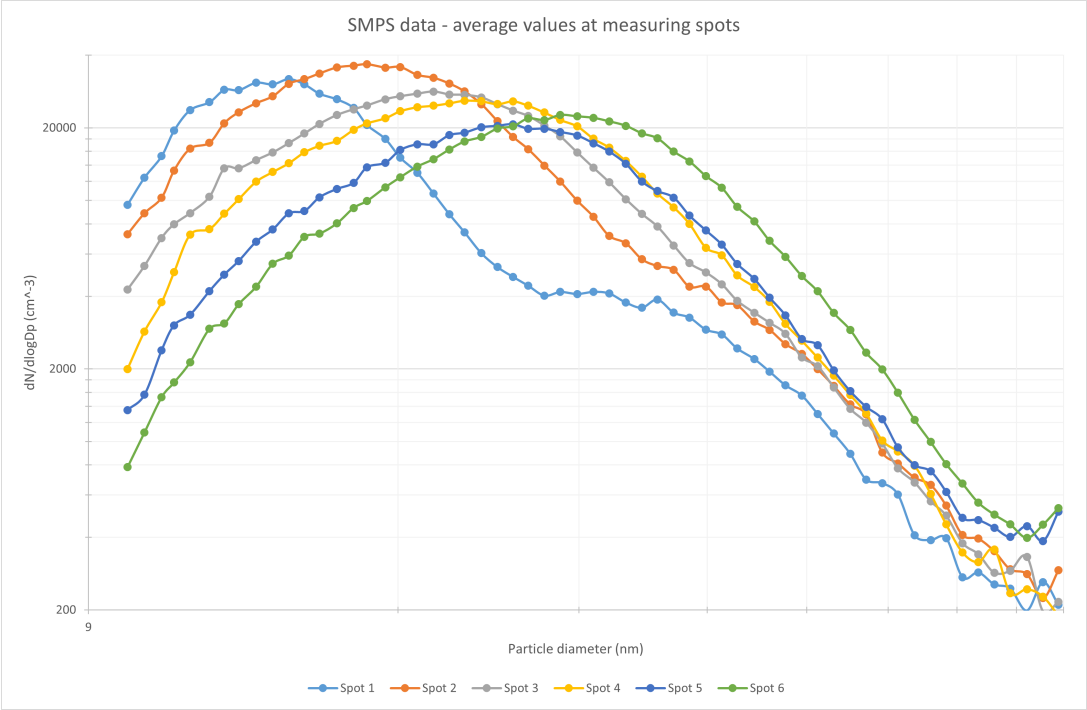

Figure 36: Average values of particle size distribution at the measurement spots, 2nd case study of the continental Lagrangian experiment, 21st of April 2021.

However, it was still possible that new particle formation took place also close to Spot 1 during the case study, although these particles could only be observed several hours later when they grew to sizes above 9 nm diameter. Therefore, if new particle formation happened in western Skåne, the 1 nm diameter particles formed around Spot 1 were likely seen as 9 nm particles in Blekinge some hours later. This hypothesis could be supported by the measurements in Spots 4 to 6, which still show relatively high concentrations of particles at 9 nm (Figures 33 and 36).

The nucleation particles were observed to grow from the moment when the new particle formation was detected for the first time until the end of the Lagrangian case study, five hours later. The increase in size can be seen in Figures 33 and 36, with a growth rate around 3.0 nm/h. The sudden decrease in the concentration of accumulation particles that led to the NPF also allowed condensational growth for the newly formed particles, making the geometric mean diameter of the NPF mode reach sizes around 40 nm when the air arrived at Karlskrona at 17:00. Although the NPF seemed to stop around 13:00 for the lowest size range,

the remaining oxidation compounds like OH radicals and ozone continued to contribute to oxidation and lowering the volatility of compounds, which participated in the condensational growth until the end of the measurements. To the author's knowledge, this diploma work is the first reported experiment where NPF could be followed in a Lagrangian way and particle growth by condensation was observed during air mass transport. Normally, this growth is only reported for fixed field sites, meaning it is only an apparent growth rate, since new air masses with different properties pass through the field site throughout the day.

A comparison of the data from the SMPS in the car and the DMPS at Hyltemossa was made for the measurements around 14:00, when the car was positioned at Spot 3, located about 17 km north of Hyltemossa. The particle size distribution for particle diameters below 80 nm was quite similar for Figures 33 and 34 showing high concentrations of particles between 20 and 40 nm diameter. Although larger particle sizes could not be compared for this case study, the similarities in the particle size distribution for small particles were a positive indication of the validity of the SMPS results measured in the car.

4.3.2 Sensors analysis

The modifications in the inlet system contributed to decreasing the particle losses in the tubes, showing stronger agreement between the sensor in the sealed box and the sensor outside for PM values (Figure 37). In contrast with the first case study, there was a noticeable difference between PM_{10} and $PM_{2.5}$, showing the presence of large particles such as dust, which is expected to be higher with higher wind speeds, or with increasing biological pollen particle concentrations. There is a smooth decrease in PM values for the consecutive measurement spots. This decrease is more distinct for PM_{10} than for $PM_{2.5}$, and the reason for this is unclear, since the winds were even increasing during the day, which would suggest higher emissions of dust particles in the coarse mode. The stability of the $PM_{2.5}$ concentration during the case study indicated that the accumulation mode particle concentration remained more stable when presumably following the same air mass in the Lagrangian approach.

It is noticeable in Figure 37 that a peak appeared for the sensor in the box a few minutes before 17:00. This is likely due to the location of Spot 6, at the end of a gravel road, where dust was lifted from the ground when driving. The peak in PM values was only observed by the sensor in the box due to the position of the inlet, slightly tilted down at the side of the car, providing a more direct transport for the particles from the gravel road. Since this pollution was of local nature, it

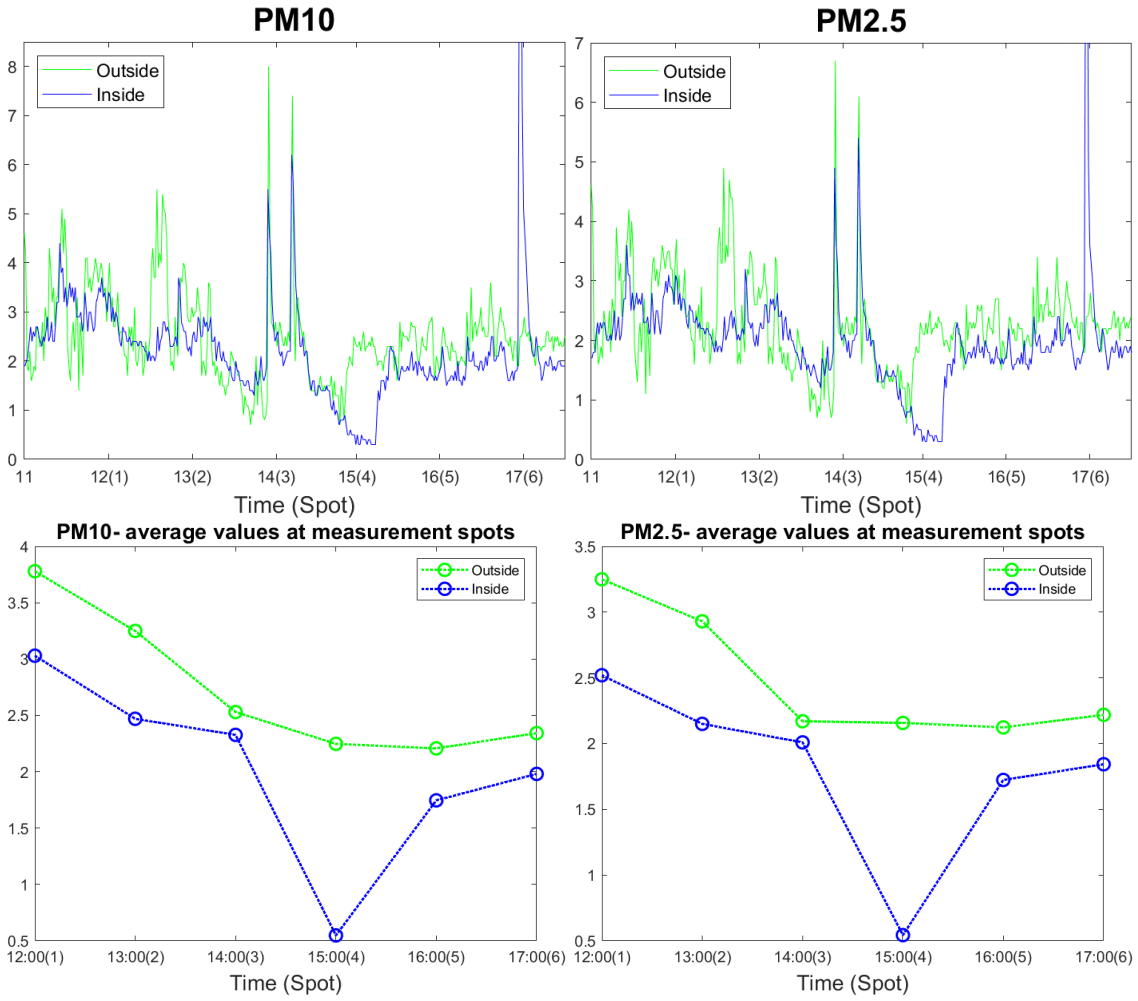

Figure 37: PM_{10} and $PM_{2.5}$ mass concentrations, second case study, 21st of April 2021.

was excluded in the average calculation of concentrations at spot 6 in the bottom panels of Figure 37.

The ozone and NO_2 measurements in Figure 38 showed that the modifications in the inlet system did not help to provide reliable results for the sensor inside and the gases were still subject to high losses in the inlet tubing, often reporting negative values. For this reason, only the AirNode outside the car was used in the analysis for subsequent case studies. The NO_2 plots also showed very intense fluctuations while driving as a consequence of changing the position of the sensor

node outside from the side to the roof of the car, although the measurements were rather stable at the measurement spots, hence reliability was not compromised by this modification. However, the changes in NO_2 values at the measurement spots did not allow for obtaining substantial conclusions, and more precise data would be needed for an appropriate analysis, for example, from the NOx 2BTech 405 monitor. The measurements from this instrument were not shown for this case study because the data was affected by problems in the inlet.

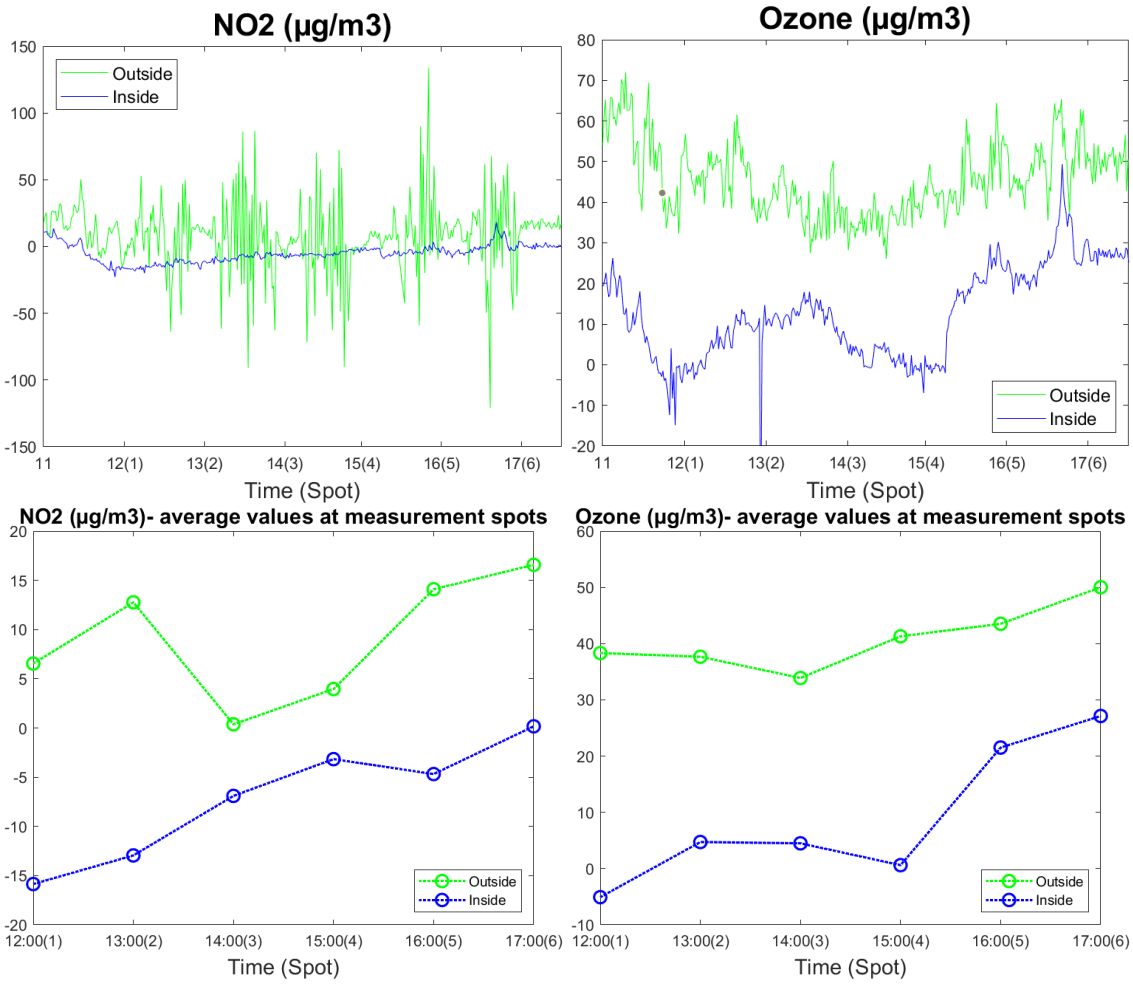

Figure 38: Nitrogen dioxide and ozone concentrations, second case study, 21st of April 2021.

The relatively high values of ozone observed for the sensor outside could have

contributed to the strong new particle formation observed in the SMPS. However, data from other atmospheric gases would be needed to understand the conditions that led to the NPF event. A comparison of the ozone values measured in the car with the data obtained in Hyltemossa was made to check the validity of these results (Figure 39). Hyltemossa showed even higher values for ozone during the whole measuring campaign, varying from 93 to 97 $\mu g/m^3$. These results are considerably higher than the 34 $\mu g/m^3$ measured by the AirNode at Spot 3, located 17 km north of Hyltemossa. Hence, it was concluded that the measurements in the car could not provide reliable results for ozone.

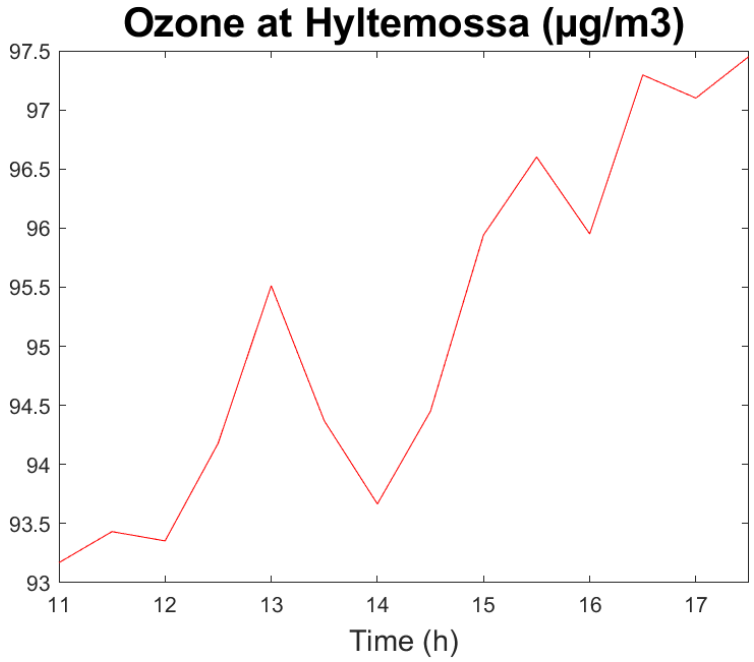

Figure 39: Ozone values measured at Hyltemossa, 21st of April 2021.

The sensors data for CO_2 and temperature and RH are shown in Figure 40. The sensor in the sealed box reported CO_2 values close to the background level during the whole measurements. The temperature values measured in the sensor outside are closer to the real temperatures for this case study, although, as previously stated, these values could not be trusted and were not used for the analysis.

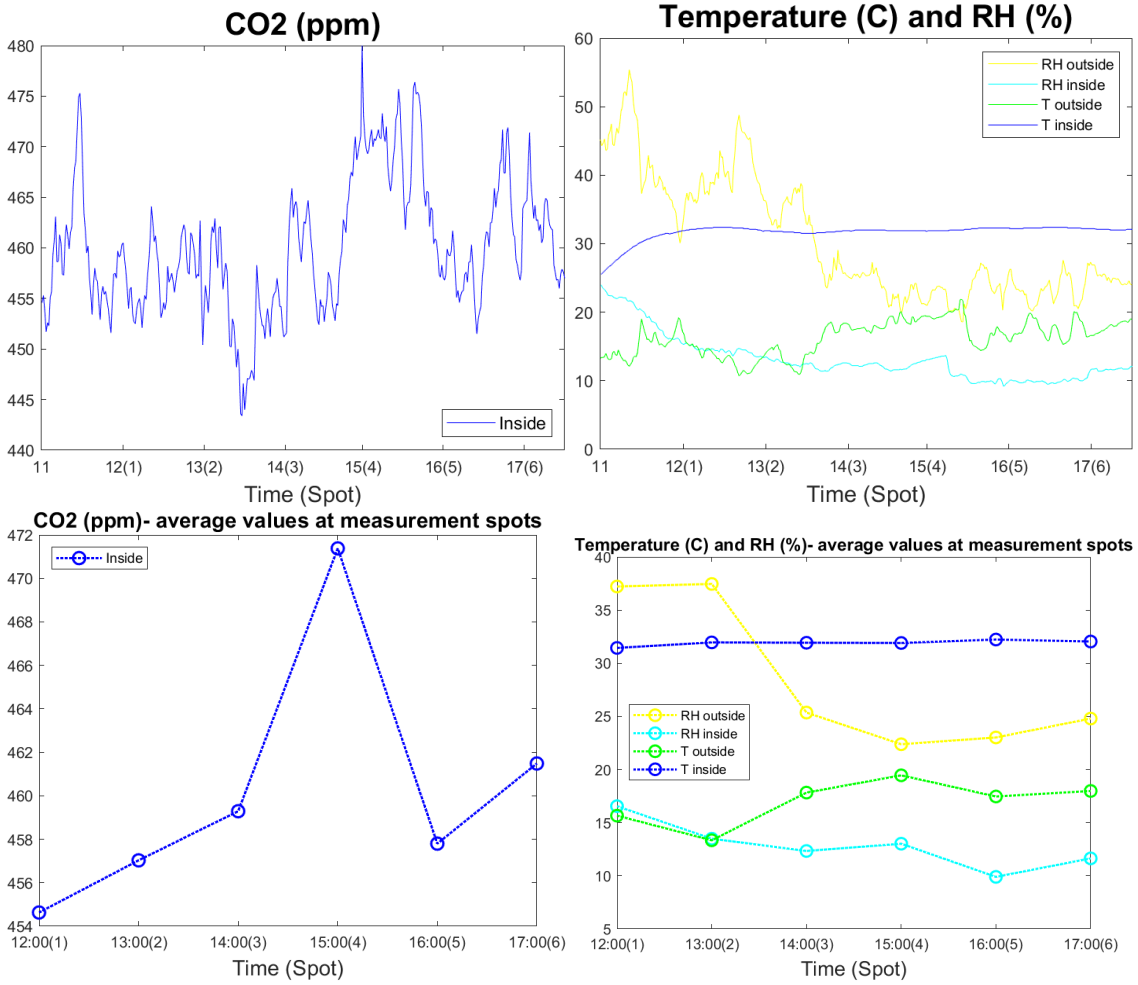

Figure 40: Carbon dioxide concentration and temperature and relative humidity, second case study, 21st of April 2021.

4.3.3 Limitations and improvements

The issues that affected the SMPS data during the first case study, which were attributed to the power outages, appeared again for the second case study, despite having no electricity interruptions. The SMPS in the car seemed to report faulty data for the largest particle sizes in a similar way to the previous campaign. The investigation of these issues was performed at first by comparing the size distribution measurements in the mobile system with the data from Hyltemossa station

for different times on the same case study day (Figure 41).

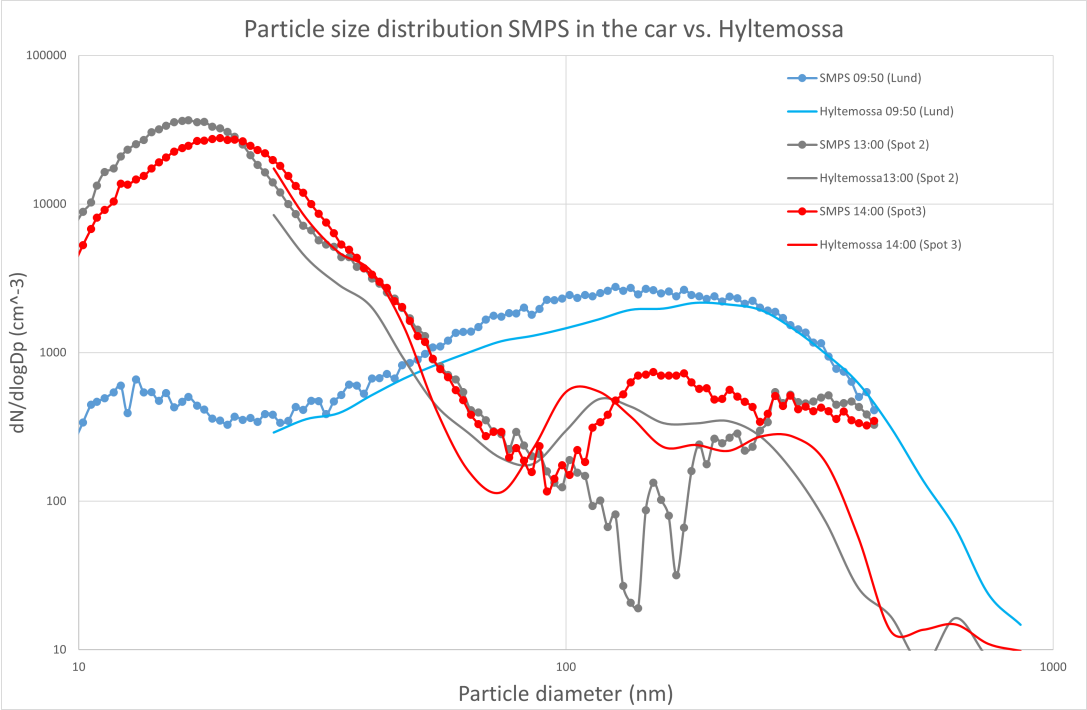

Figure 41: Size distribution measured in Hyltemossa and the portable monitoring station at different times, 21st of April 2021.

The size distribution measured in Hyltemossa in the accumulation mode was expected to be similar to the measurements in Lund, 45 km south of Hyltemossa, when the car used for the Lagrangian experiments was prepared in the Lund laboratory before each Lagrangian case study experiment. The agreement between the instruments was quite close for the measurements at 09:50 before the second case study began a few hours later. However, the data started to differ a few minutes later when the car headed to the first measurement spot. To be able to investigate this problem further, a comparison was attempted between the SMPS in the car and Hyltemossa DMPS size distribution at Spot 3, situated around 17 km north of Hyltemossa (red line in Figure 41). The particle size distribution of both instruments seemed to have a similar shape, but the diameters of some particle modes were shifted to larger sizes. This shifting seemed to increase with the particle size, barely affecting the values of the smallest particles while changing drastically the concentration of particles in the accumulation mode. Therefore the

data for sizes larger than 80 nm diameter were not presented in the results section for the second Lagrangian case study.

It could be seen that several size distribution 3-minute scans returned the error *DMA not detected*. After a closer examination of the data from the first and second case studies, it was speculated that the problem arose not only due to the power outage but also due to the movement of the car and the vibrations in the system. The SMPS stopped recognising the DMA at times, remaining unrecognised even when the car was standing still. This problem seemed to be the reason for the shift in sizes observed in Figure 41. The data also showed discontinuous jumps in the concentrations at 200 and 250 nm diameters, which could indicate that there were no stable voltages in the DMA [49]. Unfortunately, this was hard to detect during the actual case studies, since the size distribution in the SMPS AIM software was shown on a linear scale, hence, the skew in the data was not recognised until a closer examination of the SMPS data in retrospect.

The issues with the erroneous data were also discussed with personnel of TSI© [50], manufacturer of the SMPS and CPC instruments, who came in contact after the presentation of the aerosol-chase project at the NOSA conference [51]. They were interested in the continental Lagrangian experiments and wondered about the performance of the instruments in a mobile vehicle. The conversations with them regarding the data obtained in the first and second case studies were very helpful to understand the issues that affected the measurements. They suggested cleaning the chip underneath the DMA used to recognise the DMA by the SMPS system to solve the problems with connections, and suggested that additional issues might have arisen by a mismatch between the inlet flow entered in the software and the real aerosol flow entering the system. They also suggested purchasing a bracket to stabilise the DMA to the SMPS but, since there was no time for the delivery of the bracket before the following case study, the SMPS instrument was substituted for another SMPS of the same model.

After the switch of SMPS systems, the new instrument was tested in the laboratory to check that the previous issues would not affect the data from the third case study. The DMA chip was thoroughly cleaned, and the flows and pressure in the CPC and SMPS were measured to ensure that the flow registered by the SMPS corresponded to the real flow in the instrument. The movement in the car was simulated in the SMPS box while the instruments were functioning, by tilting the box and shaking it with different frequencies. It could be seen that vibrations did not affect the particle size distribution measured by the SMPS, hence no skew in the data was expected for the following case study.

Regarding the measurements of atmospheric chemistry, the main issue was the

lack of data from the 2BTech NOX monitor. The instrument was calibrated at the factory and installed in the boot of the car next to the power supply, but the inlet tubing was squeezed during the travel to the first measurement spot and the data had to be removed. For the third case study, the monitor was properly attached to the backseats and shielded to prevent the tubes from being squeezed.

4.4 Third case study

The third case study of the aerosol-chase project was performed on the 24th of May of 2021. The wind speed was around 5-6 m/s at half of the mixing layer height from south to north. The measurements lasted for six hours, measuring at seven different spots separated by 115 km, starting at the south coast of Skåne, near Ystad town (Figure 42).

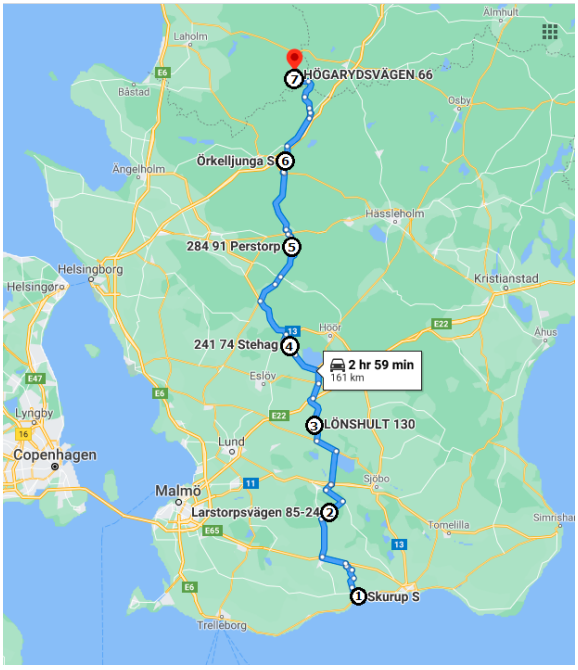

Figure 42: Route for the third case study of the continental Lagrangian experiment, 24st of May 2021. From Google Maps.

4.4.1 Particle size distribution

Figure 43 shows the particle size distribution, the total number concentration and total $PM_{0.45}$ mass concentration measured with the SMPS in the car during the third case study. For the first time in this pilot project, valid data were collected for the seven measurement spots for particle size distribution in the range of 9.3 to 437 nm. Figure 44 shows the average values of the particle size distribution calculated for each measurement spot.

Two main particles modes could be observed at around 12:00 at Spot 1, located only a few meters downwind of the sea. The highest concentration was in the Aitken mode at around 40-60 nm diameter. These particles were either originated from slightly aged ship emitted particles from the Baltic sea, which were emitted at around 30-40 nm diameter, or from slightly more aged traffic exhaust particles and other combustion generated particles in Northern Germany and Poland. The second mode covered particle diameters between 200 and 300 nm. The concentration of particles of this size was considerably higher than for any other measurement spot, which suggests that these particles were originated from sea spray close to the shore where Spot 1 was located.

The concentration of the two particle modes observed in Spot 1 decreased drastically towards Spot 2. This observation could be explained by the presence of a marine boundary layer in Spot 1 with different height and conditions than the terrestrial boundary layer in the subsequent measurement spots. The marine layer was affected by different winds, and the mixing was potentially less intense, trapping the pollutants close to the sea surface. During the transition from the marine to the continental boundary layer, in less than one hour, the air likely entered a region with more intense turbulence due to solar heating of the surface, and therefore higher mixing layer height and lower particle concentrations.

Figure 44 shows an accumulation mode of particles around 100-150 nm present in all the measurement spots that remained practically unchanged through the whole campaign. These particles might have originated in Central and Southern Europe, and they were not as affected by the mixing as the other particle modes. A more detailed trajectory analysis backwards could probably explain the origin and evolution of this mode.

Spots 3 and 4 presented similar accumulation and Aitken modes as Spot 2. However, an increase in the concentration of particles below 15 nm could be seen for these measurement spots, being especially noticeable for Spot 4. These differences might have been caused by emissions of particles and gases by road vehicles or by new particle formation.

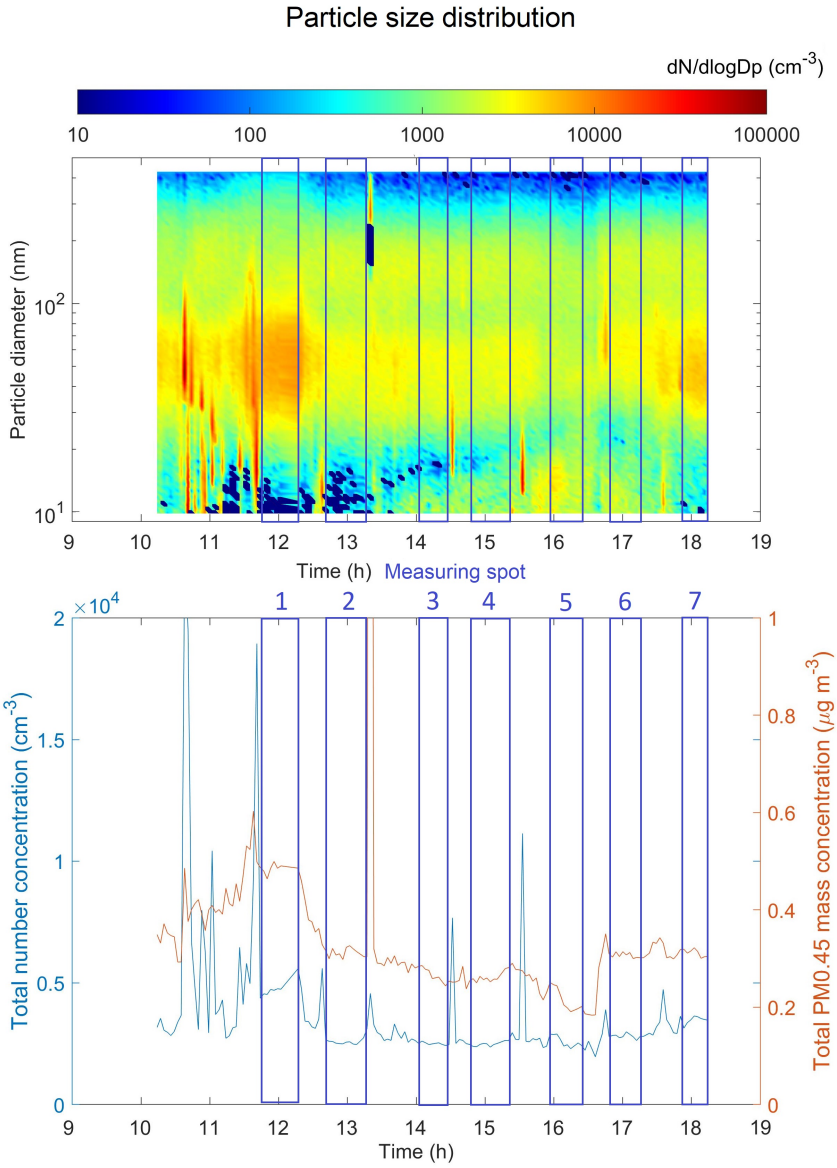

Figure 43: Particle size distribution measured with the SMPS in the car, 3rd case study of the continental Lagrangian experiment, 24th of May 2021.

The particle size distribution changed considerably at Spot 5, located in a forest, with a decrease in particles in the Aitken and accumulation modes and a dramatic increase in particles below 15 nm diameter. These observations suggested

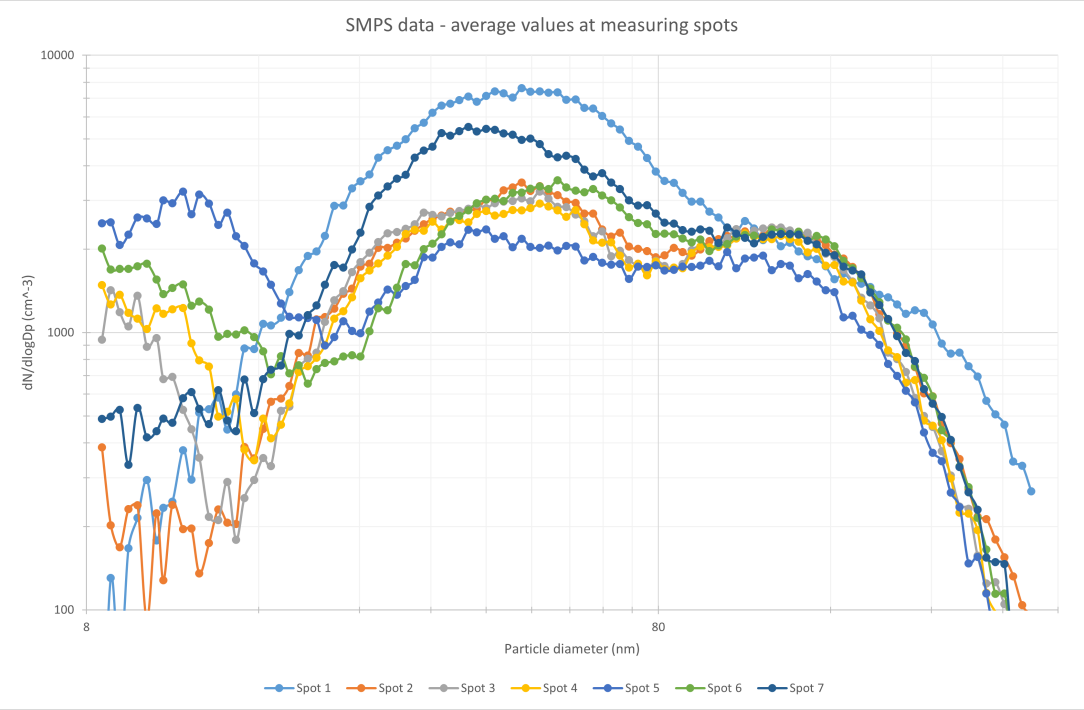

Figure 44: Average values of particle size distribution at the measurement spots, 3rd case study of the continental Lagrangian experiment, 24th of May 2021.

the appearance of new particle formation driven by the forest emissions at this spot. The increase in nucleation particles did not seem to be related to car emissions, since Spot 5 was at longer distances from roads or towns than the rest of the measurement spots.

For Spot 6, the Aitken and accumulation modes returned to values similar to Spots 2 to 4, although with a slightly higher concentration of particles around 70 nm. The increase in the Aitken mode could be caused by continued condensation of particles along the route.

For the last measurement spot, the concentration in the Aitken mode increased substantially, while most of the nucleation particles were already removed. An explanation for this could be a decrease in the mixing caused by lower heating at that time of the day, creating a new more stable layer at the bottom of the original mixing boundary layer that would trap the pollutants close to the ground. However, the creation of the lower layer would entail trapping recently emitted particles from traffic, which are in the size range around 20 nm instead of the 40-50 nm particles that were observed in the SMPS data. Although the lowering

of the boundary layer might still have happened, the sudden changes in the size distribution would be more easily explained by the intrusion of other air masses from horizontal directions carrying pollution from, for example, Malmö, Copenhagen or Kristianstad, which was not seen for previous spots since these spots did not seem to be downwind of these towns. There could have also been a deviation from the Lagrangian path due to a non accurate wind trajectory forecast. To understand the situation in Spot 7, it would be necessary to look at the analysed HYSPLIT trajectories in retrospect or 3D FLEXPART trajectories, which is planned after this diploma work.

4.4.2 Sensors analysis

For the AirNode sensors outside the car and the unit inside the sealed box, the reported PM_{10} concentrations had the same values as the $PM_{2.5}$ concentrations measured in the same unit for each data point. In other words, one of these parameters was duplicated, and in retrospect, it was not possible to deduce if it was $PM_{2.5}$ or PM_{10} data. Therefore, only one graph is presented for the third case study of this project (Figure 45). Despite that statistical issues seemed to affect the measurements, the PM data showed agreement with the $PM_{0.45}$ concentration measured in the SMPS system (Figure 43) for the whole measuring campaign. The AirNode sensors reported high PM concentrations for the first measurement spot, which can be related to the hypothesised sea spray particles measured by the SMPS instrument. As was the case for $PM_{0.45}$, the PM concentration measured in the AirNodes dropped towards Spot 2, decreasing further after that at Spots 3 to 5 before it increased slightly at Spots 6 and 7. Spot 5 showed a more drastic decrease in PM concentrations, which was in agreement with the observed decrease in SMPS data.

The PM concentrations reported by the AirNode sensors were compared to the data from the PALAS FIDAS instrument at Hallahus field station (Figure 46), located 10 kilometres east of Spot 4. Measurements at Hallahus showed distinctly higher values of $PM_{2.5}$ and PM_{10} between 3 and 6 $\mu g/m^3$ than the PM sensor at Spot 4. Nevertheless, the agreement between the SMPS and the PM sensor proved that the sensors have a good correlation with the SMPS mass measurements, which need further detailed analysis after the diploma work.

It was observed in the previous case study that the NO_2 values measured in the sensor inside, occasionally reported negative values, which could be due to losses in the inlet system that would compromise the reliability of the results. For this campaign, negative values were observed again in the AirNode placed in the

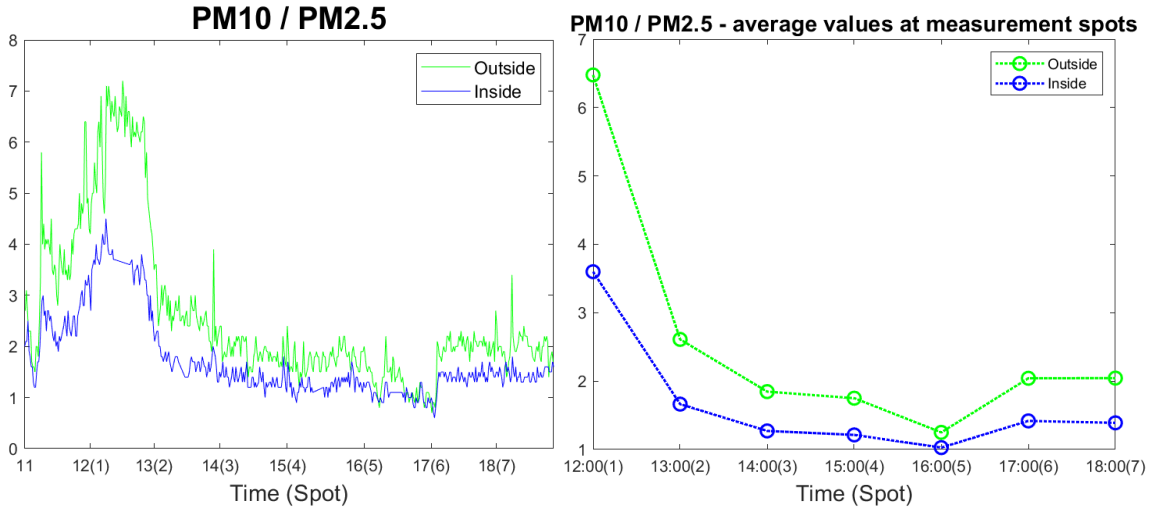

Figure 45: PM_{10} or $PM_{2.5}$ mass concentrations, third case study, 24th of May 2021.

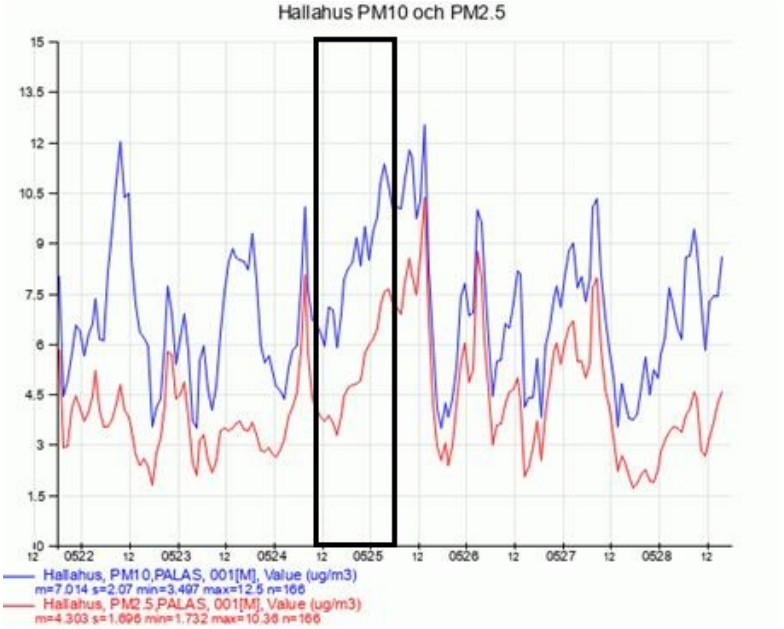

Figure 46: PM_{10} (blue) and $PM_{2.5}$ (red) concentrations from the PALAS FIDAS instrument at Hallahus field station. The marked area corresponds to the time frame when the third case study was performed. From Hallahus measuring station.

sensor box, hence only the data for the sensor outside are shown (Figure 47). The NO_2 values were not at all stable, for which it is hard to find an interpretation. The ozone measurements from the AirNode outside showed a similar tendency as the NO_2 measurements, with roughly the same increases and decreases at the different measurement spots. It was already concluded from the second case study that the ozone measurements were not reliable for the sensor nodes.

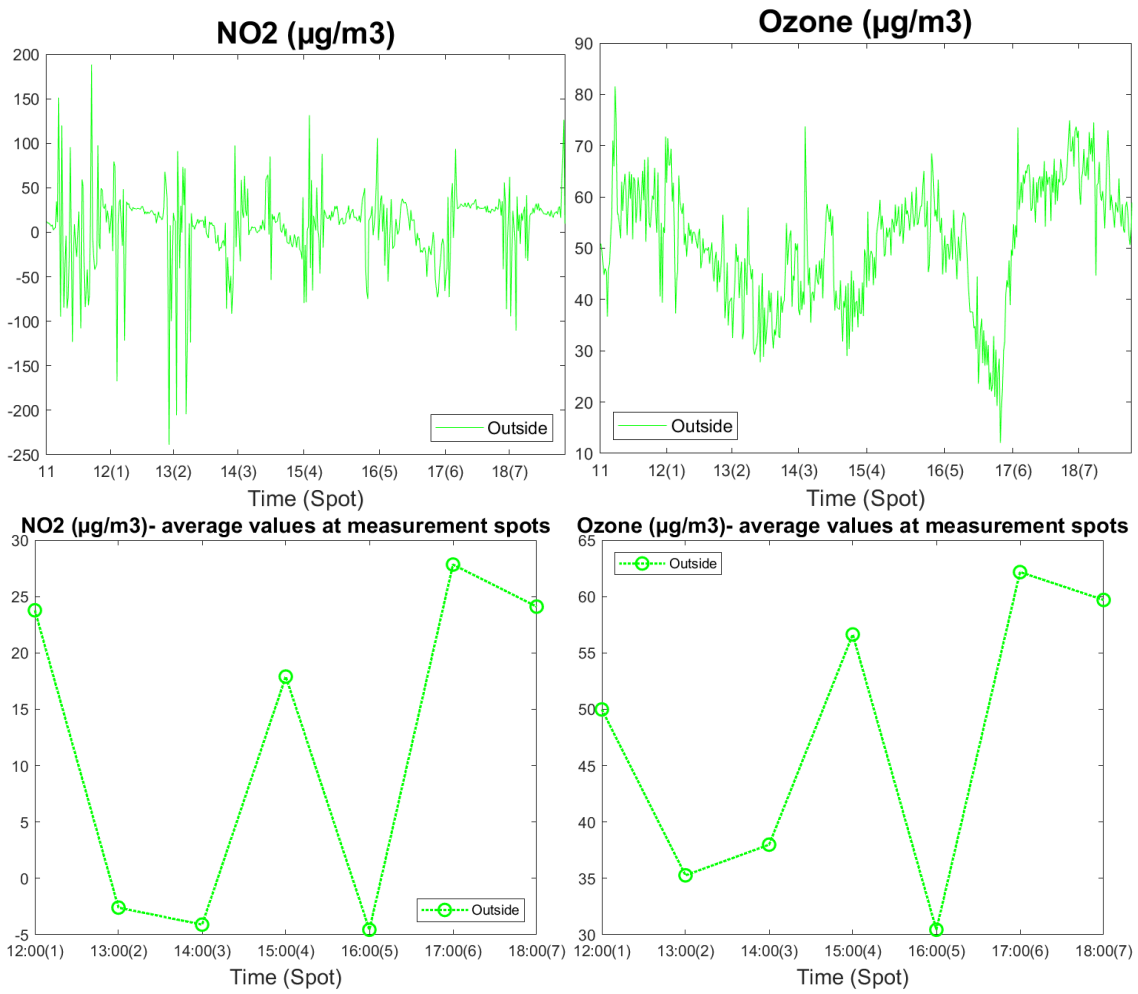

Figure 47: Nitrogen dioxide and ozone concentrations, third case study, 24th of May 2021.

The concentration of CO_2 in the sealed sensor and the values for temperature and relative humidity for both sensor nodes are shown in Figure 48. In contrast

with the data from the second case study, the continuous measurements of CO_2 showed clear differences between the data obtained on the road and the measurement spots. However, it took quite a long time before the CO_2 values dropped to background values at the spots. Hence, when stopping for a shorter duration at each spot during case studies with higher wind speeds, such as at the second case study, the values from the CO_2 sensor will likely not be reliable.

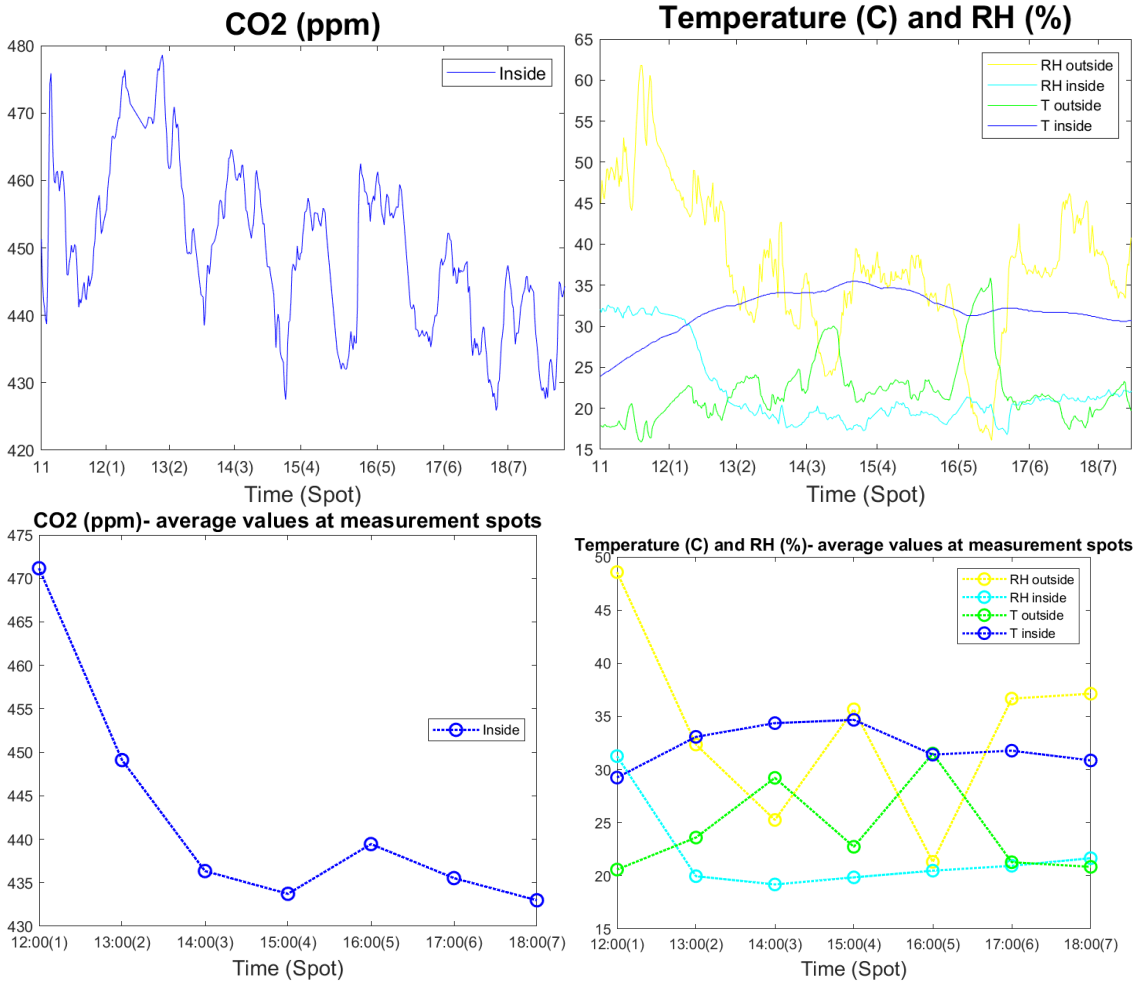

Figure 48: Carbon dioxide concentration and temperature and relative humidity, third case study, 24th of May 2021.

4.4.3 NOx 2BTech 405 monitor data

The third case study of the aerosol-chase project was the first measuring campaign where NO_2, NO and NOx data were successfully collected with the NOx 2BTech 405 monitor (Figure 49). Throughout the case study, there were very low concentrations of NO since the monitor reported values between -1 and +1 ppb(v). Hence, most NOx was in the form of NO_2. It was not easy to interpret the lower values for the first four spots and the higher concentrations for the remaining spots just based on studying the geographical map and potential source areas of emissions. NOx undergoes chemical reactions during long range transport, and a chemistry model is likely required to explain the concentration changes.

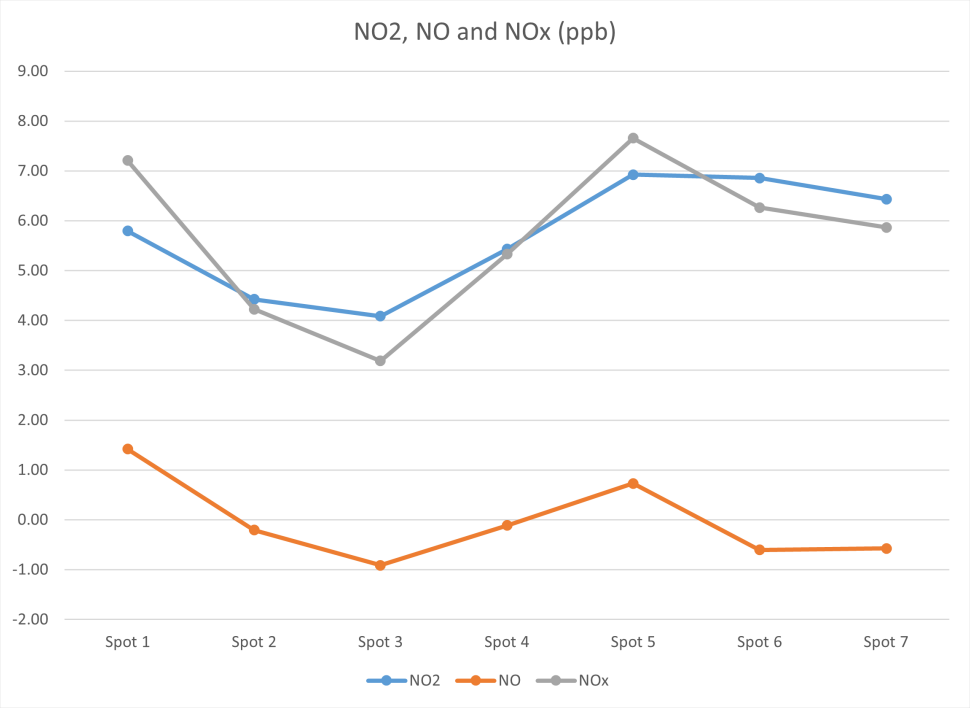

Figure 49: NO_2, NO and NOx from NOx 2BTech 405 monitor, third case study, 24th of May 2021. The plot shows average values at each measurement spot.

The 2BTech 405 NO_2 concentrations converted to $\mu g/m^3$ were on the order of 11-12 $\mu g/m^3$ and much more stable than the values from the AirNode sensors. However, the average NO_2 concentrations from the AirNode sensors were also on the order of 11-12 $\mu g/m^3$ hence, averaged over a longer period, the sensors might be reliable.

4.4.4 Limitations and improvements

As mentioned in the previous case studies, the forecast wind trajectories were not validated in this study. The lack of knowledge about the air mass history further back in time, also made it harder to interpret data. Therefore, future Lagrangian experiments should investigate winds at different heights and different directions, and study the air mass history.

The sensors data presented for the three case studies do not show error bars, due to the difficulty to estimate the systematic error in the instruments and the time constraints to calculate statistical uncertainties. The comparison of the NO_2 concentrations measured in the AirNode sensors and the NOx 2BTech 405 monitor provided an estimation of the error in the AirNode sensors on the order of 15 $\mu g/m^3$ for the average values. Similar tendencies could be expected for the remaining sensors in the AirNode, showing large uncertainty, although more data from additional instruments would be needed to perform a quantitative estimation. For the NOx 2BTech 405 monitor, which seemed to be more reliable, an error on the order of 2 ppb could be estimated based on the preliminary analysis of the data. However, a more detailed study would be necessary to accurately calculate the errors in the presented results, involving a proper calibration of the sensors and statistical analysis. Such study is planned after the conclusion of this diploma work.

The quality of the sensors data was still largely uncertain. Future ideas of how to test the accurateness of the AirNode sensors have been suggested in the section *Future research*.

5 Conclusions

The aim of this pilot project was to test a novel method to perform Lagrangian measurements over continental areas using a mobile vehicle. The three case studies showed that the method can be applied to follow an air mass during its Lagrangian path over land, measuring changes in particle size distribution, PM concentrations and atmospheric chemistry. This diploma work is meant to be a first step in the application of such methods and it is expected that future experiments will improve the methodology and investigate further factors influencing the analysis of air masses.

The first set of conclusions from this work involves the performance of the measurement equipment:

- A power supply with 360 Ah of battery power, as the one used for this pilot project, can provide power to run an SMPS system and a few more instruments with about 300 W power usage for, at least, ten hours.

- AirNode units that accommodate several different types of sensors in the same node should not have an inlet system. Different sensors in the node require different types of tubing inlets to minimize losses. Hence, the nodes should be placed on the outside of the mobile vehicle, or sensors should be separated inside the mobile vehicle to be able to use different inlet tubing to different sensors.

- The instruments should be secured to the structures in the vehicle to provide stability and protect the inlet and outlet tubes from being squeezed due to the movement of the vehicle.

- If an SMPS system is used, it should be ensured that the DMA is stabilised and that it will not lose contact with the SMPS because of the vibrations of the system due to the movement of the vehicle.

- AirNode sensors from the company AirLabs provided relatively trustworthy results for changes in PM concentrations, although comparison with field stations showed that the absolute values reported by the sensor nodes were often lower than the real values. Measurements of NO_2, ozone and temperature provided inaccurate results for the setup used in the case studies. The CO_2 sensors seemed to provide reliable data, although, at least, 20 minutes were required to obtain stable results. A proper calibration would be needed before using the AirNode sensors in future continental Lagrangian experiments.

- Using different instruments for the same atmospheric parameters would help to validate the data and having a better estimation of the reliability of the instruments, as was the case for the NO_2 measurements performed with the AirNode sensors and the NOx 2BTech 405 monitor. All sensors and instruments should preferably be installed in a rack if a larger vehicle is used, which makes the packing and unloading in the vehicle faster.

Other conclusions involve the Lagrangian approach and wind trajectories:

- The wind trajectory forecast can be successfully performed with the HYSPLIT trajectory model, as it has been proven for the three case studies. However, the accuracy of the study would considerably increase by performing

a more detailed forecast which integrates local winds intruding the air mass from the sides and above the mixing layer. Calculating backward trajectories after the measurements would also help verify the quality of the forecast and detect possible deviations from the Lagrangian path.

- The measurements for particle size distribution and atmospheric chemistry should be performed at static measurement spots, switching off the vehicle engine at locations far away from strong local sources of pollutants.

- It is possible to follow the air mass trajectory according to the methods explained in this report for wind speeds of, at least, 12 m/s. Although the limitations depend strongly on the speed limit and detour on roads where the measurements are performed, too fast winds would reduce the time that can be used for data collection at each spot, compromising the accuracy of the results.

- Having two people in the vehicle who can drive during the campaign would allow for increasing the duration of the measurements. Additionally, it would help to solve unexpected issues with the equipment and increase safety on the road by reducing tiredness and stress of the driver. Additional people would be needed to perform experiments of a longer duration than 10 hours. This logistical preparation and execution have not been tested in this diploma work.

Additional conclusions involve the data analysis aspect:

- Comparison with field stations for the parameters measured in the mobile system allows an estimation of the accuracy of the instruments and reliability of the results. In order to do this, the chosen Lagrangian path should be planned to include a measurement spot close to a field station, as it was done in this project for the stations of Hyltemossa and Hallahus.

- An analysis of the air mass history in retrospect would help locate particle emission source regions.

- CO_2 measurements are useful to verify that the measurement spots are not affected by local combustion emissions, which should be true for environments where the CO_2 values are close to the background levels.

- The data collected at the measurement spots will often be affected by intermittent local sources of pollutants, for example, a passing vehicle. This

data can be discovered in the data analysis and should be excluded from the calculation of the average values at the measurement spots.

The application of this knowledge to the Lagrangian experiments allowed for obtaining relevant observations during the three case studies of this pilot project. Although they are preliminary conclusions, some of the most relevant observations are listed below.

- New particle formation was detected during the second case study, and it was possible to observe the particle growth by condensation during several hours of transport. To the author's knowledge, this diploma work is the first reported experiment where this is done.
- Transition from a marine boundary layer close to the ocean to a terrestrial boundary layer a few kilometres inland was observed for the third case study with subsequent changes in particle and gases concentrations, showing that transitions from different boundary layer types give changing air pollutant properties.
- New emissions from combustion sources could be identified along the air mass path as an increase in nucleation mode particles between subsequent measurement spots. Hence, the type of source and the location of the source emissions can be more readily tracked by the Lagrangian approach than at a fixed measurement station.

6 Future research

As the next step of this project, the data from the case studies are planned to be connected to the ADCHEM model [13]. Taking aerosol processes, radiation, atmospheric chemistry and wind trajectories into consideration, ADCHEM can model the concentration of aerosol particles, assuming completely mixed air vertically within a certain MBL height. Based on measured meteorology data along trajectories at different heights, it is possible to simulate the mixing from aloft (from layers above the MBL). The data from these Lagrangian experiments are expected to improve the ADCHEM model.

As it was mentioned previously in the report, the forecast wind trajectories performed with HYSPLIT were not able to account for the influence of local winds from the sides of the air mass and above the mixing layer. A more accurate forecast trajectory will be performed for future Lagrangian experiments using FLEXPART

[48]. FLEXPART is able to calculate influence at a certain receptor point from several vertical layers and different horizontal wind directions backwards in time (Figure 50).

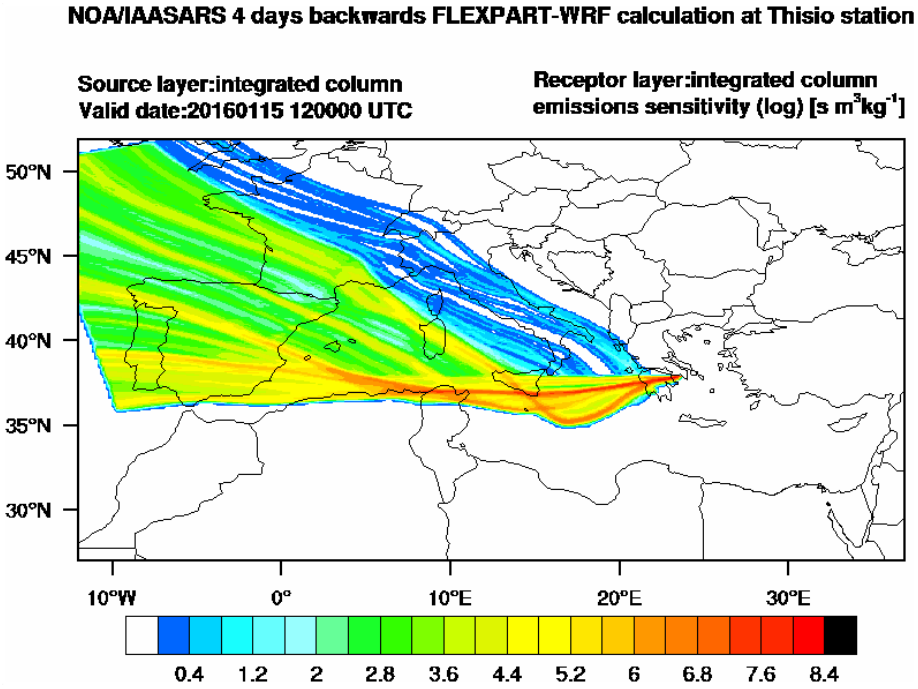

Figure 50: Forecast wind trajectories calculated with FLEXPART. From ACTRIS Athens.

For future projects, finding a commercial solution to power the instruments might be more efficient than building a battery box from scratch, as was done for this project. The building of the power supply was one of the most time-consuming parts at the beginning of the project, including several safety issues and inspections that delayed the start of the first test campaign. For these reasons, it would be recommended for future experiments to purchase a commercial power station.

The equipment in the car could be extended with more instruments to measure different atmospheric parameters. After the presentation of the aerosol-chase project at the NOSA conference [51], researchers from Magee Scientific [52] got in contact, expressing their interest in introducing the Aethalometer AE43 in the system for carbonaceous aerosol measurements.

The third case study of the aerosol-chase project was originally planned as a joint experiment performed with an additional car with similar experimental

equipment in Denmark. This car was donated by Google to Aarhus University for atmospheric measurements (Figure 51). The plan consisted of following the Lagrangian path of an air mass in Denmark and continuing the measurements when it reached Sweden. However, since the wind flows between Denmark and Sweden were not connected, this experiment has to be continued at a later occasion.

Figure 51: Interior of the Google car. Photo: Hugo Savill Russel.

Other types of campaigns could be performed for future studies in different conditions, depending on the availability of the equipment and the funds supporting the research. For example, the geographical limitations of the measurements could be overcome by installing the equipment on a boat that could follow the air mass after it reaches the sea. Another option is equipment on drones. To investigate the mixing of air masses from the sides and from aloft, additional mobile vehicles or vertical measurements can be employed.

In general, to be able to quantify source emissions and the processes acting on aerosol particles during long range transport requires extensive Lagrangian measurement campaigns repeated over all seasons for each region. A wider spread of these measurements to other regions in the world is also necessary.

7 Acknowledgements

This project was possible thanks to the tireless work of my supervisor, Adam Kristensson. He guided me in every step of the project and supported me from the first until the last day, proving to be not only an excellent supervisor but also an extraordinary person. It has been an honour and a pleasure to share this journey with you.

Thank you to my co-supervisor Matthew Stanley Johnson for trusting me with his car for the measurements, opening his garage to build the power station and keeping an eye on the whole project. I hope we get to work together again in the near future.

Thank you to the rest of the people who have contributed to making this project possible. The company AirLabs and Hugo Savill Russell for the assistance with the sensor nodes. Sadath Ismayil, for his help with the humongous project of the battery box. The Aerosol Department at Lund University, for letting me work in the lab and supporting me with the safety of the experiment. To the board of the NOSA conference for giving me the opportunity to share this project with the Aerosol research community. Mikael Elfman, for the advice with the electrical system. And Florian Dahlkoetter, from TSI, for helping us solve the issues with the SMPS data.

I would like to thank my friends and family for their support. Special thanks to Victor for being the best brother I could have wished for and to Laura for sharing the best moments with me and supporting me in the hardest ones. Lastly, I can only express my love and gratitude to my family in Spain. I would like to dedicate this project to my abuelos and my parents, who have supported me all this time despite me being so far away. Gracias por todo.

References

[1] C. I. Davidson, R. F. Phalen and P. A. Solomon (2005). Airborne Particulate Matter and Human Health: A Review, Aerosol Science and Technology, 39:8, p. 737-749.

[2] C. A. Pope III and D. W. Dockery (2006). Health effects of fine particulate air pollution: Lines that connect. J. Air Waste Manag. Assoc. 2006, 56, p. 709–742.

[3] World Health Organization (2018). Global Ambient Air Quality Database.

[4] IPCC, Climate Change (2013). Cambridge University Press, NY, USA, pp. 1535.

[5] P. Hari, T. Petäjä, J. Bäck et al. (2015). Conceptual design of a measurement network of the global change, Atmos. Chem. Phys. Discuss., 15, p. 21063–21093.

[6] R. C. Henry, C. W. Lewis, P. K. Hopke et al. (1984). Review of receptor model fundamentals, Atmospheric Environment Vol. 18. No. 8. pp. 1507-1515

[7] I. Rivas, D. C. S. Beddows, F. Amato et al. (2020). Source apportionment of particle number size distribution in urban background and traffic stations in four European cities, Environment International Volume 135, February 2020, 105345.

[8] P. Krecl, E. Hedberg Larsson, J. Strom et al. (2008). Contribution of residential wood combustion and other sources to hourly winter aerosol in Northern Sweden determined by positive matrix factorization, Atmospheric Chemistry and Physics, 8, p. 3639–3653.

[9] E. V. Sebille, S. M. Griffiesc, R. Abernathey et al. (2018). Lagrangian ocean analysis: Fundamentals and practices, Ocean Modelling, Volume 121, January 2018, p. 49-75.

[10] E. Hermansson, P. Roldin, A. Rusanen et al. (2014). Biogenic SOA formation through gas-phase oxidation and gas-to-particle partitioning – a comparison between process models of varying complexity, Atmos. Chem. Phys., 14, p. 11853–11869.

[11] S. Businger, R. Johnson and R. Talbot (2006). Scientific Insights from Four Generations of Lagrangian Smart Balloons in Atmospheric Research, American Meteorological Society, November 2006 BAMS- 1539-1554.

[12] F. Rabier, S. Cohn, P. Cocquerez et al. (2013). The Concordiasi Field Experiment over Antarctica: First Results from Innovative Atmospheric Measurements, Bulletin of the American Meteorological Society, Volume 94, Issue 3, March 2013.

[13] P. Roldin, E. Swietlicki, G. Schurgers et al. (2011). Development and evaluation of the aerosol dynamics and gas phase chemistry model ADCHEM, Atmospheric Chemistry and Physics, Vol. 11, No. 12, 2011, p. 5867-5896.

[14] W. C. Hinds (1999). Aerosol Technology. Properties, behavior, and measurement of airborne particles. Second edition, John Wiley and Sons, Inc., New York, USA.

[15] C. Tomasi and A. Lupi (2017). Primary and Secondary Sources of Atmospheric Aerosol, Atmospheric Aerosols: Life Cycles and Effects on Air Quality and Climate, First Edition, Wiley-VCH Verlag GmbH Co. KGaA.

[16] V. R. Despres, J. A. Huffman, S. M. Burrows et al. (2012). Primary biological aerosol particles in the atmosphere: a review. Tellus B, 64, 15598, doi: 10.3402/tellusb.v64i0.15598.

[17] P. H. McMurry and S. K. Friedlander (1979). New particle formation in the presence of an aerosol. Atmos. Environ., 13, p. 1635-1651.

[18] L. Sogacheva, M. Dal Maso, V. M. Kerminen et al. (2005). Probability of nucleation events and aerosol particle concentration in different air mass types arriving at Hyytiälä, southern Finland, based on back trajectories analysis. Boreal Env. Res. 10: p. 479-491.

[19] M. Kulmala and V. M. Kerminen (2008). On the formation and growth of atmospheric nanoparticles. Atmospheric Research. doi:10.1016/j.atmosres.2008.01.005.

[20] J. A. Aitken (1897). On some nuclei of cloudy condensation, Trans. Roy. Soc., XXXIX, p. 1897.

[21] M. Kulmala, G. Mordas, T. Petäjä et al. (2007). The condensation particle counter battery (CPCB): a new tool to investigate the activation properties of nanoparticles, J. Aerosol Sci., 38, p. 89-304.

[22] M. Kulmala, I. Riipinen, M. Sipilä et al. (2007). Toward direct measurement of atmospheric nucleation, Science, 318, p. 89-92.

[23] J. Curtius (2009). Nucleation of atmospheric particles. Eur. Phys. J. Conferences, 1, 199-209.

[24] J. Curtius (2006). Comptes Rendus Phys. 7, 1027.

[25] M. Hallquist , J. C. Wenger, U. Baltensperger et al. (2009). The formation, properties and impact of secondary organic aerosol: current and emerging issues, Atmos. Chem. Phys. Discuss., 9, p. 3555–3762.

[26] D. Lamb and J. Verlinde (2011). Physics and chemistry of clouds. Cambridge University Press, Cambridge, UK. First edition. ISBN 978-0-521-89910-9.

[27] R. Jaenicke (1980). Atmospheric aerosols and global climate. J. Aerosol Sci., 11, p. 577-588.

[28] B. Sportisse (2007). A review of parameterizations for modelling dry deposition and scavenging of radionucleids. Atmos. Env., 41, p. 2683-2698.

[29] K. Osada, S. Ura, M. Kagawa et al. (2014). Wet and dry deposition of mineral dust particles in Japan: factors related to temporal variation and spatial distribution. Atmos. Chem. Phys., 14, p. 1107-1121.

[30] Deutscher Wetterdienst: https://www.dwd.de/ Homepage - Research - Observing the atmosphere - Atmospheric composition - Aerosols - Particle Size Distribution (last accessed June 20, 2021).

[31] A. Lindroth, J. Holst, M. Linderson et al. (2020). Effects of drought and meteorological forcing on carbon and water fluxes in Nordic forests during the dry summer of 2018, Phil. Trans. R. Soc. B3752019051620190516.

[32] A. Kristensson, M. Dal Maso, E. Swietlicki et al. (2008). Characterization of new particle formation events at a background site in Southern Sweden: relation to air mass history. Tellus B, 60: 330-344. doi: 10.1111/j.1600-0889.2008.00345.x.

[33] J. Martinsson, H. Abdul Azeem, M. K. Sporre et al. (2017). Carbonaceous aerosol source apportionment using the Aethalometer model – evaluation by radiocarbon and levoglucosan analysis at a rural background site in southern Sweden, Atmos. Chem. Phys., 17, 4265–4281, https://doi.org/10.5194/acp-17-4265-2017 (last accessed June 20, 2021).

[34] M. Pandolfi, L. Alados-Arboledas and A. Alastuey (2018). A European aerosol phenomenology – 6: scattering properties of atmospheric aerosol particles from 28 ACTRIS sites, Atmos. Chem. Phys., 18, 7877–7911, https://doi.org/10.5194/acp-18-7877-2018 (last accessed June 20, 2021).

[35] J. Schmale, S. Henning, S. Decesari et al. (2018). Long-term cloud condensation nuclei number concentration, particle number size distribution and chemical composition measurements at regionally representative observatories, Atmos. Chem. Phys., 18, 2853–2881, https://doi.org/10.5194/acp-18-2853-2018 (last accessed June 20, 2021).

[36] L. Poulain, G. Spindler, A. Grüner et al. (2020). Multi-year ACSM measurements at the central European research station Melpitz (Germany) – Part 1: Instrument robustness, quality assurance, and impact of upper size cutoff diameter, Atmos. Meas. Tech., 13, 4973–4994, https://doi.org/10.5194/amt-13-4973-2020 (last accessed June 20, 2021).

[37] A. Wiedensohler (1987). An approximation of the bipolar charge distribution for particles in the submicron size range, Journal of Aerosol Science, Volume 19, Issue 3, 1988, p. 387-389, ISSN 0021-8502, https://doi.org/10.1016/0021-8502(88)90278-9 (last accessed June 20, 2021).

[38] J. Zhou (2001). Hygroscopic Properties of Atmospheric Aerosol Particles in Various Environments. Department of Nuclear Physics, Lund University. ISBN 91-7874-120-3.

[39] D. R. Collins, R. C. Flagan and J. H Seinfeld (2002). Improved Inversion of Scanning DMA Data. Aerosol Sci. Tech., 36, p. 1-9.

[40] Airlabs (2021). https://www.airlabs.com/ (last accessed June 20, 2021

[41] AirNode Datasheet (2021). AirLabs: https://www.airlabs.com/wp-content/uploads/2021/01/AirNode-Technical-specs.pdf (last accessed June 20, 2021).

[42] L. B. Frederickson, S. Lim, H. S. Russell et al. (2020). Monitoring Excess Exposure to Air Pollution for Professional Drivers in London Using Low-Cost Sensors, Atmosphere 2020, 11, 749.

[43] H. Y. Liu, P. Schneider, R. Haugen et al. (2019). Performance Assessment of a Low-Cost $PM_{2.5}$ Sensor for a near Four-Month Period in Oslo, Norway. Atmosphere 2019, 10, 41.

[44] L. Frederickson, E. Petersen-Sonn, Y. Shen et al. (2019). Low-Cost Sensors for Indoor and Outdoor Pollution; R.A. Meyers; Ed.; Springer: New York, NY, USA.

[45] A. Soares, C. Catita and C. Silva (2020). Exploratory Research of CO_2, Noise and Metabolic Energy Expenditure in Lisbon Commuting. Energies 2020, 13, 861.

[46] Sensirion (2011). A.G. Data Sheet SHT7x (SHT71, SHT75). Humidity and Temperature Sensor IC; Technical Report Version V5; Data sheet; Sensirion: Stäfa, Switzerland.

[47] A. F. Stein, R. R. Draxler, G. D. Rolph et al. (2015). NOAA's HYSPLIT Atmospheric Transport and Dispersion Modeling System, Bulletin of the American Meteorological Society, 96(12), p. 2059-2077.

[48] FLEXPART (2021). https://www.flexpart.eu/ (last accessed June 20, 2021).

[49] A. Wiedensohler, A. Wiesner, K. Weinhold et al. (2018). Mobility particle size spectrometers: Calibration procedures and measurement uncertainties, Aerosol Science and Technology, 52:2, p. 146-164, doi: 10.1080/02786826.2017.1387229.

[50] TSI (2021). https://tsi.com (last accessed June 20, 2021).

[51] Nordic Society for Aerosol Research (NOSA) (2021). https://www.nosa-aerosol.org/ (last accessed June 20, 2021).

[52] Magee Scientific (2021) https://mageesci.com/ (last accessed June 20, 2021).

Appendix 1: Risk evaluation

1. Description of experiments

The experiment will use a Scanning Mobility Particle Sizer (SMPS) and a collection of compact sensors that will measure particle concentration and atmospheric conditions. The equipment will be placed inside a car that will follow the trajectory of the wind to sample a certain airmass. An inlet pipe will let air flow from outside the car to the SMPS and the case where the sensors are placed, and an outlet pipe will eject the air after the measurements have been performed.

The SMPS will provide the particle size distribution of the airmass. The sensors will be compact, low-powered and with high time resolution for O_3, NO_2, RH, T, CO_2, $PM_{2.5}$ and PM_{10}.

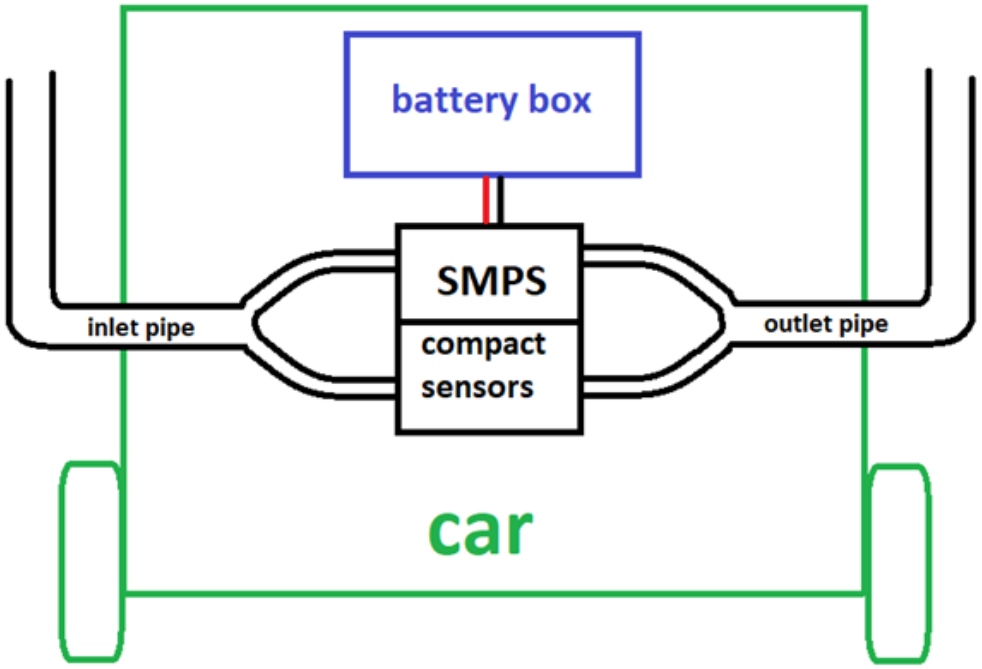

Figure 52: Experimental setup inside the car.

The system will be sustained by a battery box consisting of three gel 12 V batteries of 120 Ah capacity connected in parallel and a 1500 W inverter that transforms the 12 V direct current to 230 V pure sine wave alternating current. The three batteries can be charged at the same time by a charger that will also be placed

inside the box. A fan will make it possible to keep a moderate temperature inside the box when the batteries are being used.

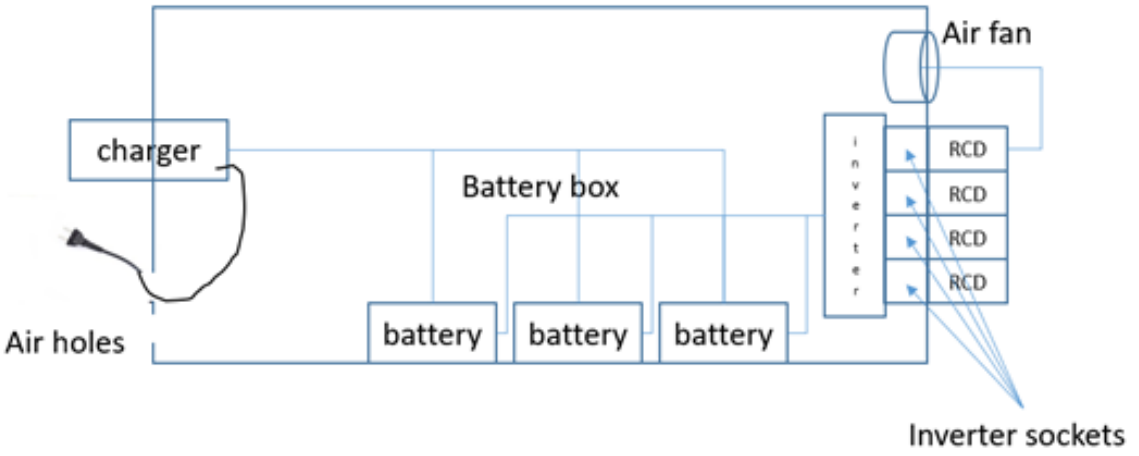

Figure 53: Drawing of the battery box.

Before the system is installed in the car, different tests will be conducted in the Aerosol laboratory at Ingvar Kamprad Design Center (IKDC) in Lund. The battery box and necessary connections will also be built in the laboratory. The sensors will be sent to Lund by the company Airlabs, in Copenhagen, and their calibration will be performed in IKDC laboratories. The system will be built and tested during December 2020 and January 2021 and the measurements in the car will be taken during February and March 2021.

2. Identification of risks

Since powerful gel batteries are being used, there is a risk of electrical shock or damage to the batteries when they are shorted. Before building the battery box, the design of the electrical system should be approved by an electricity expert. When the battery box is built, it will be enclosed, and the box will be marked with signs that indicate that no one should open the box without the needed training. Rubber gloves will be used at any time when handling the batteries, and the poles will be covered with isolation tape when possible, to make sure that both poles are not touched at the same time by people or objects. When the box is ready to be used, the tape will be replaced by more solid structures such as plastic 3-D printed covers, to achieve better isolation. All cables that are loose inside the box should be attached to the sides with clamps to avoid that they accidentally touch the poles

or other cables. Additionally, residual current devices (RCD) will be installed in the outlets of the inverter to avoid electrical shock and damage of the equipment, having no need for grounding. A 3-nod switch will be installed in the box to change between the use of the inverter (when measurements are performed) and charger (when the batteries need to be charged). By doing this, the box does not need to be opened at any time during the performance of the experiments. After building the battery box, before connecting the SMPS and measuring in the field, the electricity expert should check the system again and advise about how to use it. The battery box should not be used before the expert gives their approval and the safety suggestions they provide have been implemented.

In the current situation when, most of the times, the work is performed alone, there are extra risks to consider. A security device should be worn when working alone in the lab, which will send an alert in case the person falls and do not incorporate in a few seconds. Following the aerosol lab security rules, it is also not allowed to climb ladders or take actions that can be considered as dangerous when working alone. Additionally, no one should work alone in the lab without notifying another person involved in the experiment (for example, diploma student and supervisor).

Powerful batteries working in an enclosed box entail risk of fire or explosion due to overheating. To ensure a moderate temperature inside the box, a fan will be installed, and holes will be drilled in the top and side of the box. There must be enough holes to guarantee proper ventilation, and they must be small enough to block objects from possibly falling in the box or people accidentally touching the batteries. Before the battery box is used on the road, a test run will be performed in the lab, where the temperature inside the box is monitored to test if the batteries can run for several hours without overheating. When performing the measurements in the field, ventilation should be examined every time that the car is stopping for static measurements (approximately, once an hour) by checking that the fan is working and that the air coming from the ventilation holes is not too warm. If the temperature in the box is suspected to be higher than expected, the batteries will be turned off and the measurements, interrupted. A fire extinguisher must be carried in the car when the box is inside.

When charging lead batteries, there is a risk of hydrogen gas leak. In order to avoid accidents, it should be ensured that no flammable goods are placed around the batteries while charging and that good ventilation is possible. A charging station has been created in the corner next to the sink in the cloud room where, in case of hydrogen formation, it will diffuse immediately out in the big space. The place has been marked with a sign “charging space for batteries” and the needed

precautions are listed next to it. No other electrical devices are allowed within 1 meter and the batteries are placed far enough from the power outlets on the wall. For extra ventilation, the box door will always remain open during charging (with extra signs marking the area, discouraging non-trained personnel to get close to the system), avoiding overheating and formation of hydrogen pockets. If the batteries are charged outside of the laboratory (for example, in a hotel in-between measurements) the same security conditions should be kept.

Since the measurements will be performed in a car in movement, there is a certain risk while driving on the road. To avoid possible accidents due to distractions, at least two people will be monitoring the measurements the entire time; one person will be focused on driving while keeping in contact with another person by a phone call, using a hands-free device, that will give instructions about the direction to follow and when and where to stop, as well as ensuring that the instruments are in operation and the measurements are successfully performed. All the instruments will be properly attached to the car to avoid objects hitting people in case of an accident or a non-steady drive. The inlet and outlet system will also be secured from the inside to ensure that no objects fall to the road and compromise the security of other users and the loss of the laboratory material.

The SMPS contains a particle charger that consists of a radioactive source. The radioactive source is enclosed in a special case to avoid radioactive leakage. The particle charger will be properly secured when the system is inside the car to avoid damages in the enclosure or other elements of the system in case of an accident or a non-steady drive. The compulsory radiation safety document will accompany the car during driving the vehicle with the SMPS.

The Condensation Particle Counter (CPS) of the SMPS contains butanol. This is a flammable and toxic compound that can cause irritation in the respiratory system, skin and eyes. To avoid fire and explosions in the car, the amount of butanol carried in the SMPS will be reduced to the minimum needed for the performance of the experiment. The SMPS will be properly attached to the car to avoid leakages. For the tests performed in the laboratory, the CPC should be connected to the fume hood. The butanol will escape outdoors via the outlet tubing in the car.

RISK IDENTIFICATION

RISK NO.	TYPE	MOMENT / ACTIVITY	RISK / ATTRIBUTE	LOCATION
1	Batteries	Handling of the batteries, connection of cables and changes in the circuit	Electrical shock	Battery box
2	Batteries	Charging and discharging of batteries	Fire or explosion	Battery box in laboratory and car
3	Charging of the batteries	Charging between experiments	Hydrogen leakage	Ventilated corner in the cloud room
4	Driving	Performance of the measurements in the car in movement	Traffic accident/ contusion by instruments getting out of place	The road where the measurements are performed
5	Radioactive source of particle charger	Use of SMPS	Radioactive leakage	SMPS
6	Butanol	Use of SMPS	Leakage of toxic compound / fire	SMPS
7	Batteries	Handling of the batteries, connection of cables and changes in the circuit	Short of batteries, leading to destruction of batteries	Battery box

RISK ESTIMATION AND ASSESSMENT (without any risk-reducing measures)

RISK NO.	PROBABILITY	CONSEQUENCE	RISK ESTIMATION	RISK ASSESSMENT
1	Medium (3)	High (4)	Very high risk (12)	Not acceptable
2	Low (2)	High (4)	High risk (8)	Not acceptable
3	Low (2)	Medium (3)	Moderate risk (6)	Acceptable
4	Medium (3)	High (4)	Very high risk (12)	Not acceptable
5	Low (2)	Low (2)	Moderate risk (4)	Acceptable
6	Low (2)	High (4)	High risk (8)	Not acceptable
7	High (4)	High (4)	Very high risk (16)	Acceptable

RISK REDUCING MEASURES

RISK NO.	TYPE	RISK REDUCING MEASURES
1	Batteries (electrical shock)	1. Electricity expert supervising system before connections and after building the box, before measuring in the field. 2. Danger signs discouraging untrained personnel to open the box. 3. Use of rubber gloves when handling the batteries. 4. Isolation tape covering the battery poles when possible. Permanent isolation covers for the poles after system is built. 5. Loose cables attached with clamps to the side of the box. 6. Residual current devices (RCD) in the outlets of the inverter. 7. The box remains always closed during measurements and charging. 8. When working alone, use security alarm, avoid dangerous actions and notify another person.
2	Batteries (fire/explosion)	1. Fan installation. 2. Ventilation holes on top and side of the box. 3. Test run with temperature monitoring. 4. Hourly ventilation checks when working in the field. 5. Fire extinguisher in the car.
3	Charging of the batteries	1. Ventilated charging station. 2. No flammable goods placed around the batteries. 3. No other electrical devices allowed within 1 meter. 4. Batteries placed far enough from the power outlets on the wall. 5. Needed precautions listed next to charging station. 6. Box door open during charging.
4	Driving	1. Two people monitoring the measurements at all time. One person gives instructions by a hands-free phone call and takes care of the measurements while the driver is only focused on driving. 2. All the instruments properly attached to the car, including inlet and outlet system.
5	Radioactive source of particle charger	1. Particle charger properly secured when the system is inside the car.
6	Butanol	1. Reduction of the amount of butanol in the SMPS when driving. 2. SMPS properly attached to the car
7	Batteries	1. Danger signs discouraging untrained personnel to open the box. 2. Isolation tape covering the battery poles when possible. 3. The box remains always closed during measurements and charging.

SUMMARY AND CONCLUSION

The major risks of this experiment have been examined and safety measures have been taken in order to preserve the safety needed for the laboratory personnel to work in a safe environment.

It has been concluded that the highest risks for humans are taken when handling the batteries. The battery box has been designed in a way that once the

RISK ESTIMATION AND ASSESSMENT (with risk reducing measures applied)

RISK NO.	PROBABILITY	CONSEQUENCE	RISK ESTIMATION	RISK ASSESSMENT
1	Very low (1)	High (4)	Moderate risk (4)	Acceptable
2	Very low (1)	High (4)	Moderate risk (4)	Acceptable
3	Very low (1)	Very low (1)	Low risk (1)	Acceptable
4	Very low (1)	High (4)	Moderate risk (4)	Acceptable
5	Very low (1)	Low (2)	Low risk (2)	Acceptable
6	Very low (1)	Medium (3)	Low risk (3)	Acceptable
7	Medium (3)	High (4)	Very high (12)	Acceptable

system is built, it is not necessary to open the box or handle the batteries, so the risk is only present during the building of the system. It is therefore in this part of the process when the security measurements should be taken more into consideration.

Another dangerous side of the experiment comes from the risk of fire or explosion due to batteries overheating. The risk factors have been minimized and correct ventilation will be ensured based on the advice of an electricity expert.

When driving a car on the road, there are always risks that are difficult to prevent such as interactions with other vehicles or atmospheric conditions. To minimize risks, a person will give instructions to the driver by a hands-free call and will supervise the measurements to reduce the probability of distractions.

Other risks such as leakage and intoxication are reduced by properly attaching elements to the car and avoiding the possibility of containers being broken or damaged.

Finally, it is safe to say that the safety precautions and measures ensure that the laboratory personnel can work in a safe environment.

The greatest risk is damage to batteries during short circuit of batteries (when plus pole and negative poles get connected with conductor). However, this risk is acceptable, since it only poses a risk to damage goods, and not humans. Personnel is handling the batteries with insulation gloves.

3. Waste handling

The experiments do not generate any hazardous waste that needs to be handled or stored in any special way. The instruments cannot be considered as contaminated after the experiments are performed.

The butanol is disposed in the butanol disposal storage in IKDC aerosol lab.

COMPILATION OF DOCUMENT

Risk evaluation performed by:	*(Include name in block letters)*
ADRIAN REYES	ADAM KRISTENSSON
Responsible for experiment Adam Kristensson	Supervisor Adam Kristensson